Title
Mechanisms of Co-regulator Recruitment to the Glucocorticoid and Androgen Receptors

Author
Pfaff, Samuel James

Publication Date
2009

Peer reviewed|Thesis/dissertation

Mechanisms of Co-regulator Recruitment to the Glucocorticoid and Androgen Receptors

by

Samuel J. Pfaff

DISSERTATION

Submitted in partial satisfaction of the requirements for the degree of

DOCTOR OF PHILOSOPHY

in

Biophysics

in the

GRADUATE DIVISION

of the

UNIVERSITY OF CALIFORNIA, SAN FRANCISCO

To Hezi, Mom, and Dad

Acknowledgements

My time at UCSF has been the greatest learning experience of my life, and from the beginning, it was a team effort. Biology was new to me when I arrived, so I was very lucky to be surrounded by brilliant, hard-working classmates who set examples I am still trying to live up to today. I am greatly indebted to Caleb Bashor, Clement Chu, Chris Farady, Quincey Justman, Neema Salimi, Ben Sellers, and Jeremy Wilbur for teaching me how to ask biological questions and succeed in the lab. Special thanks also to Julie Ransom and Rebecca Brown. Their presence was always a comforting reminder that the biophysics group was in good hands.

The Fletterick lab was a great home for me during my graduate career. Starting from the top, the group is full of scientists whose deep curiosity and true expertise make successful research inevitable. I can never thank Robert enough for his support, patience, and guidance. His unique ability to see all aspects of a biological question and his willingness to go after tough projects give the lab its identity, and foster a truly intellectual environment. My lab mates were always generous, helpful, and full of ideas especially when things at the bench were not going well. Special thanks to Eugene Hur, Kris Kuchenbecker, and Jeremy Wilbur for always pushing me to achieve more, and challenging me to understand their own research.

Noting the collaborative nature of UCSF might be cliched, but my work would not have been possible without contributions from several labs on campus. The Agard lab was like a second home to me, and I thank them dearly for reagents, excessive time on their equipment, and

prescient scientific advice. The Craik, Guy, Stroud, and Wells labs also deserve thanks for letting me use their equipment and reagents without hesitation. Special thanks to my thesis committee members Jim Wells and Keith Yamamoto. Their insights and encouragement were crucial in helping me to form more complete, cohesive scientific stories. I would also like to thank Pam England and KaroBio for allowing me to participate in two very interesting and fruitful collaborations early in my scientific career.

Finally, I would like to thank my family and friends for their constant love and support. My parents have always encouraged me to follow my interests wherever they take me, and I truly appreciate that gift. Angela has been my partner in this endeavor from day one. Her love, humor, and unwavering support have always kept me afloat, and for that I am eternally grateful.

Mechanisms of co-regulator recruitment to the glucocorticoid and androgen receptors

Samuel J. Pfaff

ABSTRACT

Steroid receptors are regulated by a diverse array of cellular effectors. Interactions with chaperone proteins, steroid hormones, kinase cascades, motor proteins, co-regulator proteins, and DNA determine the functional output of a receptor. Co-regulator proteins directly bind SRs at a surface site on the C-terminal ligand binding domain, apart from the buried ligand binding pocket, and are capable of activating and repressing transcriptional activity through the receptor. Most SRs prefer to bind co-regulators bearing the NR box motif LXXLL, where X is any amino acid. The sequences surrounding the Leu residues and the amino acids that comprise the receptor's activation function-2 surface determine the specificity of the interaction. The recruitment patterns of co-regulator proteins to SRs is key in determining cell and tissue-specific responses to natural and synthetic therapeutic steroids.

Androgen receptor is unlike the other SRs in that it preferentially binds co-regulators with aromatic residues comprising the NR box. To investigate this unusual preference, we solved X-ray structures of several aromatic-containing peptides bound to AR's AF-2 surface, and determined binding constants for the interactions by surface plasmon resonance (Chapter 2).

Several AR residues were shown to be involved in an induced-fit mechanism that allows the receptor to recognize a wider variety of motifs.

Co-regulator recruitment to GR's AF-2 surface was investigated biochemically, revealing that binding events at AF-2 and the ligand binding pocket are allosterically coupled (Chapter 1). We found that NR box binding to GR's AF-2 slows association and dissociation of a fluorescent GR agonist, using fluorescence polarization. The effect on steroid binding was NR box sequence dependent with 7 of 18 peptides assayed showing the ability to reduce steroid binding rates significantly. Dissociation constants were determined for 8 of 18 peptides, revealing a more complete consensus sequence for NR box binding to GR. Additionally, mutation of a residue conserved in SRs shown to effect chaperone, steroid, and co-regulator binding to GR in cells was confirmed as a key component of the network connecting steroid and co-regulator binding sites.

Table of Contents

List of Tables

List of Figures

Chapter 1

Hormone and co-regulator binding to the glucocorticoid receptor are allosterically coupled

Manuscript submitted to EMBO Journal, 11/2009

ABSTRACT

The glucocorticoid receptor initiates the cellular response to glucocorticoid steroid hormones in vertebrates. Co-regulator proteins dock to the receptor in response to hormone binding and potentiate the transcriptional activity of the receptor by modifying DNA and recruiting essential transcription factors like RNA polymerase II. Hormones and co-regulators bind at distinct sites in the ligand binding domain, yet function cooperatively to mediate transcriptional control. This study reveals and quantifies energetic coupling between two binding sites using purified components. Using a library of peptides taken from co-regulator proteins, we determine the pattern of co-regulator recruitment to the glucocorticoid receptor ligand binding domain. We show that peptides from co-regulators differ in their effects on hormone binding and kinetics. Peptides from DAX1 and SRC1 bind with similar affinity but DAX1 binding is coupled to hormone binding and SRC1 is not. Mechanistic details of co-regulator recruitment and coupling to the hormone binding pocket are uncovered by analysis of properties endowed by mutation of a key residue in the allosteric network connecting the sites.

INTRODUCTION

Vertebrate endocrine signaling by steroids is primarily mediated by the steroid receptor (SR) class of nuclear receptors. **(Katzenellenbogen, 1980)** Members of this family, including receptors for androgens, estrogens, progestins, mineralocorticoids, and glucocorticoids, regulate target gene mRNA levels through transcriptional activation and active repression. The patterns of genes regulated by each receptor specify the cell's response to a steroid hormone signal. Aberrant signaling through SRs is a hallmark of several syndromes and diseases, including most cancers, and as such SRs are widely targeted in pharmaceutical discovery. **(Gronemeyer et al, 2004)**

The glucocorticoids (GC) steroids are the primary stress hormones released by hypothalamic-pituitary-adrenal axis in humans, and regulate numerous physiological processes, including homeostasis, cell differentiation, apoptosis, and metabolism. **(Chrousos & Kino, 2007; Rhen & Cidlowski, 2005)** Disruption of GC signaling is a component of many, diverse disease states, including depression, leukemia, and asthma. Natural and synthetic GCs are among the most prescribed drugs for their anti-inflammatory and immune-suppressive profiles. However, long term GC treatment may result in severe side effects including diabetes, glaucoma, and osteoporosis. **(Chrousos et al, 2004; Chrousos & Kino, 2007; Rhen & Cidlowski, 2005)**

The first localized step in translating a glucocorticoid signal toward a genomic outcome is the binding of GC to the glucocorticoid receptor (GR) in the cytosol. In the absence of hormone, GR is sequestered outside the nucleus where it is stabilized by regulatory complexes of chaperone proteins, that include Hsp90, Hsp70, Hsp40, HOP, and p23. **(Hutchison et al, 1994; Picard et al, 1990a; Pratt & Dittmar, 1998)** Interaction with this complex is required for high

affinity ligand binding to GR, and all other SRs. **(Bresnick et al, 1989; Pratt et al, 2004)** Following ligand binding, GR is transported to the nucleus **(Echeverria et al, 2009; Htun et al, 1996; Picard & Yamamoto, 1987; Tanaka et al, 2003)**, where it initiates a multistep series of events that are cell and tissue-specific programs of gene activation and repression. **(Galon et al, 2002; Rogatsky et al, 2003)** The simplistic model of GR-mediated transcriptional control posits two basic modes of receptor action: activation of gene expression by direct interaction with specific GC response element (GRE) sequences of DNA, and repression of pro-inflammatory genes under the control of transcription factors AP-1 and NF-κB. Recently, a more dynamic model has emerged that builds on these two basic modes to explain the temporal and kinetic characters of GR-mediated transcriptional control. **(Biddie & Hager, 2009; John et al, 2009; McNally et al, 2000; Stavreva et al, 2004)**

GR, like fellow members of the steroid receptor family, is a modular scaffolding protein, consisting of three major functional domains. The N-terminal 400 residues comprise a mostly unstructured region that importantly harbors a transcriptional activation region, dubbed activation function 1 (AF-1). AF-1 can bind co-regulator proteins and its transcriptional activity is not ligand-dependent. **(Iniguez-Lluhi et al, 1997; Warnmark et al, 2000)** Residues 430-500 comprise a direct DNA-binding domain (DBD) that is the most well-conserved domain across all nuclear receptors (NRs). **(Baumann et al, 1993; Hard et al, 1990; Luisi et al, 1991)** GR forms homo-dimers through this domain, and uses zinc-finger motifs coded in this region to recognize and bind specific glucocorticoid binding sequences (GBSs) associated with target genes on DNA. **(Kumar & Thompson, 2005)** Long thought to simply dock to DNA, a recent study has

elucidated a role for the DBD, and the specific GBS to which it is bound, in allosteric, inter-domain communication through the receptor. **(Meijsing et al, 2009)**

The C-terminal 250 residues of GR encompass the ligand binding domain (LBD), which initiates the cell's response to GCs. GR's preference for its natural hormone cortisol evolved through mutations in the LBD ~400 million years ago when it diverged from the mineralocorticoid receptor. **(Ortlund et al, 2007)** Interestingly, the molecular basis of its evolved specificity involves mutations at the receptor : hormone interface, as well as sets of permissive mutations to other regions of the LBD shown to be critical in stabilizing a functional receptor conformation. **(Bridgham et al, 2006; Bridgham et al, 2009; Ortlund et al, 2007)** Well conserved through the nuclear receptor superfamily, the LBD is a three-layered α-helical sandwich structure, whose hydrophobic core is completed by lipophillic hormone binding to the protein's interior. **(Bourguet et al, 1995; Renaud et al, 1995; Wagner et al, 1995)** The surface of the nuclear receptor LBD typically contains at least two protein-protein interaction sites: a dimerization surface, more prevalent in the class II receptors (TR, VDR, RAR) that are regulated by forming hetero-dimmers with RXR **(Mangelsdorf & Evans, 1995)**, and a co-regulator protein docking site termed activation function-2 (AF-2). Comprised of residues from helices 3, 4, 5, and 12, AF-2 is a shallow, mainly hydrophobic groove surrounded by polar residues that allows for specific docking of co-regulators to the LBD surface. **(Darimont et al, 1998; Feng et al, 1998; Shiau et al, 1998)**

Co-regulators are essential players in the transduction of hormone signals through nuclear receptors. **(McKenna et al, 1999; McKenna & O'Malley, 2002; Xu & Li, 2003)** Canonically, ectopic expression of co-activators, including the p160 family, **(Hong et al, 1996; Voegel et al,**

1996; Zhu et al, 1996) leads to an enhancement of target gene expression upon hormone treatment, whereas co-repressors such as NCoR and SMRT silence hormone-induced gene expression. **(Chen et al, 1996)** The intrinsic functionality of co-regulators is varied, with many implicated in chromatin remodeling and recruitment of the basal transcription machinery. **(Belandia & Parker, 2003; Fryer & Archer, 1998)** As their docking to nuclear receptors typically follows ligand binding and subsequent localization to the nucleus, co-regulators represent a vital, cell-specific layer of control that can be employed to modify the cellular response to hormone.

Both co-activators and co-repressors interact with NR LBDs by docking short, amphipathic, helical segments at the AF-2 surface. **(Darimont et al, 1998; Heery et al, 1997)** Many co-regulators contain several of these NR interaction sites, referred to henceforth as NR boxes. The canonical co-activator NR box is comprised of the sequence LXXLL, where L is leucine and X is any amino acid. The most well-characterized co-activators, the p160 family, **(Hong et al, 1997; Hong et al, 1996; Onate et al, 1998; Voegel et al, 1998; Voegel et al, 1996; Zhu et al, 1996)** each contain at least three NR boxes that share the LXXLL core, but differ in the residues at the +2 and +3 positions in addition to the flanking sequence. These residues have been shown to be key determinants of selectivity between co-regulators and the wide array of NRs with which they interact. **(Chang et al, 1999)**

Several studies have determined patterns of co-regulator recruitment to NR LBDs by structural, biochemical, or cell-based methods. **(Bramlett et al, 2001; Estebanez-Perpina et al, 2005; Hur et al, 2004; Moore et al, 2004; Teichert et al, 2009; Wu et al, 2004)** Interestingly, many NRs assayed show different patterns of co-regulator recruitment based on the identity of

the ligand in the binding pocket, implying allosteric coupling between the two sites. This allosteric link between NR functional sites has been explored computationally by Shulman et al., who used co-variation within the protein's evolved sequences to determine the network of residues involved in communication between the dimerization, AF-2, and ligand binding regions of the Class II NR RXR. **(Shulman et al, 2004)**

This report presents the first quantitative assessment of GR LBD's key functional sites using purified components. Allosteric modulation of ligand binding kinetics by co-regulators at the AF-2 surface is revealed and characterized using fluorescence polarization (FP). A similar technique is applied to determine and quantify the pattern of co-regulator recruitment to agonist-bound GR LBD, using a library of 18 NR box peptides from physiologically important co-regulators. Additionally, the mechanism of action of a recently discovered mutation with profound functional consequences in the cell is elucidated. **(Ricketson et al, 2007)** Together these results represent a first step in the development of a quantitative framework for the description of coupling between the co-regulator docking site and the ligand binding site.

RESULTS

GR ligand binding kinetics

Crystal structures show a spectrum of physical interactions of GR LBD with peptides, drugs and self. **(Biggadike et al, 2008; Bledsoe et al, 2002; Kauppi et al, 2003; Madauss et al, 2008; Suino-Powell et al, 2008)** However, quantitative evaluation of these interactions and their relationships is scant. Biochemical interrogation of GR LBD and its various interaction partners has long been hindered by difficulty in obtaining stable, functional receptors for in vitro studies.

The majority of published work using recombinantly-expressed GR LBD, including this study, has been aided by incorporation of solubility-enhancing mutations discovered by yeast screens of GR activity. **(Bledsoe et al, 2002; B. Darimont, personal communication; Frego & Davidson, 2006; Kauppi et al, 2003; Kroe et al, 2007)** GR containing the mutations F602S and C638D will be referred to henceforth as GR_{SD}.

To assess the functionality of purified GR LBD, binding kinetics of fluorescein-labeled dexamethasone (dex-fl) (Figure 1-1) were measured using fluorescence polarization (Figure 1-2). Dex-fl is a fluorescent analogue of the potent, synthetic GC dexamethasone, that has been shown to bind GR with a similar affinity. **(Lin et al, 2002)** To facilitate this ligand binding study, unlabeled dex remaining from the protein preparation was removed from solution through dialysis or desalting. Previous studies **(Frego & Davidson, 2006; Kauppi et al, 2003; Kroe et al, 2007)** have shown that recombinantly expressed GR LBD can readily exchange ligand under non-denaturing conditions, in sharp contrast with the androgen receptor (unpublished results), suggesting ligand binding pocket accessibility may be a feature of GR. Figure 1-2(a and b) shows association and dissociation of the GR_{SD} : dex-fl complex monitored to equilibrium. Both processes were fit to a single exponential model that yielded half times of 41 s and 160 s at 25^0 C, for association and dissociation, respectively.

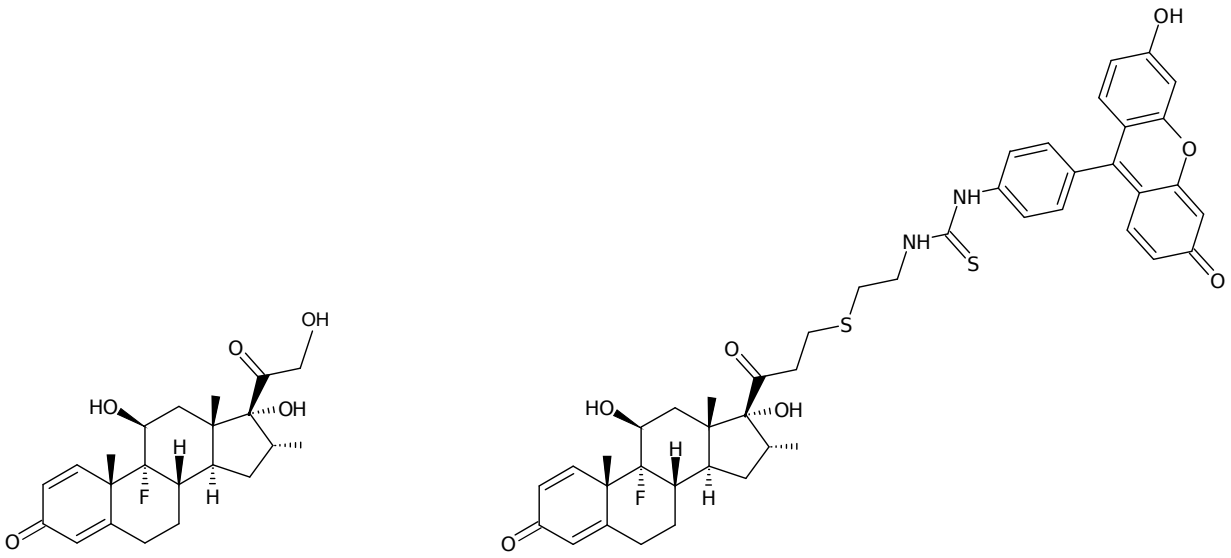

Figure 1-1. *Chemical structures of dex and dex-fl*

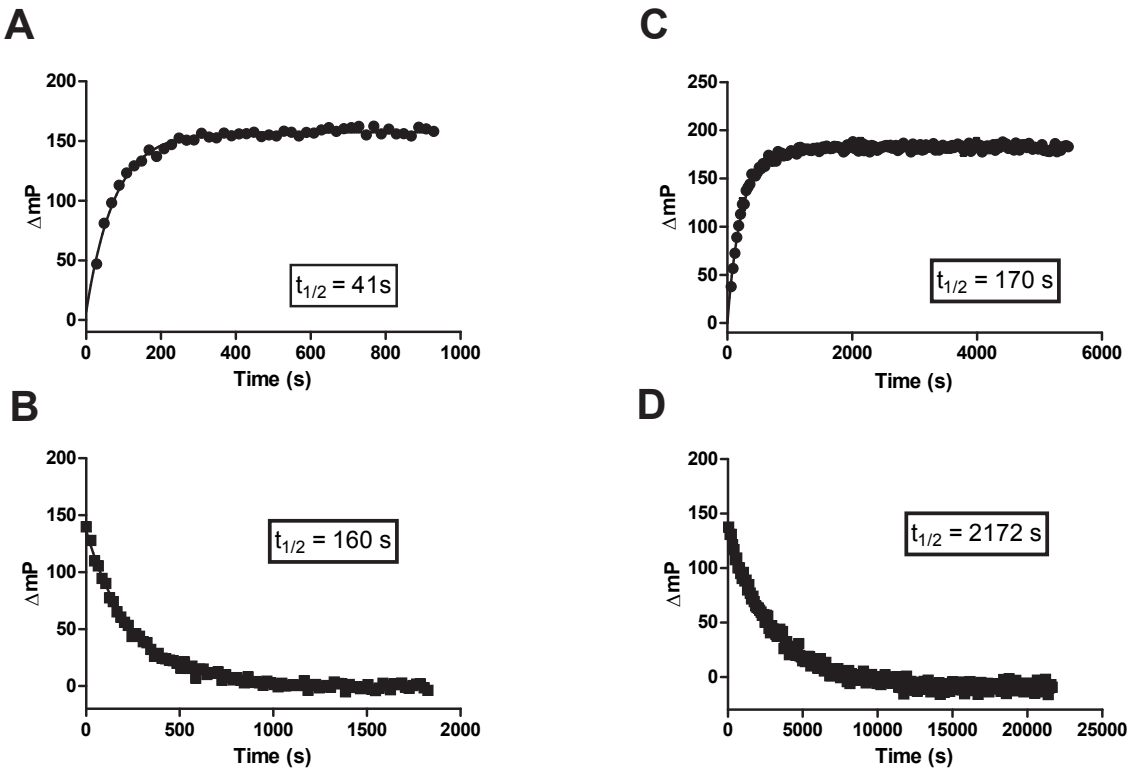

Figure 1-2. *GR : dex-fl binding kinetics.* (A) 1 μM GR_{SD} (F602S, C638D), 20 nM dex-fl association monitored by fluorescence polarization. (B) 1 μM GR_{SD}, 20 nM dex-fl dissociation induced by addition of 50 μM unlabeled dex. (C) 1 μM GR_{M752I}, 20 nM dex-fl association. (D) 1 μM GR_{M752I}, 20nM dex-fl dissociation. All data fit to one-phase exponential models to yield half times.

NR box peptides slow ligand binding

Previous studies have shown NR box peptides have a stabilizing effect on the AF-2 regions of NRs. **(Gee et al, 1999; Kallenberger et al, 2003; Nahoum et al, 2007; Perez Santin et al, 2009)** Reflecting this, several NRs, including GR and MR, require addition of NR box peptides to obtain complexes stable enough for crystallographic study. **(Li et al, 2005; Suino-Powell et al, 2008)** Helix 12 and other structural elements that form the AF-2 binding site have been postulated to form a lid on the ligand binding pocket. **(He et al, 1999)** This encouraged us to evaluate the functional interplay between NR box binding to GR's AF-2 and dex-fl binding to the ligand binding pocket using FP kinetics.

GR was incubated with 10x molar excess of each of 18 physiological NR box peptides, and was then assayed for binding to dex-fl (Figure 1-3, Table 1-I). Association of the GR_{SD} : dex-fl complex in the presence of peptides from the DAX1 co-repressor and SRC2 co-activator are shown in figure 1-3a. Both peptides alter two components of the exponential association process; the binding plateau is heightened, and time to equilibrium is extended, 5 fold for SRC2-3, and 6 fold for DAX1-3. Figure 1-3c shows $t_{1/2}$ values for GR_{SD} : dex-fl complex formation in the presence of peptides from our NR box library. Many NR box peptides showed little influence on the on rates of the hormone analog, but large changes in rates were found for SRC1-4, SRC2-3, SRC3-3, PGC1α-1, DAX1-2, DAX1-3 and SHP-2 indicating that peptide residence at AF-2 affects the ligand binding pocket. A more dramatic effect was observed during dissociation of the GR : dex-fl complex (Figure 1-3b and d), initiated by addition of 50 μM unlabeled dex. In this library, SRC2-3 and DAX1-3 slowed ligand dissociation by 10 and 27-

fold respectively (Figure 1-3b). This biased modulation of dissociation kinetics was apparent for all NR box peptides that affected ligand binding (Figure 1-3c and d, Table 1-I).

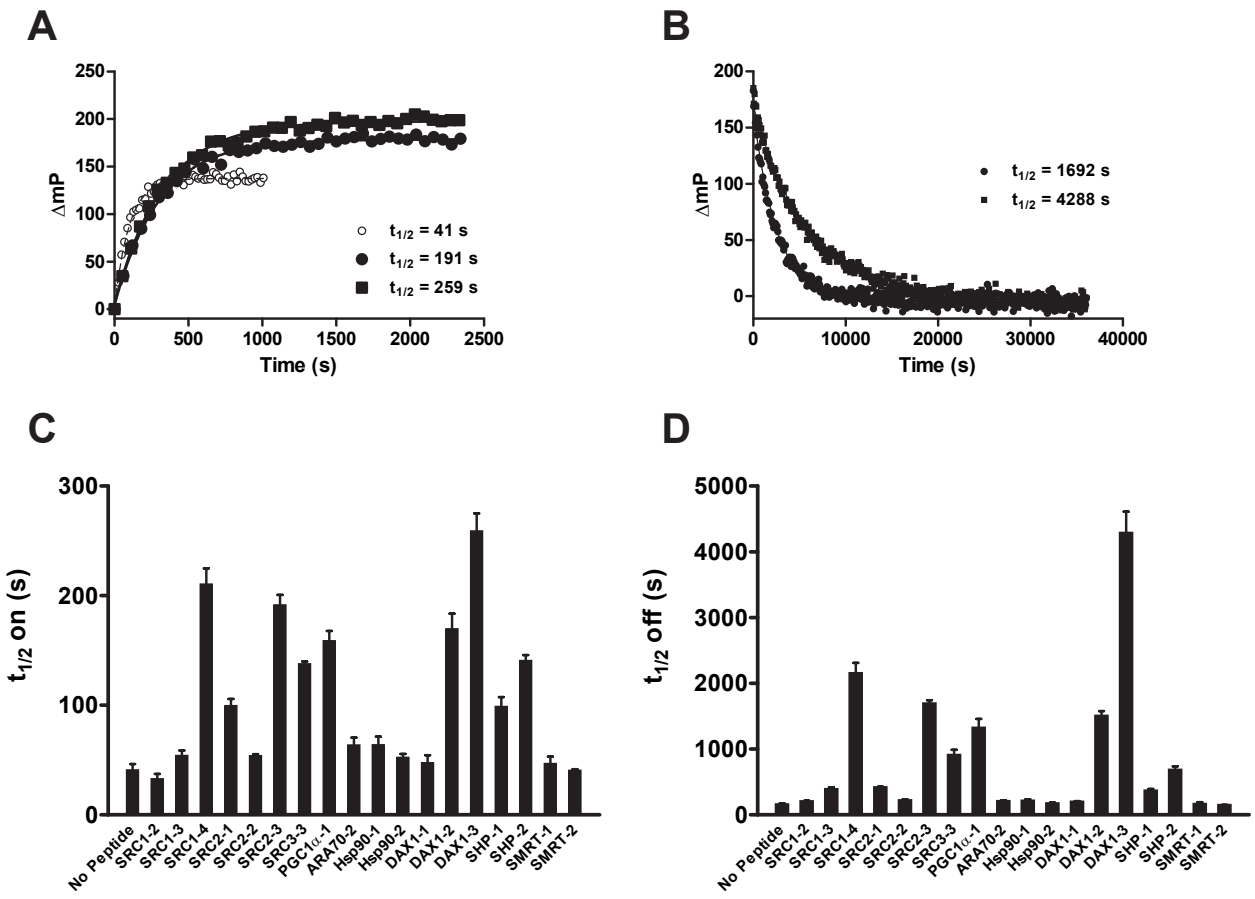

Figure 1-3. *NR box binding is coupled to ligand binding kinetics.* (A) 1 μM GR_{SD}, 20 nM dex-fl association in the presence of 10 μM SRC2-3 (circles), DAX1-3 (squares), and no NR box (grey circles). Baseline-subtracted data fit to one-phase exponential model. (B) 1 μM GR_{SD}, 20 nM dex-fl dissociation in the presence of 10 μM SRC2-3 (circles), DAX1-3 (squares). (C) Half times of GR_{SD} : dex-fl association in the presence of 10 μM NR box. Bars represent mean ± S.E.M. of at least 3 independent experiments. (D) Half times of GR_{SD} : dex-fl dissociation in the presence of 10 μM NR box.

M752I throttles GR ligand binding

In a recent study, Ricketson and co-workers identified several mutations of the GR LBD that increase responsiveness to dex, while also reducing the receptor's dependence on ubiquitous molecular chaperone Hsp90. **(Ricketson et al, 2007)** One of the mutations identified was M752I, which in addition to the aforementioned effects, was shown to increase GR's affinity for co-regulator SRC2. Structurally, Met-752 is positioned at a key location for inter- and intra-protein interactions. **(Bledsoe et al, 2002)** At the N-terminus of helix 12, it directly contacts bound NR box peptides at its -1 position, a conserved hydrophobic residue, and packs against hydrophobic side chains from residues in neighboring helices of the receptor. Methionine side chains are both hydrophobic and flexible. Receptors naturally possessing a more constrained Leu at this position, including those for thyroid hormone, retinoic acid, and vitamin D, typically do not depend on Hsp90 in the unliganded state. These receptors are localized to the nucleus in the absence of ligand, and are repressed by the nuclear receptor RXR through hetero-dimerization. **(Dalman et al, 1990; Dalman et al, 1991; Mangelsdorf & Evans, 1995)** Figure 1-2 (c and d) shows association and dissociation of dex-fl from GR_{M752I}. Both processes were fit to a single exponential model that yielded half times of 170 s and 2172 s respectively, for association and dissociation. Thus mutation of a flexible, hydrophobic surface residue 10 Å from the dex-fl molecule slowed both processes, with a greater impact being observed on dissociation, suggesting the amino acid residue at position 752 affects ligand binding pocket stability through a mechanism likely similar to that shown by NR box binding.

M752I AF-2 binding preferentially slows hormone association

NR box modulation of dex-fl binding kinetics was also explored with GR_{M752I}. Interacting NR box peptides produced highly stable complexes, with $t_{1/2}$ association as high as 9,400 s (DAX1-3; Figure 1-4 a and c) and $t_{1/2}$ dissociation reaching 74,000 s (DAX1-3; Figure 1-4 b and d). Dex-fl dissociation was not monitored to equilibrium for reactions with strong interacting peptides, as the time required to reach a lower plateau was too long to ensure high protein quality for the duration of the assay. To acquire an estimate of the $t_{1/2}$ in this situation, we measured the reaction for typically at least 50,000 s and extrapolated the fit curve to a lower polarization plateau of 20 mP. Data sets for SRC1-4, SRC2-3, PGC1α-1, DAX1-2, and DAX1-3 were treated this way. Strikingly, the effect of NR box on ligand association and dissociation rates was reversed from GR_{SD} in the context of M752I, with the peptide having greater influence on dex-fl association (Table 1-I).

To test the hypothesis that NR box peptides have more affinity for unliganded GR_{M752I}, SRC3-3 was covalently labeled with Alexa-Fluor 555 through its N-terminal cysteine for direct-binding fluorescence polarization measurements (Figure 1-5). **(Moore et al, 2004; Teichert et al, 2009)** In the presence of 10 μM dex, GR_{M752I} bound SRC3-3-fluor with K_D = 349 nM (Figure 1-5b). GR_{M752I} that had been stripped of ligand, bound SRC3-3-fluor with a nearly identical K_D of 327 nM, indicating that both holo and apo GR_{M752I} present interaction-competent AF-2 surfaces. For comparison, the analogous experiments were carried out with GR_{SD}. SRC3-3-fluor bound apo and holo GR_{SD} similarly, with K_D = 676 nM for apo and K_D = 741 nM for dex-bound GR_{SD} (Figure 1-5a). Thus each GR binds this peptide nearly as well with our without hormone, but the stronger interaction is with GR_{M752I}.

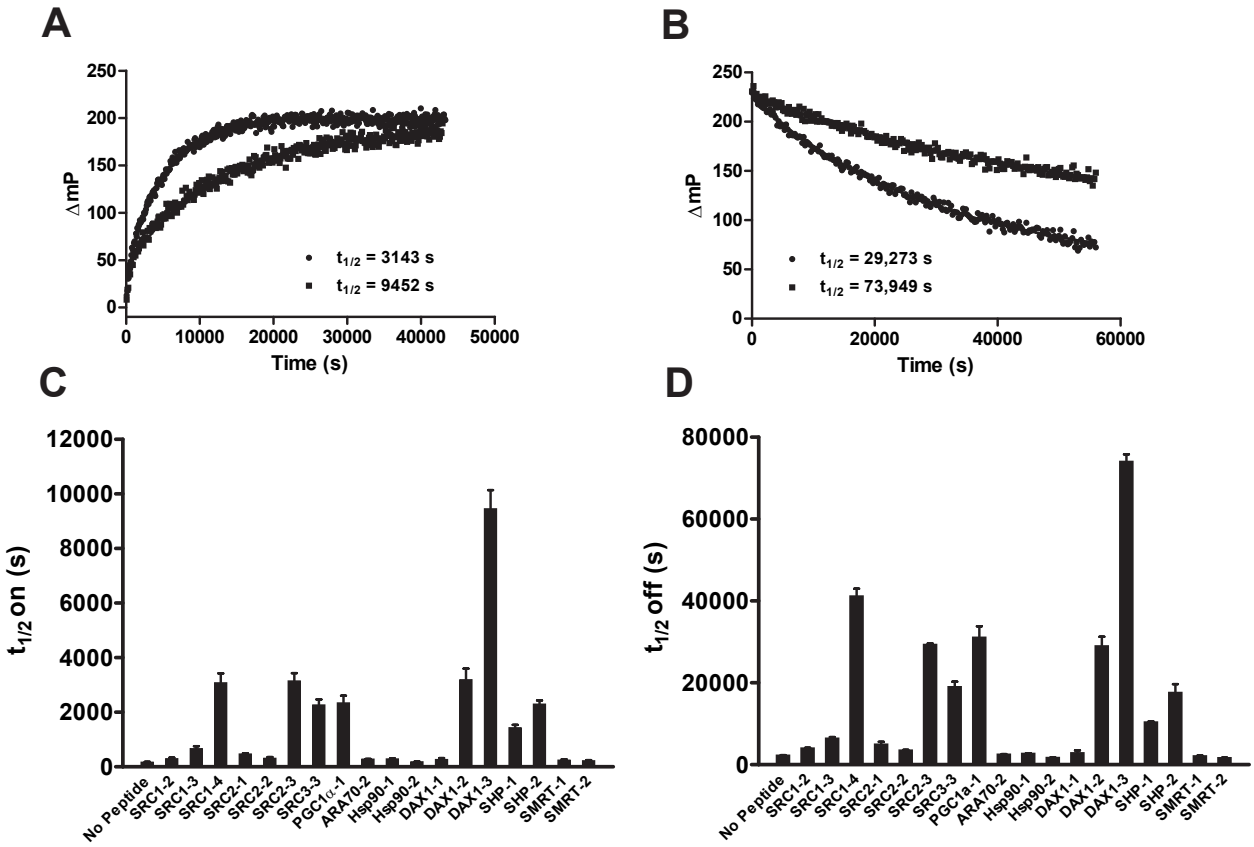

Figure 1-4. *GRM752I : dex-fl binding kinetics in the presence of NR box peptides.* (A) 1 μM GRM752I, 20 nM dex-fl association in the presence of 10 μM SRC2-3 (circles), DAX1-3 (squares). Baseline-subtracted data fit to one-phase exponential model. (B) Half times of GRM752I : dex-fl association in the presence of 10 μM NR box. Bars represent mean ± S.E.M. of at least 3 independent experiments. (C) 1 μM GRM752I, 20 nM dex-fl dissociation in the presence of 10 μM SRC2-3 (circles), DAX1-3 (squares). (D) Half times of GRM752I : dex-fl dissociation in the presence of 10 μM NR box.

	GR_{SD}				GR_{M752I}			
	$t_{1/2}$ on		$t_{1/2}$ off		$t_{1/2}$ on		$t_{1/2}$ off	
No Peptide	41	**1**	160	**1**	170	**1**	2172	**1**
SRC1-2	33	**1**	206	**1**	301	**2**	3931	**2**
SRC1-3	54	**1**	392	**2**	668	**4**	6326	**3**
SRC1-4	211	**5**	2152	**13**	3078	**18**	41069	**19**
SRC2-1	100	**2**	418	**3**	471	**3**	4887	**2**
SRC2-2	54	**1**	222	**1**	312	**2**	3455	**2**
SRC2-3	192	**5**	1692	**11**	3143	**18**	29273	**13**
SRC3-3	138	**3**	910	**6**	2265	**13**	18907	**9**
PGC1α-1	159	**4**	1325	**8**	2341	**14**	31007	**14**
ARA70-2	64	**2**	207	**1**	281	**2**	2444	**1**
Hsp90-1	64	**2**	215	**1**	292	**2**	2613	**1**
Hsp90-2	53	**1**	175	**1**	188	**1**	1622	**1**
DAX1-1	48	**1**	198	**1**	264	**2**	2790	**1**
DAX1-2	170	**4**	1506	**9**	3193	**19**	28890	**13**
DAX1-3	259	**6**	4288	**27**	9452	**56**	73949	**34**
SHP-1	99	**2**	368	**2**	1432	**8**	10301	**5**
SHP-2	141	**3**	683	**4**	2295	**13**	17496	**8**
SMRT-1	47	**1**	165	**1**	244	**1**	2021	**1**
SMRT-2	41	**1**	150	**1**	225	**1**	1588	**1**

Table 1-I. *Half-times of association and dissociation of the GR : dex-fl complex.* Bold numbers represent fold half-time increase over no peptide condition.

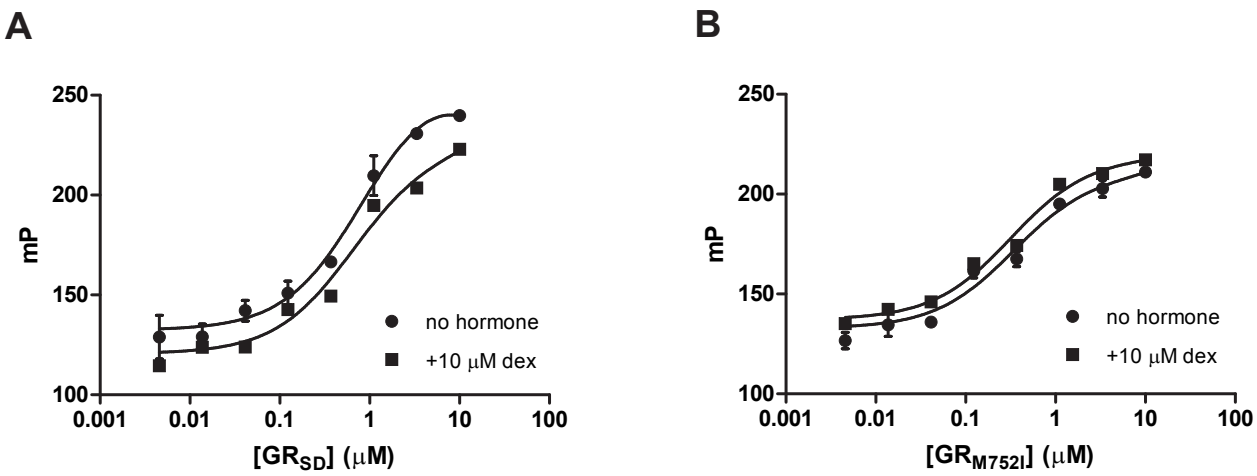

Figure 1-5. *GR binding to SRC3-3-fluor with and without dex.* (**A**) GR_{SD} titrated against 20 nM SRC3-3 conjugated to Alexa-Fluor 555 in the presence (circles) or absence (squares) of 10 μM dex. (**B**) GR_{M752I} titrated against 20 nM SRC3-3 conjugated to Alexa-Fluor 555 in the presence (circles) or absence (squares) of 10 μM dex.

Determination of NR box binding affinities by FP

NR box binding to AF-2 alters the plateau in polarization in addition to the kinetics of GR : dex-fl complex formation (Figure 1-3a). This finding allowed determination of NR box binding affinities using dex-fl polarization as a readout. This modulation of the binding plateau can be caused by at least two complimentary processes. The affinity of dex-fl could be increased in the presence of binding at AF-2. Alternatively, the bound peptide might change the spectrum of conformations available to GR. NR box binding appears to cause the receptor ligand pair to move from fast exchange to a slow exchange regime as demonstrated by our kinetic experiments (Figures 1-3 and 1-4, Table 1-1). As FP is sensitive to molecular dynamics, the observed increase in polarization could be caused by longer-lived receptor : ligand complexes. Titrations of NR box peptide were performed against constant concentrations of GR and dex-fl, yielding K_D values for 8 of 18 peptides tested (Table 1-II, Figure 1-S1). Example titration curves representing the various binding modes observed are shown in figure 1-6.

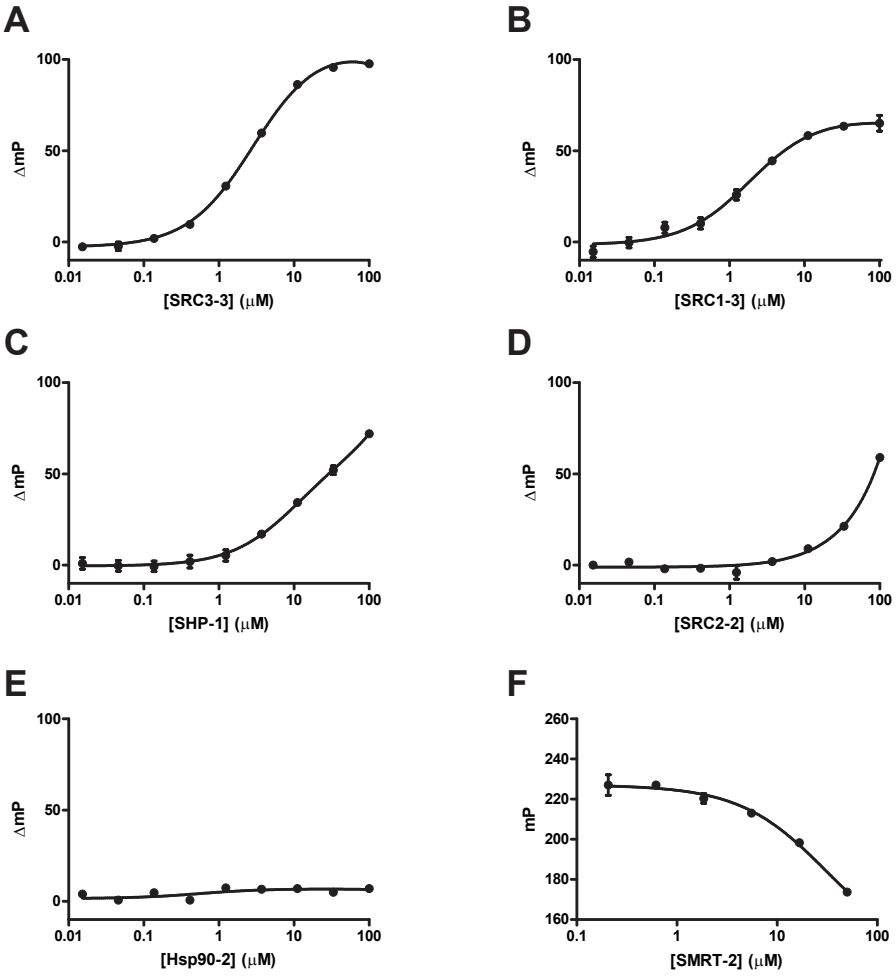

Figure 1-6. *GR binding to NR box peptides by allosteric FP reveals six binding modes.* NR box peptides titrated against 500 nM GR_{SD}, 20 nM dex-fl. (**A**) SRC3-3, high-plateau saturation. (**B**) SRC1-3, low-plateau saturation. (**C**) SHP-1, non-saturable binding. (**D**) SRC2-2, weak binding. (**E**) Hsp90-2, no binding. (**F**) SMRT-2, co-repressor binding. All data fit to one site saturation binding model.

NR box binding to GR occurred in six distinct modes: high-plateau saturable binding (a), low-plateau saturable binding (b), non-saturable binding (c), weak binding (d), no binding (e), and co-repressor binding (f). As expected, NR box peptides identified as having the greatest effect on ligand binding kinetics were primarily those that displayed saturable binding behavior. K_D values for these peptides are listed in Table 1-II. Of these NR box peptides, four belong to the p160 family of co-activators (SRC1-3, SRC1-4, SRC2-3, SRC3-3), while the others (PGC1α-1, DAX1-2, DAX1-3, and SHP-2) represent different families of co-regulators. PGC1α-1 is derived from a co-activator, while the remaining NR box peptides come from the unusual nuclear receptors/co-repressors DAX1 and SHP. SHP contains a putative LBD and has no identified ligand; the structure of DAX1's C-terminal 230 amino acids shows a nearly complete LBD with no hormone binding pocket. **(Sablin et al, 2008)** Both are implicated in GR signaling in an NR box-dependent manner **(Borgius et al, 2002; Zhou et al, 2008)**. DAX1 and SHP are thought to silence NR-mediated transcription by competing with co-activators for binding to AF-2, and each appears to contain multiple NR box peptides with affinity for GR. In the case of the nuclear receptor LRH-1, DAX-1's NR- boxes were not implicated in repression of transcription, and a different motif was identified. **(Sablin et al, 2008)** SHP-1 peptide showed non-saturable binding behavior, yet had a significant effect on ligand binding, suggesting moderate (>10 μM) affinity for GR. DAX1-3 bound well to GR with K_D = 1.3 μM. However, its relative advantage in K_D doesn't appear great enough to explain its exaggerated effect on dex-fl binding kinetics (Figures 1-3, 1-4 and Table 1-I). Together these observations imply either a unique binding mode or multiple binding sites for this peptide.

Half-times of association and dissociation of the GR:dex-fl complex which are NR box-dependent, in both GR contexts, were used to cluster the kinetic data for the 18 NR box peptides in our library (Figure 1-7). In agreement with the equilibrium data, two primary clusters consisting of 6 binders and 11 non-binders result, with two notable exceptions: DAX1-3, whose exaggerated effects make it an outlier, while SRC1-3, found to have a strong affinity for GR in our equilibrium assay, clusters with non-binders due to its weak effect on ligand binding kinetics (Table 1-I).

SRC1-3 is grouped in the unique low-plateau saturable binding mode (Figure 1-6b). This novel binding mode, characterized by strong affinity (1.3 μM) with a diminished maximum binding signal, can be attributed to SRC1-3's weak effects on ligand binding kinetics (Table 1-I). Increasing GR : dex-fl association and dissociation half-times only 1- and 2-fold, the tight binding SRC1-3 shows the weakest coupling to the ligand-binding pocket. This suggests a transient or passive docking to AF-2 that fails to stabilize this region of the receptor, in stark contrast to the other seven saturable binders, most notably DAX1-3. As previous studies using two-hybrid or peptide competition approaches have reported either moderate **(Wu et al, 2004)** or very weak **(Suino-Powell et al, 2008)** interactions between GR and SRC1-3, it is likely that these techniques were not sensitive to the binding mode of SRC1-3.

The co-repressor NR box SMRT-2 displayed a different binding mode (Figure 1-6f). SMRT-2, not thought to interact with agonist-bound GR, contains the putative co-repressor motif ΦXXΦΦXXXΦ, where Φ is a hydrophobic residue. Co-repressors bind to a structurally modified AF-2 region in which helix 12 is displaced from its active agonist-bound position. **(Madauss et al, 2007; Xu et al, 2002)** In contrast with the LXXLL containing NR box peptides,

titration of SMRT-2 caused a dose-dependent decrease in polarization of the GR : dex-fl complex. Although saturation was not reached in the assayed concentration range, SMRT-2 appears to act as a low-affinity, non-competitive inhibitor of ligand binding. Due to its weak affinity (IC_{50} > 25 μM), the biological relevance of this interaction is questionable. However, GR's ability to interact with SMRT-2 in an agonist-bound context indicates that the receptor has enough intrinsic flexibility to sample conformations capable of binding co-repressors. **(Madauss et al, 2007)**

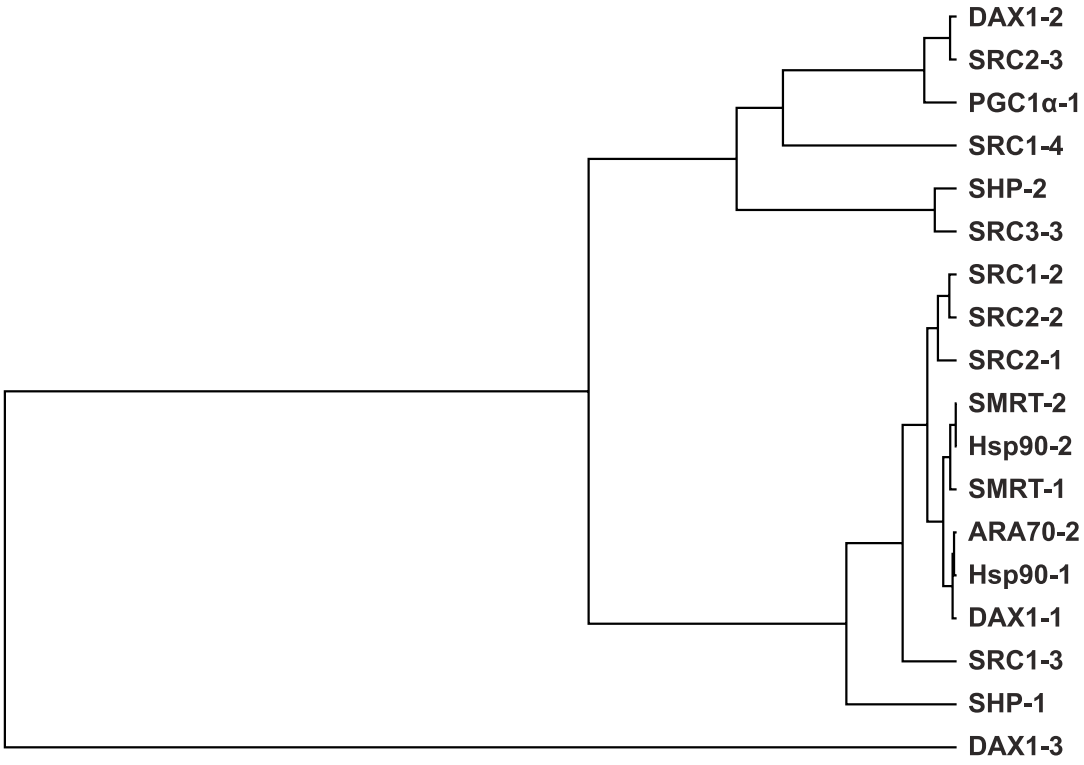

Figure 1-7. *Hierarchical clustering of NR box peptides.* NR box peptides were clustered using half-times shown in figures 1-3 and 1-4.

M752I increases NR box affinity

In addition to its alteration of GR's interactions with hormone and Hsp90, the M752I mutation was also shown to produce qualitatively tighter binding of co-activator SRC2 in a pull-down assay. **(Ricketson et al, 2007)** The peptides identified as binders to GR_{SD} were assayed for binding to GR_{M752I} using a similar experimental setup (Figure 1-S2, Table 1-II). A lower concentration of GR (250 nM as opposed to 500 nM) was used with GR_{M752I} as binding signal was empirically found to be optimal at this concentration. Two distinct behaviors were seen across the eight peptides tested for binding (Table 1-II). In agreement with the previous study, 7 of 8 NR box peptides showed at least a 2 fold increase in binding affinity as compared to GR_{SD}, while affinity for SRC1-3 remained unchanged. SRC2-3's interaction with GR_{M752I} strengthened most dramatically, with a 6.8-fold decrease in K_D from GR_{SD}, while the strongest interaction remained the DAX1-3 : GR interaction, with K_D = 280 nM.

Characterization of the GR : SRC1-3 interaction

SRC1-3 emerged as an NR box peptide with novel properties by displaying a relatively strong interaction with GR_{SD} (K_D = 1.4 μM) that didn't strengthen upon mutation of Met-752 to Ile, while showing weak coupling to ligand binding kinetics, seemingly incongruous with its high affinity (Figure 1-3, Table 1-I). To more fully probe the GR : SRC1-3 interaction, an Alexa-Fluor 555-conjugated SRC1-3 peptide was created for direct-binding, fluorescence polarization studies. Kinetics of peptide binding were impossible to measure with our assay setup, as the reaction between GR and NR box peptides reaches equilibrium within 30 s (Data not shown). This finding is in line with surface plasmon resonance-derived kinetics of androgen receptor

binding NR box peptides **(K. Kuchenbecker, personal communication)**. Steady state equilibrium binding assays were carried out with both GR constructs and SRC1-3-fluor in the presence of 10 μM dex (Figure 1-9). As can be appreciated from the isotherms and accompanying error bars, the interaction between GR and SRC1-3-fluor appears much less stable than the interaction between GR and SRC3-3-fluor (Figure 1-5). The high variance observed between duplicate wells is indicative of rapidly shifting molecular populations, which may be the defining feature of the GR : SRC1-3 interaction. SRC1-3 appears to be passively docking at the AF-2 surface without coupling to the ligand binding pocket, whereas other interacting NR box peptides dock and effectively register the receptor for ligand binding.

	GR_{SD}	GR_{M752I}	
NR Box	**K_D ± SEM (μM)**	**K_D ± SEM (μM)**	**Fold Decrease**
SRC1-3	1.4 ± 0.21	1.3 ± 0.16	1.1
SRC1-4	2.1 ± 0.24	0.44 ± 0.014	4.8
SRC2-3	2.6 ± 0.64	0.38 ± 0.11	6.8
SRC3-3	3.5 ± 0.69	0.63 ± 0.11	5.6
PGC1α-1	2.3 ± 0.54	0.65 ± 0.11	3.5
DAX1-2	1.9 ± 0.36	1.0 ± 0.14	1.9
DAX1-3	1.3 ± 0.14	0.28 ± 0.035	4.6
SHP-2	5.8 ± 1.1	1.1 ± 0.29	5.3

Table 1-II. *NR box peptide dissociation constants*

	-4	-3	-2	-1	+1	+2	+3	+4	+5	+6	+7
DAX1-3	Q	G	S	I	L	Y	S	L	L	T	S
SRC1-4	Q	K	S	L	L	Q	Q	L	L	T	E
SRC2-3	E	N	A	L	L	R	Y	L	L	D	K
DAX1-2	Q	G	S	I	L	Y	S	M	L	T	S
PGC1α-1	E	P	S	L	L	K	K	L	L	L	A
SRC3-3	N	N	A	L	L	R	Y	L	L	D	R
SHP-2	V	P	S	I	L	K	K	I	L	L	E
SRC1-3	D	H	Q	L	L	R	Y	L	L	D	K

Figure 1-8. *Core sequences of GR binders.* GR-binding NR box core sequences with conserved residues highlighted. LXXLL Leu residues in black, GR-specific conserved positions in gray.

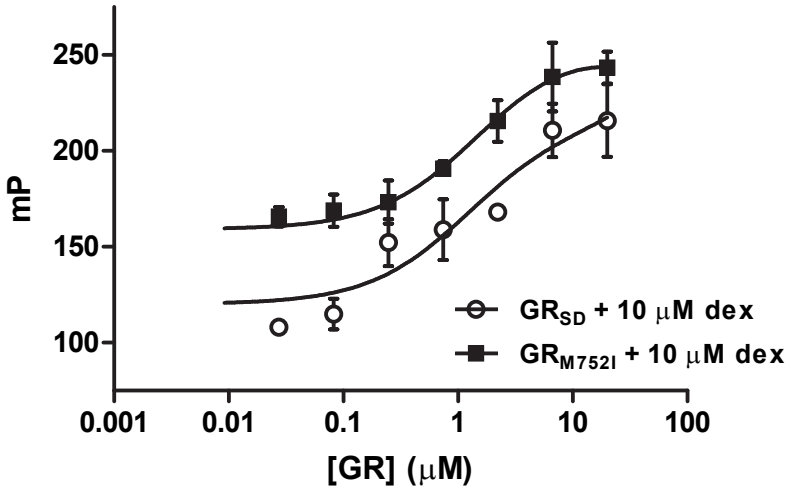

Figure 1-9. *GR binding to SRC1-3-fluor.* GR_{SD} (open cirlces) and GR_{M752I} (closed squares) were titrated against 20 nM SRC1-3 conjugated to Alexa-Fluor 555 in the presence of 10 μM dex. Data fit to one site saturation binding model.

DISCUSSION

GR ligand binding pocket and AF-2 are allosterically coupled

Allosteric mechanisms abound in the realm of signaling proteins. **(del Sol et al, 2006)** NRs represent signaling nodes that mediate vast transcription networks though a diverse array of protein-protein, protein-DNA, and protein-small molecule interactions. In the case of the NR LBD, conformational changes induced by the binding of small molecule ligand to the protein's interior are echoed throughout the domain to distant, functional sites. **(Shulman et al, 2004)** An integral step in signal transduction through NRs is the formation of the AF-2 surface. AF-2 formation and subsequent recruitment of co-regulators is necessary for full potentiation of a hormone signal. The energetic coupling of these two functional sites has primarily been explored biochemically by manipulating the bound ligand and observing perturbations in the subsequent recruitment pattern of co-regulators to AF-2. **(Moore et al, 2004; Moore & Guy, 2005; Teichert et al, 2009)** In this study, we examined the coupling between two of the GR LBD's functional sites by fluorescence polarization from the opposite perspective, using a fluorescein-labeled GR agonist (dex-fl : Figure 1-1) and a library of unlabeled co-regulator NR box peptides. The pattern of co-regulator recruitment to AF-2 was determined using kinetic and equilibrium polarization measurements of dex-fl binding in the ligand binding pocket (Figures 1-3, 1-4, 1-7, 1-S1). Of the 18 NR box peptides we examined, 7 showed significant ability to decrease the rates of GR : dex-fl association and dissociation, effectively limiting access to the ligand binding pocket through a kinetic mechanism (Table 1-I). GR_{SD} : dex-fl association and dissociation were slowed as much as 6- and 27-fold, respectively, in the presence of 10 μM peptide. DAX1-3 showed by far the greatest effect on hormone binding kinetics, slowing dex-fl

dissociation 2-fold more than any other peptide in our library (Table 1-I). As DAX1 has been shown to preferentially repress GR-mediated gene activation and not repression **(Zhou et al, 2008)**, a desirable pharmaceutical profile referred to as dissociated, the binding of its third NR box may represent a new direction for discovery of GR antagonists.

Pattern of co-regulator recruitment to GR AF-2

In order to more quantitatively assess NR box recruitment to GR, we employed an equilibrium peptide binding assay, again using unlabeled NR box peptides and dex-fl polarization as the readout (Figures 1-6, 1-S1, 1-S2 and Table 1-II). Binding of NR box at AF-2 induced a dose-dependent increase in dex-fl polarization, resulting from the peptide's ability to slow both ligand association and dissociation. Six distinct binding modes were observed among the 18 NR box peptides in our library, with 8 of the peptides showing saturation binding behavior (Figures 1-6, 1-S1 and Table 1-II). The core sequences of these 8 NR box peptides, for which K_{DS} could be determined, are shown in figure 1-8. Aside from the conserved leucine residues of the LXXLL motif, these peptides show significant conservation at three additional sites, suggesting a more complete consensus sequence for high-affinity binding to GR's AF-2. The conserved hydrophobic residue at the -1 position, directly preceding LXXLL, has been appreciated as a key component of NR box binding to several NRs **(Chang et al, 1999)**, and indeed all 8 binders contain Leu or Ile here. The data presented here reveal that 7 of 8 binders have Ala or Ser at the -2 position, indicating a preference for residues with small side chains at this position. As structural alignments of GR : NR box complexes do not indicate a role for this residue in direct AF-2 recognition, it may contribute to binding by allowing the NR box to attain

a conformation appropriate for docking. Interestingly, the non-canonical binder SRC1-3 has a Gln here, which may contribute to the novel binding mode employed by this NR box. The -4 position is also well-conserved, with a branched, polar residue (Glu, Gln, Asp, Asn) appearing in 7 of 8 binders. These four amino acid side chains would be expected to be solvent exposed as they are among the most polar of side chains. In the GR : dex : SRC2-3 crystal structure, this residue favorably packs against Asn-759, Asp in the most closely related MR, Ala and Val respectively in PR and AR, indicating a role for the -4 position in specific co-regulator recognition of the corticosteroid sub-class of SRs.

M752I alters both ligand and peptide interactions with GR

The mechanism of co-regulator recruitment was also determined for GR with the mutation M752I (Figures 1-4, 1-S2 and Tables 1-I, 1-II). This mutation was shown to increase GR's affinity for co-regulators binding at AF-2, while decreasing the receptor's dependence on Hsp90. **(Ricketson et al, 2007)** The results of our equilibrium binding assay verify this finding, with 7 of 8 GR_{SD}-binding peptides showing increased affinity for GR_{M752I} (Table 1-II). SRC1-3 was the lone NR box peptide whose affinity failed to increase, solidifying its status as an atypical binder. Co-regulator modulation of dex-fl binding kinetics was also observed for GR_{M752I} (Figure 1-4, Table 1-I). Interestingly, the two versions of GR behaved differently. Our analysis of peptide regulation of GR_{M752I} : dex-fl complex formation showed interacting NR box peptides to have a similar effect on both on and off rates for the ligand, while for GR_{SD} : dex-fl we found that NR box peptides preferentially influenced off rates (Figures 1-3 and 1-4, Table 1-I). These results suggest two mechanisms, one direct, the other indirect, underlying the binding to M752I.

In the direct mechanism (1) the strategically positioned Ile increases peptide affinity for the unliganded receptor, with a kinetic effect solely dependent on peptide residence time at AF-2. In the indirect mechanism (2) the Ile alters the coupling between AF-2 and the ligand binding pocket by introducing a more rigid side chain into the allosteric network. We demonstrated by direct measurement of peptide binding that a representative NR box, SRC3-3, has nearly identical affinities for dex bound- and apo-GR for both GR_{SD} and GR_{M752I}, suggesting mechanism (2) (Figure 1-5).

This leads to a view of Met-752 as a two-way molecular sensor whose flexible side chain allows hormone association at a reduced-rate to GR with an NR box, or presumably a co-regulator, bound at AF-2. Mutation to Ile strengthens GR's interactions with NR box peptides while dramatically slowing hormone association with peptide bound, indicating that the ligand binding pocket can no longer signal that it is empty. It is likely that disruption of this vital intra-protein communication mechanism in this manner would greatly compromise signaling through GR by effectively eliminating hormone binding as a prerequisite for receptor function.

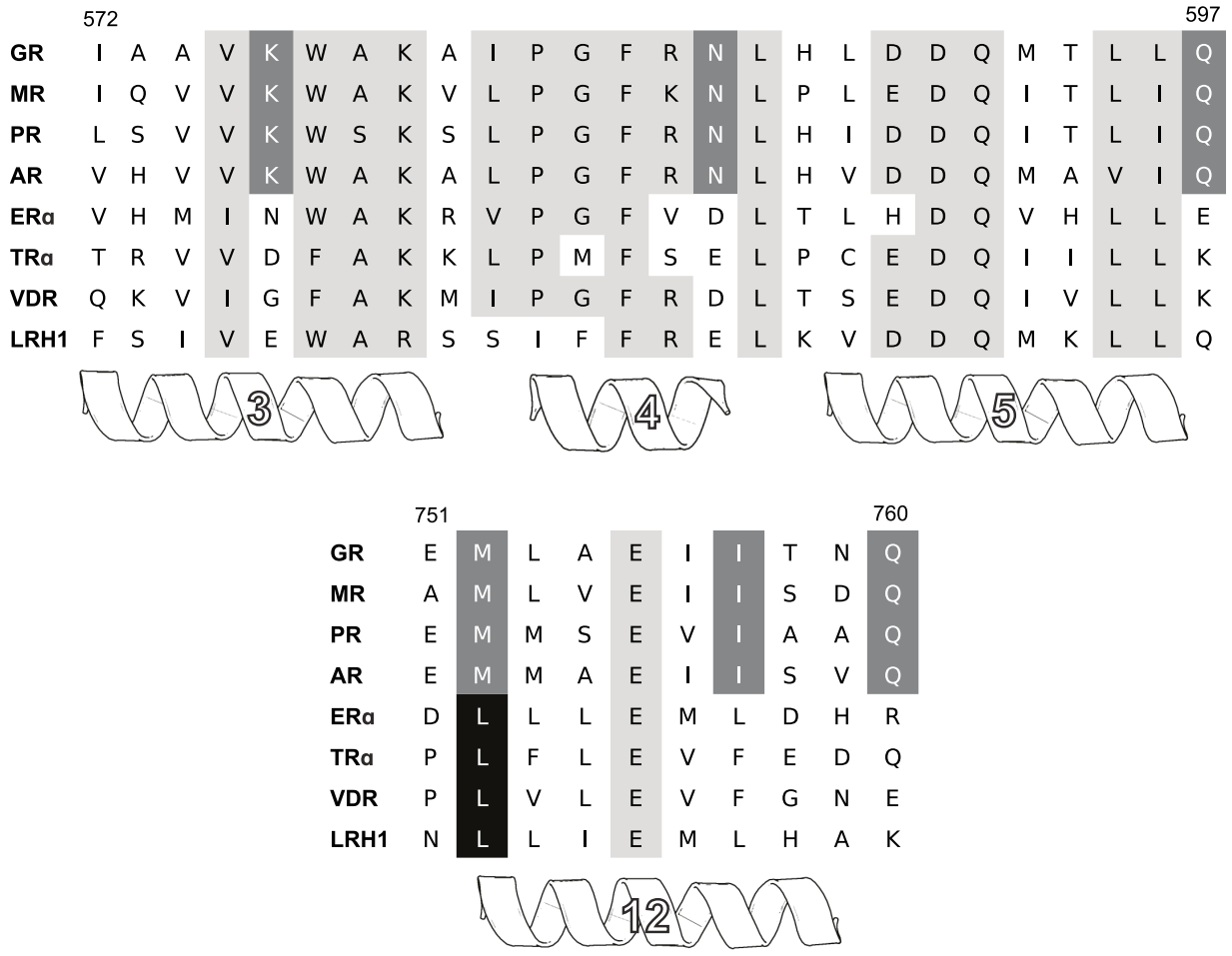

Figure 1-10. *Sequence alignment of NR AF-2 regions.* NR LBD crystal structures were aligned by structure. Residues conserved across the NR superfamily are in light gray. Residues conserved among SRs are in dark gray. Residues conserved among non-SRs are in black. The PDB codes of structures used for the alignment are GR (3BQD), MR (2ABI), PR (3D90), AR (1T7R), ER (2OCF), VDR (2ZL9), TR (3HZF), LRH-1 (1YOK)

The AF-2 surface and its surrounding residues are well conserved throughout the nuclear receptor superfamily. Sequence alignment of the SR family with representative NRs from the other classes reveals several AF-2 residues that are conserved across the superfamily, and 6, including Met-752 that are conserved among SRs with the exception of ER (Figure 1-10). At these 6 positions, the only residue that is conserved in the non-SRs as well is Leu at the position corresponding to Met-752 in GR. Receptors containing Leu here, including ER, VDR, TR, and RAR, are regulated in a dramatically different fashion from the canonical SRs. Typically, they do not depend on Hsp90 and are localized to the nucleus in the absence of hormone; two behaviors induced by the M752I mutation in GR. **(Ricketson et al, 2007)** ER is the only of the receptors bearing a Leu here to show dependence on Hsp90. However, the Hsp90 : ER interaction is less-dependent on the ER LBD than other SRs, and ER can readily translocate to the nucleus in the absence of hormone. **(Picard et al, 1990b; Schlatter et al, 1992)** Our results indicate the 752 position as a key regulator of the allosteric network connecting hormone and co-regulator binding sites in GR LBD. Conservation of this residue among Hsp90-dependent receptors and the functional consequences of mutations that rigidify the position suggest evolutionary pressure towards flexibility at this site in SRs. The mechanisms by which this flexibility is recognized and exploited by Hsp90 and other regulatory elements remain unclear.

GR is a finely-tuned molecular switch, capable of carrying out a myriad of critical functions at the organismal level. As a ligand-regulated scaffolding molecule, GR must translate extrinsic hormone signals into meaningful conformational change to promote interactions with chaperones, DNA, and a variety of co-regulator proteins. These interactions, across all of GR's domains, determine the outcome of a GC signal. This study and others have aimed to provide a

quantitative framework for the description of these interactions, and the allosteric mechanisms by which they are enabled. **(Meijsing et al, 2009)** Recent advances in the purification and structural characterization of multi-domain NR constructs should enable this work to be extended into molecules of absolute biological relevance and increasing complexity. **(Chandra et al, 2008; Simmons et al, 2008)**

METHODS

Protein expression and purification

Human GR LBD (520-777, F602S, C638D, ±M752I) was expressed as a 6xHis fusion protein from a modified pACYCDuet vector in E. coli strain BL21Star. The encoded GR sequence was optimized for expression in E. coli (GeneArt, Burlingame, CA, USA). Cells were grown at 30^0 C in 2x LB to OD_{600} = 0.8, at which time the temperature was reduced to 15^0 C and protein expression was induced by addition of 0.2 mM IPTG and 0.2 mM dexamethasone (3B Pharmachem, China). After 16-20 hours of expression, cells were pelleted by centrifugation, lysed by sonication in a buffer containing 50 mM Tris-HCl pH 8.0, 150 mM NaCl, 10% glycerol, 2 M urea, 0.2 mM TCEP, 10 mM imidazole, 0.04% CHAPS, 10 μM dexamethasone, and clarified by centrifugation at 30,000xg for 30 minutes. The lysate supernatant was bound in batch to Ni-NTA resin (Qiagen) and eluted with a buffer containing 20 mM Tris-HCl pH 8.0, 150mM Nacl, 10% glycerol, 0.2 mM TCEP, 0.04% CHAPS, 10 μM dexamethasone, 150 mM imidazole. GR containing fractions were pooled and diluted into a buffer containing 20 mM Tris-HCl pH 8.0, 10% glycerol, 0.2mM TCEP, 0.4% CHAPS, 10 μM dexamethasone (AX Buffer A), and then applied to a HiTrap Q HP (GE Healthcare) column on an Akta explorer FPLC (GE

Healthcare). Protein was eluted using a 0-30% gradient of AX Buffer B (Buffer A + 1 M NaCl). Thrombin cleavage of the 6xHIS tag was carried out during dialysis into storage buffer containing 20 mM HEPES pH 7.4, 150 mM NaCl, 10% glycerol, 0.2 mM TCEP, 0.04% CHAPS, 10 μM dexamethasone. The resultant GR LBD was purified to 100% homogeneity using a Superdex 200 column (GE Healthcare).

Ligand Removal

Ligand-free GR for fluorescence studies was prepared in two manners. For GR_{SD} (F602S, C638D), ligand removal was accomplished by passage over a NAP-25 desalting column (GE Healthcare). For GR_{M752I} (F602S, C638D, M752I), dialysis into storage buffer without dexamethasone followed by passage over a NAP-25 column was necessary.

NR Box Peptide Library

NR box peptides were obtained from Elim Biopharmaceuticals (Hayward, CA, USA) with the exception of SRC1-3 and SRC3-3, which were a generous gift of Dr. R. K. Guy. SRC1-3 and SRC3-3 each contain a non-native N-terminal cysteine residue to allow for easy coupling of fluorescent probes. All other NR box sequences are WT. Peptide sequences are as follows:

SRC1-2 CPSSHSSLTERHKILHRLLQEGSPS

SRC1-3 CESKDHQLLRYLLDKDEKDL

SRC1-4 AQQKSLLQQLLTE

SRC2-1 SKGQTKLLQLLTCSS

SRC2-2 KHKILHRLLQDSS

SRC2-3	KENALLRYLLDKDD
SRC3-3	CKKENNALLRYLLDRDDPSD
PGC1α-1	EPSLLKKLLLAPAN
ARA70-2	TSEKFKLLFQ
Hsp90-1	NLCKIMKDILEK
Hsp90-2	GWTANMERIMKAQ
DAX1-1	QWQGSILYNMLMSAK
DAX1-2	PRQGSILYSMLTSAK
DAX1-3	PRQGSILYSLLTSSK
SHP-1	ASHPTILYTLLSPGP
SHP-2	APVPSILKKILLEEPNS
SMRT-1	RVVTLAQHISEVITQDYTR
SMRT-2	TNMGLEAIIRKALMGKYD

Fluorescence polarization kinetics

All fluorescence polarization experiments were carried out in black, non-binding surface, 384-well plates (Corning), in a buffer containing 20 mM HEPES pH 7.4, 150 mM NaCl, 0.2 mM TCEP, 0.04% CHAPS at room temperature. Kinetic measurements were performed on a SpectraMax M5 plate reader (Molecular Devices). For association measurements, GR was incubated with the specified peptide for 15 min at room temperature, followed by addition of dexamethasone-fluorescein (Invitrogen) at t = 0. Final concentrations of components were, 1 μM GR, 10 μM peptide, and 20 nM dexamethasone-fluorescein. Timed measurements were

taken typically every 30 s or 1 min until after the reaction had reached equilibrium. Dissociation was initiated by addition of 50 μM unlabeled dexamethasone and measurements were taken until equilibrium was reached. Data was fit using non-linear regression to one-phase association or one-phase decay models in Prism 5 (GraphPad Software). All values reported represent the mean ± S.E.M. of at least 3 independent experiments.

Fluorescence polarization affinity

All fluorescence polarization experiments were carried out in black, non-binding surface, 384-well plates (Corning), in a buffer containing 20 mM HEPES pH 7.4, 150 mM NaCl, 0.2 mM TCEP, 0.04% CHAPS at room temperature. 1 μM GR_{SD} or 500 nM GR_{M752I} was incubated with 40 nM dex-fl until equilibrium was reached. GR:dex-fl was diluted 1:1 into samples of peptide from 200 μM to 30 nM prepared by serial dilution. Final concentrations of components were 500 nM GR_{SD}, 20 nM dex-fl, 100 μM - 15 nM peptide or 250 nM GR_{M752I}, 20 nM dex-fl, 50 μM - 7.5 nM peptide. Steady-state affinity measurements were performed on an Analyst AD, Analyst HT, or SpectraMax M5 plate reader (Molecular Devices). Data was fit by non-linear regression to a one site saturation binding model in Prism 5 (GraphPad Software). All values reported represent the mean ± S.E.M. of at least 3 independent experiments.

Fluorescent NR box probes

SRC1-3 and SRC3-3 peptides were synthesized with a non-native cysteine at the N-terminus to allow easy coupling to fluorescent probes. (Moore et al, 2004) Maleimide-Alexa Fluor-555 (Invitrogen) was coupled to each peptide in 20 mM HEPES 7.1, 0.4 mM TCEP at

room temperature for 3 h. The reaction was quenched with β-mercaptoethanol, and the peptides were separated from free probe using a Superdex Peptide column on an Akta Explorer FPLC (GE Healthcare). Peptide concentration was determined using λ = 280 nM absorbance, with the appropriate correction factor applied to account for Alexa-Fluor 555's contribution to the signal. Binding measurements were made in either FP buffer (20 mM HEPES pH 7.4, 150 mM NaCl, 0.04% CHAPS, 0.2 mM TCEP) or FP plus 10 μM dex at room temperature on a SpectraMax M5 plate reader (Molecular Devices). NR box-fluor, present at 20 nM in all wells, was titrated with GR from 10 μM to 4.5 nM. Isotherms were analyzed and fit by non-linear regression to a single-site saturation binding model in Prism 5 (GraphPad Software). All values reported represent the mean ± S.E.M. of at least 3 independent experiments.

ACKNOWLEDGEMENTS

The authors would like to thank C. Cunningham, J. Dilla, C. Farady, E. Kirschke, and K. Kuchenbecker for helpful scientific discussions. Experiments were conceived by S.J.P. and R.J.F. and performed by S.J.P.

REFERENCES

Baumann H, Paulsen K, Kovacs H, Berglund H, Wright AP, Gustafsson JA, Hard T (1993) Refined solution structure of the glucocorticoid receptor DNA-binding domain. *Biochemistry* **32**(49)**:** 13463-13471

Belandia B, Parker MG (2003) Nuclear receptors: a rendezvous for chromatin remodeling factors. *Cell* **114**(3)**:** 277-280

Biddie SC, Hager GL (2009) Glucocorticoid receptor dynamics and gene regulation. *Stress* **12**(3)**:** 193-205

Biggadike K, Bledsoe RK, Hassell AM, Kirk BE, McLay IM, Shewchuk LM, Stewart EL (2008) X-ray crystal structure of the novel enhanced-affinity glucocorticoid agonist fluticasone furoate in the glucocorticoid receptor-ligand binding domain. *J Med Chem* **51**(12)**:** 3349-3352

Bledsoe RK, Montana VG, Stanley TB, Delves CJ, Apolito CJ, McKee DD, Consler TG, Parks DJ, Stewart EL, Willson TM, Lambert MH, Moore JT, Pearce KH, Xu HE (2002) Crystal structure of the glucocorticoid receptor ligand binding domain reveals a novel mode of receptor dimerization and coactivator recognition. *Cell* **110**(1)**:** 93-105

Borgius LJ, Steffensen KR, Gustafsson JA, Treuter E (2002) Glucocorticoid signaling is perturbed by the atypical orphan receptor and corepressor SHP. *J Biol Chem* **277**(51)**:** 49761-49766

Bourguet W, Ruff M, Chambon P, Gronemeyer H, Moras D (1995) Crystal structure of the ligand-binding domain of the human nuclear receptor RXR-alpha. *Nature* **375**(6530)**:** 377-382

Bramlett KS, Wu Y, Burris TP (2001) Ligands specify coactivator nuclear receptor (NR) box affinity for estrogen receptor subtypes. *Mol Endocrinol* **15**(6)**:** 909-922

Bresnick EH, Dalman FC, Sanchez ER, Pratt WB (1989) Evidence that the 90-kDa heat shock protein is necessary for the steroid binding conformation of the L cell glucocorticoid receptor. *J Biol Chem* **264**(9)**:** 4992-4997

Bridgham JT, Carroll SM, Thornton JW (2006) Evolution of hormone-receptor complexity by molecular exploitation. *Science* **312**(5770)**:** 97-101

Bridgham JT, Ortlund EA, Thornton JW (2009) An epistatic ratchet constrains the direction of glucocorticoid receptor evolution. *Nature* **461**(7263)**:** 515-519

Chandra V, Huang P, Hamuro Y, Raghuram S, Wang Y, Burris TP, Rastinejad F (2008) Structure of the intact PPAR-gamma-RXR-alpha nuclear receptor complex on DNA. *Nature***:** 350-356

Chang C, Norris JD, Gron H, Paige LA, Hamilton PT, Kenan DJ, Fowlkes D, McDonnell DP (1999) Dissection of the LXXLL nuclear receptor-coactivator interaction motif using combinatorial peptide libraries: discovery of peptide antagonists of estrogen receptors alpha and beta. *Mol Cell Biol* **19**(12)**:** 8226-8239

Chen JD, Umesono K, Evans RM (1996) SMRT isoforms mediate repression and anti-repression of nuclear receptor heterodimers. *Proc Natl Acad Sci U S A* **93**(15)**:** 7567-7571

Chrousos GP, Charmandari E, Kino T (2004) Glucocorticoid action networks--an introduction to systems biology. *J Clin Endocrinol Metab* **89**(2)**:** 563-564

Chrousos GP, Kino T (2007) Glucocorticoid action networks and complex psychiatric and/or somatic disorders. *Stress* **10**(2)**:** 213-219

Dalman FC, Koenig RJ, Perdew GH, Massa E, Pratt WB (1990) In contrast to the glucocorticoid receptor, the thyroid hormone receptor is translated in the DNA binding state and is not associated with hsp90. *J Biol Chem* **265**(7)**:** 3615-3618

Dalman FC, Sturzenbecker LJ, Levin AA, Lucas DA, Perdew GH, Petkovitch M, Chambon P, Grippo JF, Pratt WB (1991) Retinoic acid receptor belongs to a subclass of nuclear receptors that do not form "docking" complexes with hsp90. *Biochemistry* **30**(22)**:** 5605-5608

Darimont BD, Wagner RL, Apriletti JW, Stallcup MR, Kushner PJ, Baxter JD, Fletterick RJ, Yamamoto KR (1998) Structure and specificity of nuclear receptor-coactivator interactions. *Genes Dev* **12**(21)**:** 3343-3356

del Sol A, Fujihashi H, Amoros D, Nussinov R (2006) Residues crucial for maintaining short paths in network communication mediate signaling in proteins. *Mol Syst Biol* **2:** 2006 0019

Echeverria PC, Mazaira G, Erlejman A, Gomez-Sanchez C, Pilipuk GP, Galigniana MD (2009) Nuclear import of the glucocorticoid receptor-hsp90 complex through the nuclear pore complex is mediated by its interaction with Nup62 and importin beta. *Mol Cell Biol* **29**(17)**:** 4788-4797

Estebanez-Perpina E, Moore JM, Mar E, Delgado-Rodrigues E, Nguyen P, Baxter JD, Buehrer BM, Webb P, Fletterick RJ, Guy RK (2005) The molecular mechanisms of coactivator utilization in ligand-dependent transactivation by the androgen receptor. *J Biol Chem* **280**(9)**:** 8060-8068

Feng W, Ribeiro RC, Wagner RL, Nguyen H, Apriletti JW, Fletterick RJ, Baxter JD, Kushner PJ, West BL (1998) Hormone-dependent coactivator binding to a hydrophobic cleft on nuclear receptors. *Science* **280**(5370)**:** 1747-1749

Frego L, Davidson W (2006) Conformational changes of the glucocorticoid receptor ligand binding domain induced by ligand and cofactor binding, and the location of cofactor binding sites determined by hydrogen/deuterium exchange mass spectrometry. *Protein Sci* **15**(4)**:** 722-730

Fryer CJ, Archer TK (1998) Chromatin remodelling by the glucocorticoid receptor requires the BRG1 complex. *Nature* **393**(6680)**:** 88-91

Galon J, Franchimont D, Hiroi N, Frey G, Boettner A, Ehrhart-Bornstein M, O'Shea JJ, Chrousos GP, Bornstein SR (2002) Gene profiling reveals unknown enhancing and suppressive actions of glucocorticoids on immune cells. *FASEB J* **16**(1)**:** 61-71

Gee AC, Carlson KE, Martini PG, Katzenellenbogen BS, Katzenellenbogen JA (1999) Coactivator peptides have a differential stabilizing effect on the binding of estrogens and antiestrogens with the estrogen receptor. *Mol Endocrinol* **13**(11)**:** 1912-1923

Gronemeyer H, Gustafsson JA, Laudet V (2004) Principles for modulation of the nuclear receptor superfamily. *Nat Rev Drug Discov* **3**(11)**:** 950-964

Hard T, Kellenbach E, Boelens R, Maler BA, Dahlman K, Freedman LP, Carlstedt-Duke J, Yamamoto KR, Gustafsson JA, Kaptein R (1990) Solution structure of the glucocorticoid receptor DNA-binding domain. *Science* **249**(4965)**:** 157-160

He B, Kemppainen JA, Voegel JJ, Gronemeyer H, Wilson EM (1999) Activation function 2 in the human androgen receptor ligand binding domain mediates interdomain communication with the NH(2)-terminal domain. *J Biol Chem* **274**(52)**:** 37219-37225

Heery DM, Kalkhoven E, Hoare S, Parker MG (1997) A signature motif in transcriptional co-activators mediates binding to nuclear receptors. *Nature* **387**(6634)**:** 733-736

Hong H, Kohli K, Garabedian MJ, Stallcup MR (1997) GRIP1, a transcriptional coactivator for the AF-2 transactivation domain of steroid, thyroid, retinoid, and vitamin D receptors. *Mol Cell Biol* **17**(5)**:** 2735-2744

Hong H, Kohli K, Trivedi A, Johnson DL, Stallcup MR (1996) GRIP1, a novel mouse protein that serves as a transcriptional coactivator in yeast for the hormone binding domains of steroid receptors. *Proc Natl Acad Sci U S A* **93**(10)**:** 4948-4952

Htun H, Barsony J, Renyi I, Gould DL, Hager GL (1996) Visualization of glucocorticoid receptor translocation and intranuclear organization in living cells with a green fluorescent protein chimera. *Proc Natl Acad Sci U S A* **93**(10)**:** 4845-4850

Hur E, Pfaff SJ, Payne ES, Gron H, Buehrer BM, Fletterick RJ (2004) Recognition and accommodation at the androgen receptor coactivator binding interface. *PLoS Biol* **2**(9)**:** E274

Hutchison KA, Dittmar KD, Pratt WB (1994) All of the factors required for assembly of the glucocorticoid receptor into a functional heterocomplex with heat shock protein 90 are preassociated in a self-sufficient protein folding structure, a "foldosome". *J Biol Chem* **269**(45)**:** 27894-27899

Iniguez-Lluhi JA, Lou DY, Yamamoto KR (1997) Three amino acid substitutions selectively disrupt the activation but not the repression function of the glucocorticoid receptor N terminus. *J Biol Chem* **272**(7)**:** 4149-4156

John S, Johnson TA, Sung MH, Biddie SC, Trump S, Koch-Paiz CA, Davis SR, Walker R, Meltzer PS, Hager GL (2009) Kinetic complexity of the global response to glucocorticoid receptor action. *Endocrinology* **150**(4)**:** 1766-1774

Kallenberger BC, Love JD, Chatterjee VK, Schwabe JW (2003) A dynamic mechanism of nuclear receptor activation and its perturbation in a human disease. *Nat Struct Biol* **10**(2)**:** 136-140

Katzenellenbogen BS (1980) Dynamics of steroid hormone receptor action. *Annu Rev Physiol* **42:** 17-35

Kauppi B, Jakob C, Farnegardh M, Yang J, Ahola H, Alarcon M, Calles K, Engstrom O, Harlan J, Muchmore S, Ramqvist AK, Thorell S, Ohman L, Greer J, Gustafsson JA, Carlstedt-Duke J, Carlquist M (2003) The three-dimensional structures of antagonistic and agonistic forms of the glucocorticoid receptor ligand-binding domain: RU-486 induces a transconformation that leads to active antagonism. *J Biol Chem* **278**(25)**:** 22748-22754

Kroe RR, Baker MA, Brown MP, Farrow NA, Gautschi E, Hopkins JL, LaFrance RR, Kronkaitis A, Freeman D, Thomson D, Nabozny G, Grygon CA, Labadia ME (2007) Agonist versus antagonist induce distinct thermodynamic modes of co-factor binding to the glucocorticoid receptor. *Biophys Chem* **128**(2-3)**:** 156-164

Kumar R, Thompson EB (2005) Gene regulation by the glucocorticoid receptor: structure:function relationship. *J Steroid Biochem Mol Biol* **94**(5)**:** 383-394

Lin S, Bock CL, Gardner DB, Webster JC, Favata MF, Trzaskos JM, Oldenburg KR (2002) A high-throughput fluorescent polarization assay for nuclear receptor binding utilizing crude receptor extract. *Anal Biochem* **300**(1)**:** 15-21

Luisi BF, Xu WX, Otwinowski Z, Freedman LP, Yamamoto KR, Sigler PB (1991) Crystallographic analysis of the interaction of the glucocorticoid receptor with DNA. *Nature* **352**(6335)**:** 497-505

Madauss KP, Bledsoe RK, McLay I, Stewart EL, Uings IJ, Weingarten G, Williams SP (2008) The first X-ray crystal structure of the glucocorticoid receptor bound to a non-steroidal agonist. *Bioorg Med Chem Lett* **18**(23)**:** 6097-6099

Madauss KP, Grygielko ET, Deng SJ, Sulpizio AC, Stanley TB, Wu C, Short SA, Thompson SK, Stewart EL, Laping NJ, Williams SP, Bray JD (2007) A structural and in vitro characterization of asoprisnil: a selective progesterone receptor modulator. *Mol Endocrinol* **21**(5)**:** 1066-1081

Mangelsdorf DJ, Evans RM (1995) The RXR heterodimers and orphan receptors. *Cell* **83**(6)**:** 841-850

McKenna NJ, Lanz RB, O'Malley BW (1999) Nuclear receptor coregulators: cellular and molecular biology. *Endocr Rev* **20**(3)**:** 321-344

McKenna NJ, O'Malley BW (2002) Combinatorial control of gene expression by nuclear receptors and coregulators. *Cell* **108**(4)**:** 465-474

McNally JG, Muller WG, Walker D, Wolford R, Hager GL (2000) The glucocorticoid receptor: rapid exchange with regulatory sites in living cells. *Science* **287**(5456)**:** 1262-1265

Meijsing SH, Pufall MA, So AY, Bates DL, Chen L, Yamamoto KR (2009) DNA binding site sequence directs glucocorticoid receptor structure and activity. *Science* **324**(5925)**:** 407-410

Moore JM, Galicia SJ, McReynolds AC, Nguyen NH, Scanlan TS, Guy RK (2004) Quantitative proteomics of the thyroid hormone receptor-coregulator interactions. *J Biol Chem* **279**(26)**:** 27584-27590

Moore JM, Guy RK (2005) Coregulator interactions with the thyroid hormone receptor. *Mol Cell Proteomics* **4**(4)**:** 475-482

Nahoum V, Perez E, Germain P, Rodriguez-Barrios F, Manzo F, Kammerer S, Lemaire G, Hirsch O, Royer CA, Gronemeyer H, de Lera AR, Bourguet W (2007) Modulators of the

structural dynamics of the retinoid X receptor to reveal receptor function. *Proc Natl Acad Sci U S A* **104**(44)**:** 17323-17328

Onate SA, Boonyaratanakornkit V, Spencer TE, Tsai SY, Tsai MJ, Edwards DP, O'Malley BW (1998) The steroid receptor coactivator-1 contains multiple receptor interacting and activation domains that cooperatively enhance the activation function 1 (AF1) and AF2 domains of steroid receptors. *J Biol Chem* **273**(20)**:** 12101-12108

Ortlund EA, Bridgham JT, Redinbo MR, Thornton JW (2007) Crystal structure of an ancient protein: evolution by conformational epistasis. *Science* **317**(5844)**:** 1544-1548

Perez Santin E, Germain P, Quillard F, Khanwalkar H, Rodriguez-Barrios F, Gronemeyer H, de Lera AR, Bourguet W (2009) Modulating retinoid X receptor with a series of (E)-3-[4-hydroxy-3-(3-alkoxy-5,5,8,8-tetramethyl-5,6,7,8-tetrahydronaphtha len-2-yl)phenyl]acrylic acids and their 4-alkoxy isomers. *J Med Chem* **52**(10)**:** 3150-3158

Picard D, Khursheed B, Garabedian MJ, Fortin MG, Lindquist S, Yamamoto KR (1990a) Reduced levels of hsp90 compromise steroid receptor action in vivo. *Nature* **348**(6297)**:** 166-168

Picard D, Kumar V, Chambon P, Yamamoto KR (1990b) Signal transduction by steroid hormones: nuclear localization is differentially regulated in estrogen and glucocorticoid receptors. *Cell Regul* **1**(3)**:** 291-299

Picard D, Yamamoto KR (1987) Two signals mediate hormone-dependent nuclear localization of the glucocorticoid receptor. *EMBO J* **6**(11)**:** 3333-3340

Pratt WB, Dittmar KD (1998) Studies with Purified Chaperones Advance the Understanding of the Mechanism of Glucocorticoid Receptor-hsp90 Heterocomplex Assembly. *Trends Endocrinol Metab* **9**(6)**:** 244-252

Pratt WB, Galigniana MD, Morishima Y, Murphy PJ (2004) Role of molecular chaperones in steroid receptor action. *Essays Biochem* **40:** 41-58

Renaud JP, Rochel N, Ruff M, Vivat V, Chambon P, Gronemeyer H, Moras D (1995) Crystal structure of the RAR-gamma ligand-binding domain bound to all-trans retinoic acid. *Nature* **378**(6558)**:** 681-689

Rhen T, Cidlowski JA (2005) Antiinflammatory action of glucocorticoids--new mechanisms for old drugs. *N Engl J Med* **353**(16)**:** 1711-1723

Ricketson D, Hostick U, Fang L, Yamamoto KR, Darimont BD (2007) A conformational switch in the ligand-binding domain regulates the dependence of the glucocorticoid receptor on Hsp90. *J Mol Biol* **368**(3)**:** 729-741

Rogatsky I, Wang JC, Derynck MK, Nonaka DF, Khodabakhsh DB, Haqq CM, Darimont BD, Garabedian MJ, Yamamoto KR (2003) Target-specific utilization of transcriptional regulatory surfaces by the glucocorticoid receptor. *Proc Natl Acad Sci U S A* **100**(24)**:** 13845-13850

Sablin EP, Woods A, Krylova IN, Hwang P, Ingraham HA, Fletterick RJ (2008) The structure of corepressor Dax-1 bound to its target nuclear receptor LRH-1. *Proc Natl Acad Sci U S A* **105**(47)**:** 18390-18395

Schlatter LK, Howard KJ, Parker MG, Distelhorst CW (1992) Comparison of the 90-kilodalton heat shock protein interaction with in vitro translated glucocorticoid and estrogen receptors. *Mol Endocrinol* **6**(1)**:** 132-140

Shiau AK, Barstad D, Loria PM, Cheng L, Kushner PJ, Agard DA, Greene GL (1998) The structural basis of estrogen receptor/coactivator recognition and the antagonism of this interaction by tamoxifen. *Cell* **95**(7)**:** 927-937

Shulman AI, Larson C, Mangelsdorf DJ, Ranganathan R (2004) Structural determinants of allosteric ligand activation in RXR heterodimers. *Cell* **116**(3)**:** 417-429

Simmons CA, Bledsoe RK, Guex N, Pearce KH (2008) Expression, purification, and characterization of multiple, multifunctional human glucocorticoid receptor proteins. *Protein Expr Purif* **62**(1)**:** 29-35

Stavreva DA, Muller WG, Hager GL, Smith CL, McNally JG (2004) Rapid glucocorticoid receptor exchange at a promoter is coupled to transcription and regulated by chaperones and proteasomes. *Mol Cell Biol* **24**(7)**:** 2682-2697

Suino-Powell K, Xu Y, Zhang C, Tao YG, Tolbert WD, Simons SS, Jr., Xu HE (2008) Doubling the size of the glucocorticoid receptor ligand binding pocket by deacylcortivazol. *Mol Cell Biol* **28**(6)**:** 1915-1923

Tanaka M, Nishi M, Morimoto M, Sugimoto T, Kawata M (2003) Yellow fluorescent protein-tagged and cyan fluorescent protein-tagged imaging analysis of glucocorticoid receptor and importins in single living cells. *Endocrinology* **144**(9)**:** 4070-4079

Teichert A, Arnold LA, Otieno S, Oda Y, Augustinaite I, Geistlinger TR, Kriwacki RW, Guy RK, Bikle DD (2009) Quantification of the vitamin D receptor-coregulator interaction. *Biochemistry* **48**(7)**:** 1454-1461

Voegel JJ, Heine MJ, Tini M, Vivat V, Chambon P, Gronemeyer H (1998) The coactivator TIF2 contains three nuclear receptor-binding motifs and mediates transactivation through CBP binding-dependent and -independent pathways. *EMBO J* **17**(2)**:** 507-519

Voegel JJ, Heine MJ, Zechel C, Chambon P, Gronemeyer H (1996) TIF2, a 160 kDa transcriptional mediator for the ligand-dependent activation function AF-2 of nuclear receptors. *EMBO J* **15**(14)**:** 3667-3675

Wagner RL, Apriletti JW, McGrath ME, West BL, Baxter JD, Fletterick RJ (1995) A structural role for hormone in the thyroid hormone receptor. *Nature* **378**(6558)**:** 690-697

Warnmark A, Gustafsson JA, Wright AP (2000) Architectural principles for the structure and function of the glucocorticoid receptor tau 1 core activation domain. *J Biol Chem* **275**(20)**:** 15014-15018

Wu J, Li Y, Dietz J, Lala DS (2004) Repression of p65 transcriptional activation by the glucocorticoid receptor in the absence of receptor-coactivator interactions. *Mol Endocrinol* **18**(1)**:** 53-62

Xu HE, Stanley TB, Montana VG, Lambert MH, Shearer BG, Cobb JE, McKee DD, Galardi

CM, Plunket KD, Nolte RT, Parks DJ, Moore JT, Kliewer SA, Willson TM, Stimmel JB (2002) Structural basis for antagonist-mediated recruitment of nuclear co-repressors by PPARalpha. *Nature* **415**(6873)**:** 813-817

Xu J, Li Q (2003) Review of the in vivo functions of the p160 steroid receptor coactivator family. *Mol Endocrinol* **17**(9)**:** 1681-1692

Zhou J, Oakley RH, Cidlowski JA (2008) DAX-1 (dosage-sensitive sex reversal-adrenal hypoplasia congenita critical region on the X-chromosome, gene 1) selectively inhibits transactivation but not transrepression mediated by the glucocorticoid receptor in a LXXLL-dependent manner. *Mol Endocrinol* **22**(7)**:** 1521-1534

Zhu Y, Qi C, Calandra C, Rao MS, Reddy JK (1996) Cloning and identification of mouse steroid receptor coactivator-1 (mSRC-1), as a coactivator of peroxisome proliferator-activated receptor gamma. *Gene Expr* **6**(3)**:** 185-195

SUPPLEMENTAL INFORMATION

FIGURE 1-S1. *GR_{SD} NR box binding isotherms*

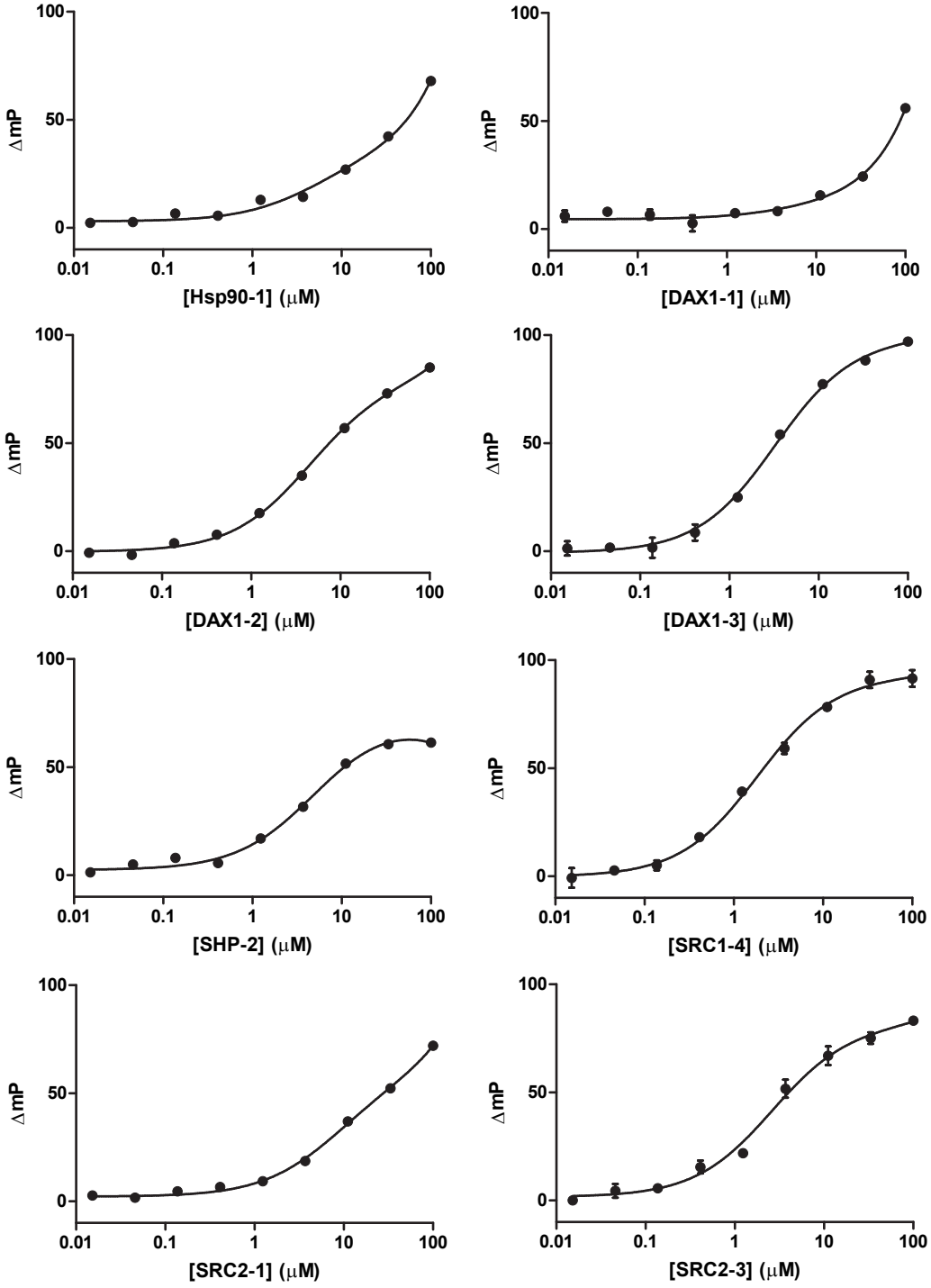

FIGURE 1-S1 cont.

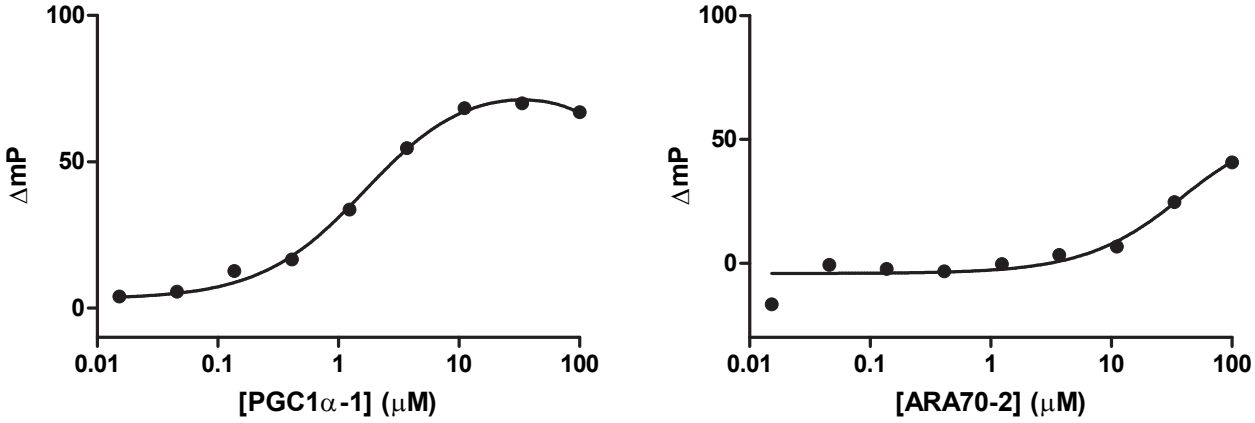

FIGURE 1-S2. *GR_{M752I} NR box binding isotherms*

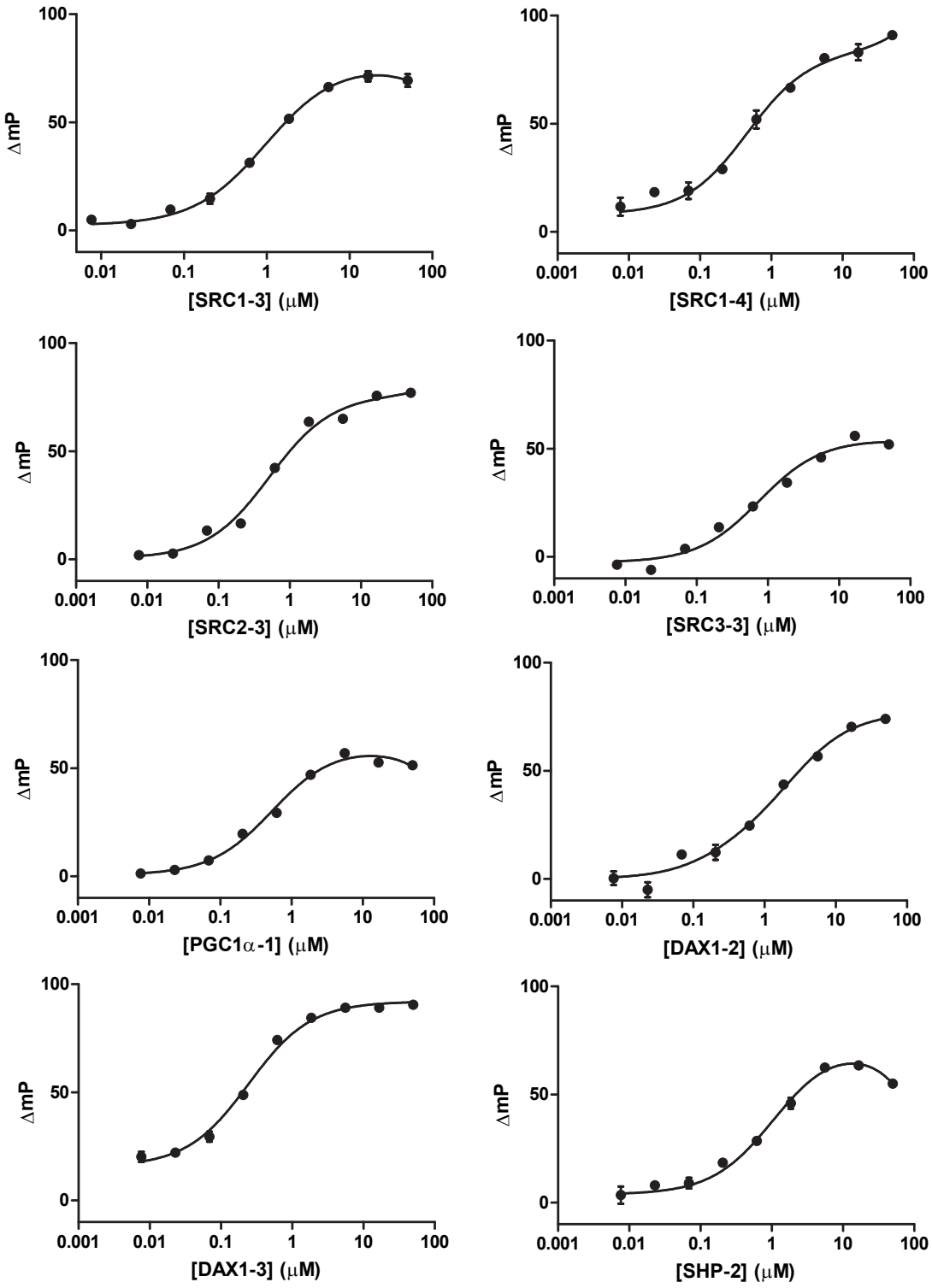

Chapter 2

Recognition and accommodation at the androgen receptor coactivator binding interface

In collaboration with:

Eugene Hur, E. Sturgis Payne, Hanne Grøn, Benjamin M Buehrer, and Robert J Fletterick

Reprinted with permission from:

Hur E, Pfaff SJ, Payne ES, Gron H, Buehrer BM, Fletterick RJ. (2004) *Recognition and accommodation at the androgen receptor coactivator binding interface.* PLoS Biol 2(9): e274.

ABSTRACT

Prostate cancer is a leading killer of men in the industrialized world. Underlying this disease is the aberrant action of the androgen receptor (AR). AR is distinguished from other nuclear receptors in that after hormone binding, it preferentially responds to a specialized set of coactivators bearing aromatic-rich motifs, while responding poorly to coactivators bearing the leucine-rich "NR box" motifs favored by other nuclear receptors. Under normal conditions, interactions with these AR-specific coactivators through aromatic-rich motifs underlie targeted gene transcription. However, during prostate cancer, abnormal association with such coactivators, as well as with coactivators containing canonical leucine-rich motifs, promotes disease progression. To understand the paradox of this unusual selectivity, we have derived a complete set of peptide motifs that interact with AR using phage display. Binding affinities were measured for a selected set of these peptides and their interactions with AR determined by X-ray crystallography. Structures of AR in complex with FxxLF, LxxLL, FxxLW, WxxLF, WxxVW, FxxFF, and FxxYF motifs reveal a changing surface of the AR coactivator binding interface that permits accommodation of both AR-specific aromatic-rich motifs and canonical leucine-rich motifs. Induced fit provides perfect mating of the motifs representing the known family of AR coactivators and suggests a framework for the design of AR coactivator antagonists.

INTRODUCTION

The androgen receptor (AR) is the cellular mediator of the actions of the hormone 5-α dihydrotestosterone (DHT). Androgen binding to AR leads to activation of genes involved in the development and maintenance of the male reproductive system and other tissues such as bone and muscle. However, it is the pivotal role of AR in the development and progression of prostate cancer that has led to increasing interest in this nuclear receptor. Presently, hormone-dependent prostate cancer is treated with a combination of strategies that reduce circulating levels of androgens, such as the administration of antiandrogens that compete for the androgen-binding pocket in the core of the C-terminal ligand-binding domain (LBD). The benefits of these treatments are typically transient, with later tumor growth associated with increases in expression levels of AR or its cofactors, or mutations that render AR resistant to antiandrogens (Gregory et al. 2001; Culig et al. 2002; Lee and Chang 2003). Alternative approaches to inhibiting AR transcriptional activity may therefore lie in disrupting critical protein associations the receptor needs for full function.

The precise details of how AR binds the dozens of coregulator proteins reported to associate with different regions of AR in vivo remain poorly understood (Lee and Chang 2003). Many nuclear receptors activate transcription by binding short leucine-rich sequences conforming to the sequence LxxLL (where "x" is any amino acid), termed nuclear receptor (NR) boxes, which are found within a variety of NR coactivators including the p160 family. Hormone binding to the LBD stabilizes the C-terminal helix of the receptor, helix 12, in a conformation that completes a binding surface for these LxxLL motifs (Darimont et al. 1998; Nolte et al. 1998; Shiau et al. 1998; Bledsoe et al. 2002). The structural elements composing this binding

interface, consisting of helices 3, 4, 5, and 12 of the receptor, are synonymous with a previously defined hormone-dependent activation function that lies within the LBD termed activation function (AF)–2. Association of p160 coactivators allows the recruitment and assembly of a number of other cofactors that together modulate the state of chromatin and interactions with components of the basal transcription machinery to initiate transcription (Glass and Rosenfeld 2000).

AR, however, utilizes multiple mechanisms to activate gene transcription. Generally, AR activity is dependent on contributions from multiple transactivation functions that lie within the N-terminal domain (NTD) collectively called AF-1. Although the AR AF-2 can bind to a restricted set of LxxLL motifs (Ding et al. 1998; He et al. 1999;Needham et al. 2000) and is relatively potent (Wang et al. 2001), it usually displays weak independent activity at typical androgen-regulated genes, with significant activity observed only in the presence of high levels of p160 coactivators, as detected in some prostate cancers (He et al. 1999; Gregory et al. 2001). Instead, the AR AF-2 exhibits a distinct preference among NRs for phenylalanine-rich motifs conforming to the sequence FxxLF (He et al. 2000; He and Wilson 2003). Such motifs have been identified in the AR NTD and in an AR cognate family of coactivators that includes AR-associated protein (ARA) 54, ARA55, and ARA70 (He et al. 2000, 2002b; Lee and Chang 2003). The NTD FxxLF motif (residues 23–27) mediates a direct, interdomain, ligand-dependent interaction between the NTD and LBD (N/C interaction) that is thought to facilitate dimerization, stabilize androgen binding, and possibly regulate AF-1 and AF-2 activity (Langley et al. 1998; He et al. 2000). In addition, the NTD also contains a related hydrophobic motif,

WxxLF (residues 433–437), that nucleates formation of an alternative N/C interaction that may serve to inhibit AR activity (He et al. 2000, 2002a; Hsu et al. 2003).

Presently, how the AR AF-2 surface can accommodate residues with bulky aromatic side chains and distinguish FxxLF motifs from LxxLL motifs is not known. To understand the structural basis of this unusual coactivator recognition preference, we characterized the full repertoire of interacting sequences using phage display to define amino acids preferred at the AR coactivator binding interface. Crystal structures of the AR LBD in complex with several phage display–derived peptides reveal the structural basis of FxxLF motif specificity and an induced fit of the receptor that allows accommodation of other related hydrophobic motifs. Comparisons of the structures suggest strategies for the design of AR coactivator antagonists.

RESULTS

AR Preference for Aromatic Groups in Coregulator Recognition. Phage display has been used to study coactivator recognition specificity and to identify coactivator motif sequence variants preferred by the estrogen receptor (ER), thyroid hormone receptor (TR) β, and most recently AR (**Chang et al. 1999**; **Norris et al. 1999**; **Paige et al. 1999**; **Northrop et al. 2000**; **Hsu et al. 2003**). Using phage display, we screened more than 2 × 1010 randomized peptides against DHT-bound AR LBD. Selections identified sequences containing hydrophobic motifs that were primarily aromatic in character, consistent with another recent study (**Hsu et al. 2003**) (Figure 2-1). Of these aromatic motifs, FxxLF and related motifs with substitutions of

phenylalanine or tryptophan for leucine at positions +1, +5, or both, dominated the selections. (Peptide residues are numbered in reference to the first hydrophobic residue of the core motif, which is numbered +1. Residues preceding the first hydrophobic residue are numbered negatively in descending order starting with −1.) Substitutions of tyrosine at the +5 position were also observed, but to a much lesser extent (unpublished data). At the +4 position, valines, methionines, and even the aromatic residues phenylalanine and tyrosine were observed (Figure 2-1; unpublished data). In general, LxxLL motifs were not selected. The LxxLL motif shown in Figure 2-1 was derived from prior phage selections with ER and subsequently demonstrated to bind AR in FRET-based screens in vitro (unpublished data).

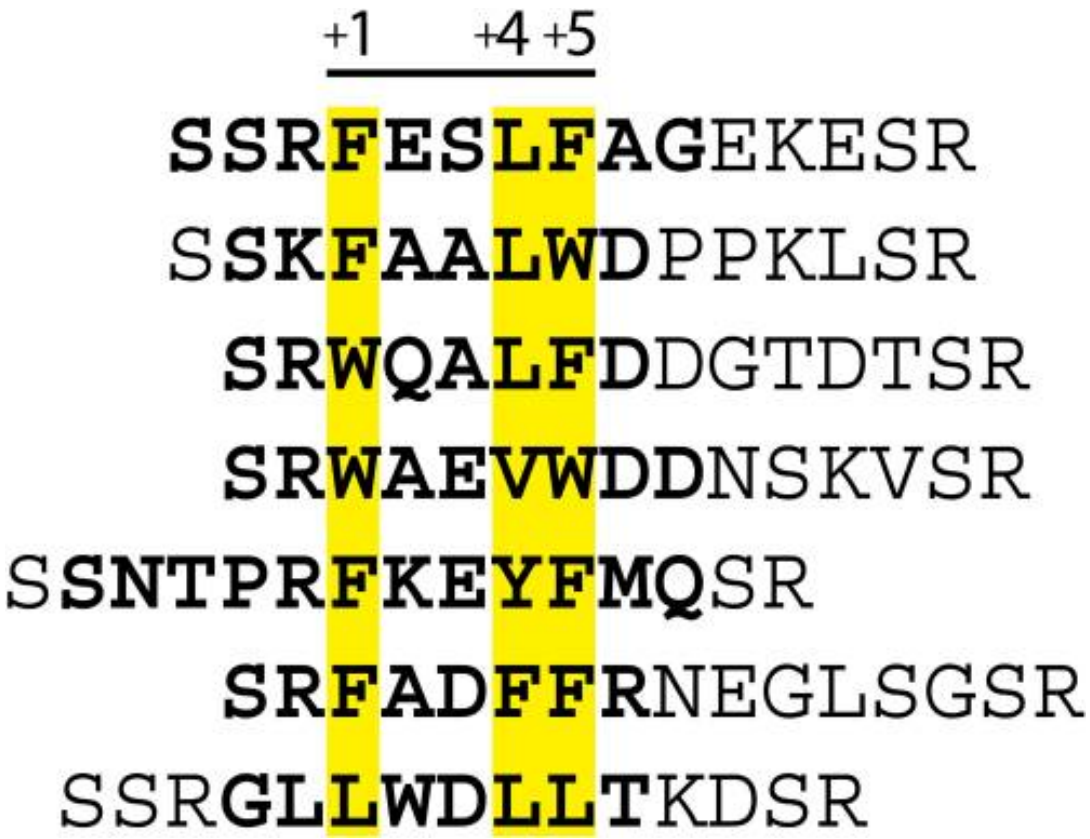

Figure 2-1. AR LBD–Interacting Peptides Selected by Phage Display

Preliminary characterization of the subset of AR-interacting peptides shown in figure 2-1 confirmed that each competed for binding of in vitro translated AR cofactors to bacterially expressed AR LBD in pulldown assays, and generally did so with modestly improved efficiency relative to the native FxxLF motif from the AR NTD and significantly greater efficiency than a native LxxLL motif from glucocorticoid receptor-interacting protein 1 (GRIP1) NR box 3 (P. Webb, personal communication). The equilibrium dissociation constants (Kd) were directly determined for the interaction between the AR LBD and FxxLF and LxxLL peptides and one variant tryptophan-containing peptide, FxxLW, using surface plasmon resonance (Table 2-1). The Kd for FxxLF was 1.1 μM, similar to the affinities of physiologically derived FxxLF motifs determined previously by isothermal titration calorimetry (He and Wilson 2003). The affinity of LxxLL was less than 2-fold weaker, with a Kd of 1.8 μM, but more than three times stronger than the tightest binding p160-derived LxxLL motif, NR box 3 of transcriptional intermediary factor 2 (TIF2) (He and Wilson 2003). Surprisingly, the affinity of FxxLW, with a Kd of 920 nM, was slightly better than FxxLF, in spite of the presence of the tryptophan residue at the +5 position. Together, our results are consistent with the notion that the phage display peptides interact with the same AR surface that binds FxxLF and LxxLL motifs in native cofactors, and that they do so with similar or improved affinities relative to their natural counterparts.

Constants	FxxLF	LxxLL	FxxLW
$k_{a1} \times 10^{-4}$ ($M^{-2}s^{-1}$)	5.2±1.0	6.2±4.3	5.9±1.5
$k_{d1} \times 10^{2}$ ($M^{-1}s^{-1}$)	2.3±0.03	7.0±0.17	3.4±0.04
K_{d1} (nM)	440±85	1120±78	580±140
$k_{a2} \times 10^{3}$ ($M^{--1}s^{-1}$)	1.3±0.5	3.2±0.4	3.6±0.3
$k_{d2} \times 10^{3}$ ($M^{-1}s^{-1}$)	3.5±0.06	5.0±0.04	5.6±0.05
K_{d2}	2.6±1.0	1.6±0.2	1.6±0.2
K_d^{app} (μM)	1.1±0.6	1.8±1.1	0.92±0.3

Surface plasmon resonance data were best fit using the two-state conformational change model (Warnmark et al. 2001, 2002). Dissociation constants were calculated from rate constants as described previously (Warnmark et al. 2001).
DOI: 10.1371/journal.pbio.0020274.t001

Table 2-1. Rate and Dissociation Constants for the Interaction between the AR LBD and Selected Peptides.

Surface plasmon resonance data were best fit using the two-state conformational change model (Warnmark et al. 2001, 2002). Dissociation constants were calculated from rate constants as described previously (Warnmark et al. 2001).

One Site Fits All. To understand the binding mode of different AR coactivators, we determined the crystal structures of DHT-bound AR LBD without peptide and in complex with each of the seven peptides listed in Figure 2-1. All complexes crystallized in the space group P212121 with one molecule per asymmetric unit and unit cell dimensions similar to those observed in previous AR LBD crystal structures (Matias et al. 2000; Sack et al. 2001). Overall structural features of the complexes are shown in Figure 2-2. Peptides assumed short α helical conformations centered on the core hydrophobic motif and bound in a solvent channel relatively free of crystal contacts on a groove formed by helices 3, 4, 5, and 12 of the receptor (Figure 2-2A). Detailed data collection and refinement statistics, as well as buried surface areas for each complex, are listed in Table 2-2. The structures confirm previous suggestions that AR utilizes a single binding interface for LxxLL and noncanonical aromatic-rich motifs (He et al. 2000, 2002a). Only side chains move to accommodate the array of peptides, sometimes considerably, with the unbranched side chains of Lys720, Met734, and Met894 making the largest conformational changes upon binding of peptide (Figure 2-2B).

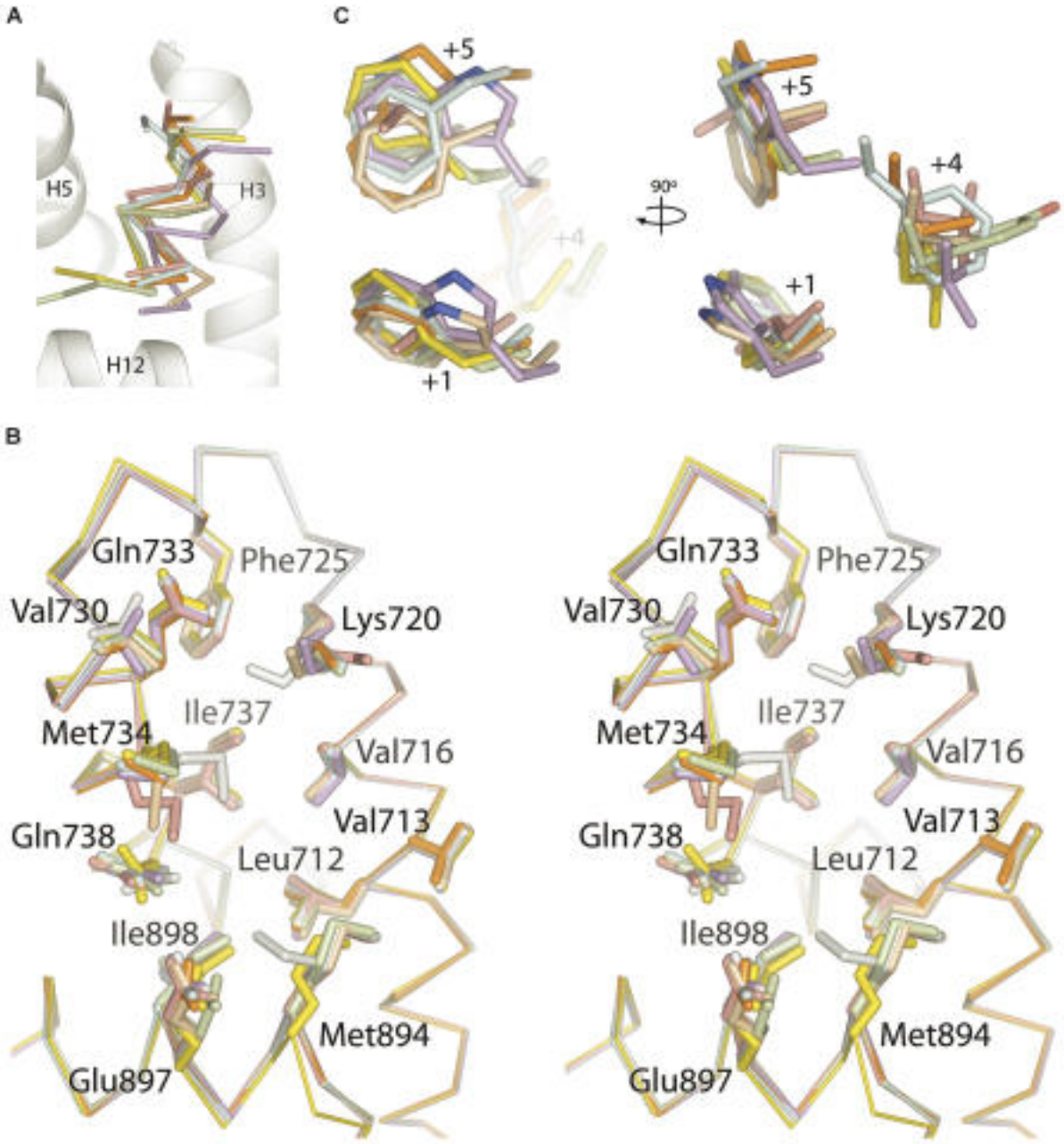

Figure 2-2. A Structural Profile of the AR Coactivator Binding Interface.

Structure		FxxLF	FxxFF	FxxYF	FxxLW	WxxLF	WxxVW	LxxLL	Unbound
Space group		$P2_12_12_1$	$P2_12_12_1$	$P2_12_12_1$	$P2_12_12_1$	$P2_12_12_1$	$P2_12_12_1$	$P2_12_12_1$	$P2_12_12_1$
Unit cell dimensions (Å)	*a*	55.4	54.3	55.6	55.8	56.4	53.4	54.2	56.2
	b	66.2	66.6	66.6	66.1	66.4	66.4	66.3	66.2
	c	68.8	70.2	72.5	68.4	72.1	70.6	69.4	68.5
Resolution (Å)		20–1.4	20–2.2	20–1.6	20–1.8	20–2.0	20–2.1	20–1.6	20–1.7
Unique reflections		49611	13332	36190	23771	18803	15170	32737	28564
Completeness (%)[a]		98.2 (88.4)	99.3 (98.6)	99.9 (99.6)	98.8 (89.6)	99.8 (85.3)	99.9 (99.9)	97.2 (93.6)	99.3 (99.2)
R_{sym} (%)[a,b]		7.2 (57.1)	9.7 (54.2)	5.2 (65.0)	8.4 (59.6)	5.9 (54.1)	6.7 (56.3)	4.5 (46.3)	6.1 (45.7)
$<I/I_{\sigma}>$[a]		21.3 (2.0)	20.4 (3.1)	54.1 (3.4)	19.1 (2.2)	28.2 (2.6)	26.2 (3.3)	31.4 (2.7)	28.5 (3.2)
R_{cryst} (%)[c]		19.6	20.0	19.7	20.0	21.6	20.8	19.9	18.1
R_{free} (%)[c]		20.5	24.5	20.8	23.4	23.9	23.9	21.8	20.5
r.m.s.d. bond lengths (Å)		0.005	0.007	0.006	0.006	0.007	0.006	0.006	0.006
r.m.s.d. bond angles (°)		1.11	1.07	1.06	1.06	1.02	1.08	1.07	1.07
Average B-factor (Å^2):	Overall	22.4	40.3	28.2	29.0	43.5	44.1	25.1	21.2
	LBD	21.2	39.7	27.1	28.3	42.3	43.1	23.9	20.3
	Peptide	30.9	56.2	35.2	37.6	71.0	65.9	44.1	–
Buried surface area (Å^2):	Total	1012	926	1197	937	970	903	984	–
	+1[d]	305	305	311	315	364	351	271	–
	+4[d]	189	204	205	187	194	149	193	–
	+5[d]	276	276	283	313	281	287	241	–
PDB accession code		1T7R	1T73	1T7M	1T79	1T74	1T76	1T7F	1T7T

[a]Numbers in parenthesis denote values for the highest resolution shell.
[b]$R_{sym} = \Sigma|I - <I>| / \Sigma (I)$.
[c]$R_{cryst} = \Sigma\ |F_o - F_c| / \Sigma\ |F_o|$, where F_o and F_c are observed and calculated structure factors, respectively; R_{free} was calculated similarly with a randomly selected set of reflections consisting of 5% of total reflections that were excluded from refinement.
[d]Values for side chain atoms only.
DOI: 10.1371/journal.pbio.0020274.t002

Table 2-2. Summary of Structures and Crystallographic Statistics

FxxLF. The mechanisms that permit AR to accommodate motifs with bulky phenylalanine residues were assessed in a crystal structure of the AR LBD in complex with the FxxLF peptide. The FxxLF peptide recapitulates the binding mode of p160-derived LxxLL motifs to other nuclear receptors (Darimont et al. 1998; Nolte et al. 1998;Shiau et al. 1998; Bledsoe et al. 2002). The peptide forms a short α helix whose hydrophobic face, composed of Phe+1, Leu+4, and Phe+5, binds an L-shaped groove formed by helices 3, 4, 5, and 12 of the LBD that is composed of three subsites that accommodate each hydrophobic residue (Figures 2-2A and and 2-3A). The conserved charged residues at either end of the cleft, Lys720 and Glu897, the so-called charge clamp residues, make electrostatic interactions with the main chain atoms at the ends of the peptide helix: Lys720 with the carbonyl group of Phe+5, and Glu897 with the amide nitrogens of Phe+1 and Arg−1 (Figure 2-3C). Glu897 also interacts with the side chain of Arg −1. The two interior residues of the motif, Glu+2 and Ser+3, are solvent exposed and do not interact with the receptor.

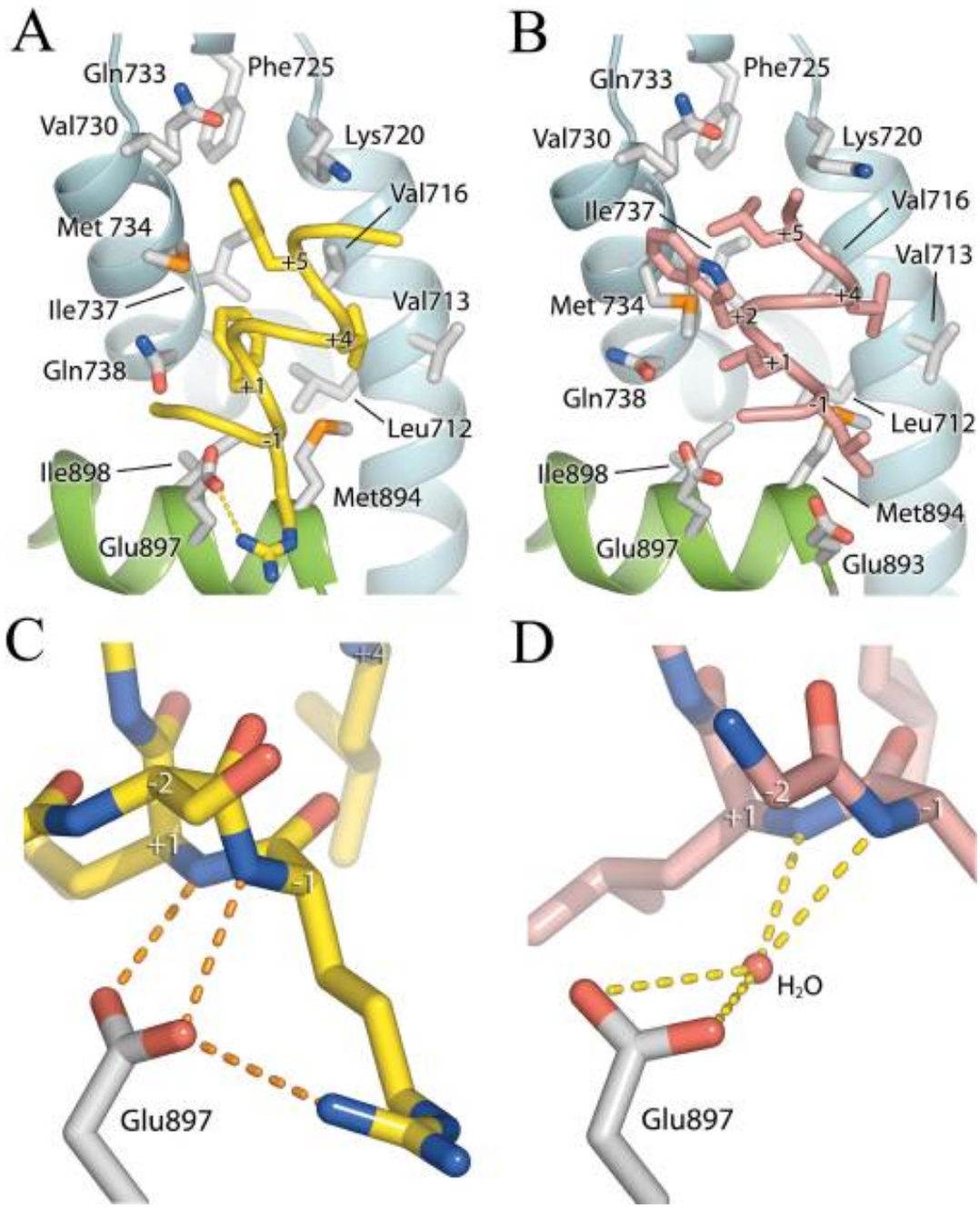

Figure 2-3. Interactions of FxxLF and LxxLL with the AR LBD

Comparison of AR alone and AR in complex with FxxLF (and other aromatic-rich peptides described below) reveals that the AF-2 cleft reorganizes to accommodate the bulky peptide side chains (see Figures 2-2B and 2-4). The unbranched side chains of Lys720 and Met734 move from an extended conformation over the +5 pocket to one almost perpendicular to the surface of the protein. The pockets for Phe+1 and Phe+5 are arranged in a line, forming a deep, extended cleft on the LBD spanning the length of the two side chains on the face of the peptide helix (see Figures 2-3A and 2-4B). Phe+1, almost entirely solvent inaccessible, binds face down at the base of this groove, making hydrophobic contacts with Leu712, Val716, Met734, Gln738, Met894, and Ile898, which define the +1 pocket. The top of the groove, composed of Val716, Lys720, Phe725, Ile737, Val730, Gln733, and Met734, narrows to form the +5 pocket. Met734 and the aliphatic portion of Lys720 constrict this subsite, forming van der Waals interactions with opposite faces of the Phe+5 benzyl ring. Together, the +1 and +5 residues are almost entirely solvent inaccessible. In contrast, Leu+4 binds in a shallow hydrophobic patch consisting of Leu712 and Val716 lined at the ridges by Val713 and Met894 and is largely solvent exposed.

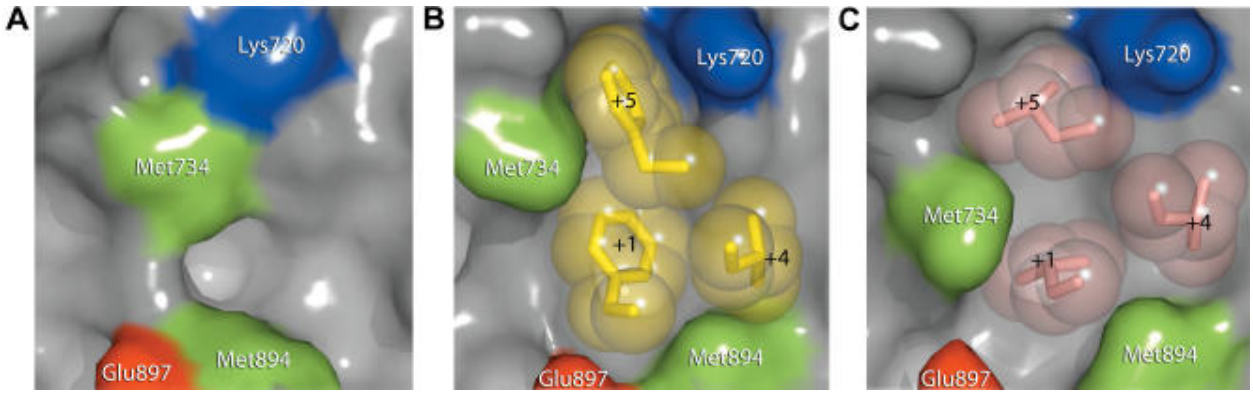

Figure 2-4. Induced Fit of the AR AF-2 Interface.

LxxLL. The preference of AR for motifs with aromatic groups over leucine-rich motifs was assessed with a crystal structure of the AR LBD in complex with the LxxLL peptide. The structure reveals similarities between the binding modes of the LxxLL and FxxLF motifs to AR, and other LxxLL motifs to other nuclear receptors. The LxxLL motif adopts a helical conformation, and interactions of the motif with the AF-2 cleft are predominantly hydrophobic, with the three leucine residues of the motif contributing most of the interactions. However, significant differences can be seen between the binding mode of the LxxLL motif to AR and that of p160-derived LxxLL motifs to other nuclear receptors. First, flanking residues were largely disordered, with only two N-terminal flanking residues and one C-terminal residue visible in electron density maps (see Figures 2-1 and 2-3B). This contrasts with extended structures seen in the p160-derived LxxLL motifs in complex with their cognate receptors (Darimont et al. 1998; Nolte et al. 1998; Shiau et al. 1998; Bledsoe et al. 2002). Second, the LxxLL peptide backbone forms hydrogen bonds with only one of the two conserved charge clamp residues, Lys720. A shift in the position of the LxxLL peptide helix precludes direct interactions with Glu897 (see Figures 2-2A and 2-3D). This shift results from changes in the geometry of the +1 and +5 subsites mediated by Met734, which moves 2.5Å toward the +1 pocket (see Figures 2-2B and 2-4C) and enables binding of a leucine at the +5 subsite by a simultaneous widening and shallowing of the pocket. This movement of Met734 causes displacement of the +1 residue, resulting in a rotation of the peptide helix away from helix 12, toward helix 3. A slight translation of the peptide helix also occurs away from helix 12 because of the shorter side chain length of leucine (see Figure 2-2A).

Side chains of residues flanking the first leucine of the motif make additional hydrophobic interactions with the AR surface (see Figure 2-3B). Trp+2 reaches over Met734, clamping the methionine in between itself and Leu+1. Leu−1 extends over Met894, abutted against Glu893. These interactions likely explain the moderate affinity of AR for this particular LxxLL motif despite suboptimal complimentarity with the residues of the core motif (as discussed below) and the loss of main chain interactions with Glu897.

WxxLF, FxxLW, and WxxVW. To understand how the AR AF-2 accommodates tryptophan residues, structures of AR in complex with peptides containing tryptophan substitutions at the +1 or +5 position, or both, were determined (Figure 2-5). Surprisingly, WxxLF, analogous to the only tryptophan-containing motif known in vivo, WHTLF in the AR NTD, was relatively disordered, with the peptide displaying the highest B-factor and least well defined density, suggesting that it binds with the lowest affinity (Table 2-2). Nonetheless, each of the tryptophan peptides adopted similar helical conformations. As described above for the LxxLL motif, substitutions at the +1 and +5 positions for non-phenylalanine residues result in shifts of the peptide helix (see Figure 2-2A). Consequently, backbone interactions with Lys720 are maintained, but interactions with the other charge clamp residue, Glu897, are lost. Once again, however, flanking residues within the peptide make additional contacts with the AR surface, and, unlike the LxxLL peptide, these contacts include Glu897. In FxxLW and WxxVW, the −2 serine (Figure 2-6) forms a bidentate hydrogen-bonding interaction, making hydrogen bonds to both Glu897 and the backbone amide group of the +2 residue. Ser−2 of WxxLF similarly interacts with Glu897, but is too distant for helical-capping interactions with the +2 amide group. Instead,

Glu893, in a more typical interaction with the +1 amide nitrogen, caps the WxxLF helix (Figure 2-6B). Thus, tryptophan substitutions are tolerated, but they induce a shift in the peptide backbone that precludes interactions with one of the charge clamp residues. This suboptimal interaction is compensated partially by interactions of flanking residues with the AR surface.

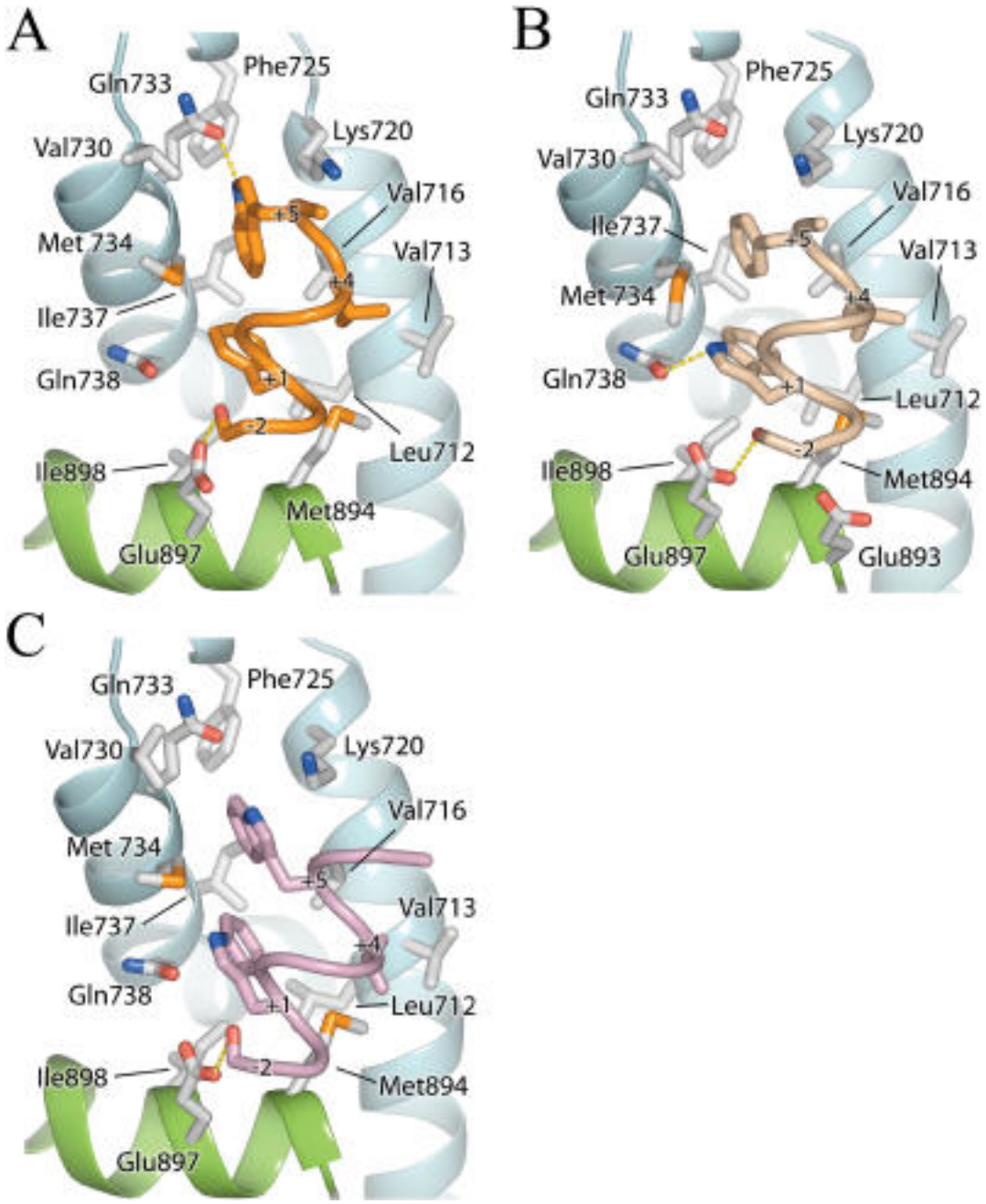

Figure 2-5. Interactions of the Tryptophan Motifs with the AR LBD.

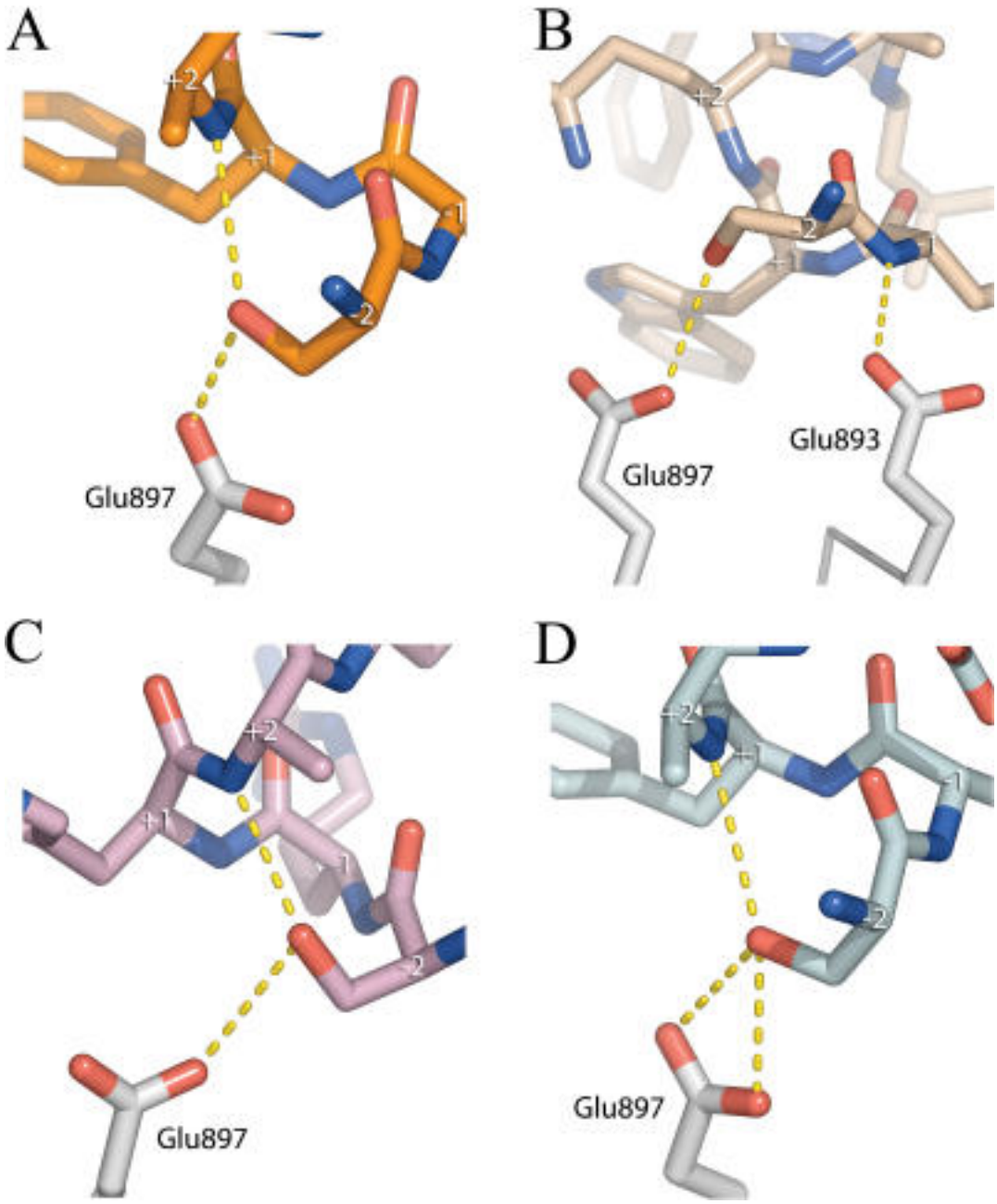

Figure 2-6. Interactions of Ser−2 with Glu897.

FxxFF and FxxYF. Finally, effects of substitutions at the +4 position were assessed in structures of AR in complex with peptides containing FxxFF and FxxYF motifs (Figure 2-7). Surprisingly, the binding mode of FxxFF to AR resembled that of the tryptophan peptides more closely than the binding mode of FxxLF (see Figures 2-2A and 2-7B). Like the tryptophan peptides, interactions with Glu897 are mediated by Ser−2 instead of the peptide backbone (see Figure 2-6D). Deviations from ideal helical geometry allow Phe+4 to bind facedown in the +4 pocket with the benzyl ring stacked against Val713.

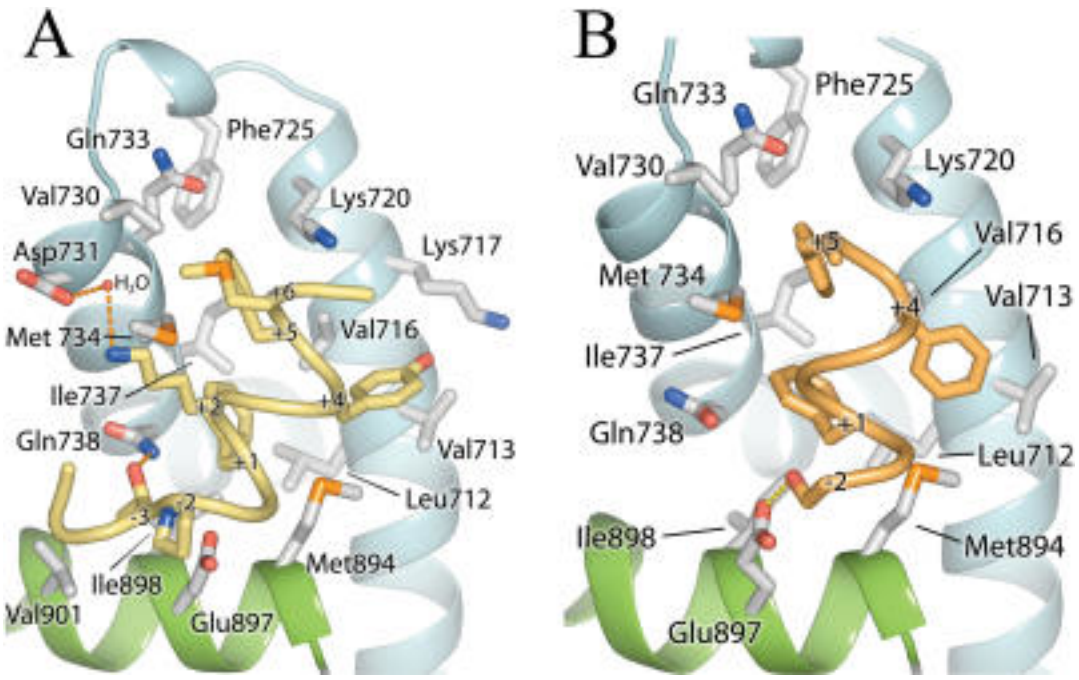

Figure 2-7. Interactions of FxxYF and FxxFF with the AR LBD.

By contrast, the conformation of FxxYF was the closest to FxxLF (see Figure 2-2A). Other than FxxLF, only FxxYF makes direct backbone interactions with Glu897. Unlike the facedown orientation of Phe+4 observed in the FxxFF peptide, Tyr+4 is bound edgewise into the shallow +4 pocket, making interactions with Val713, Val716, and the aliphatic portion of Lys717. FxxYF was the most ordered of all the peptides, with 12 out of 15 residues observed in the electron density (see Figures 2-1 and 2-7A). Significant interactions were observed involving residues other than hydrophobic residues of the motif. Lys+2 and Met+6 are predominantly solvent exposed, extending out over the protein surface. Met+6 is bound on top of Phe+5, while Lys+2 makes a water-mediated hydrogen bond with Asp731. Thr−3 of the peptide defines a new subsite, with the hydroxyl group forming a hydrogen bond to Gln738 and the methyl group making hydrophobic contacts in a pocket formed by Glu897, Ile898, and Val901. Similar interactions were observed in the glucocorticoid receptor (GR)–TIF2 complex involving the −3 glutamine of the TIF2 NR box 3 motif (Bledsoe et al. 2002). However a valine to asparagine substitution at the residue corresponding to 901 in AR creates a pocket with a more polar character in GR (Figure 2-8).

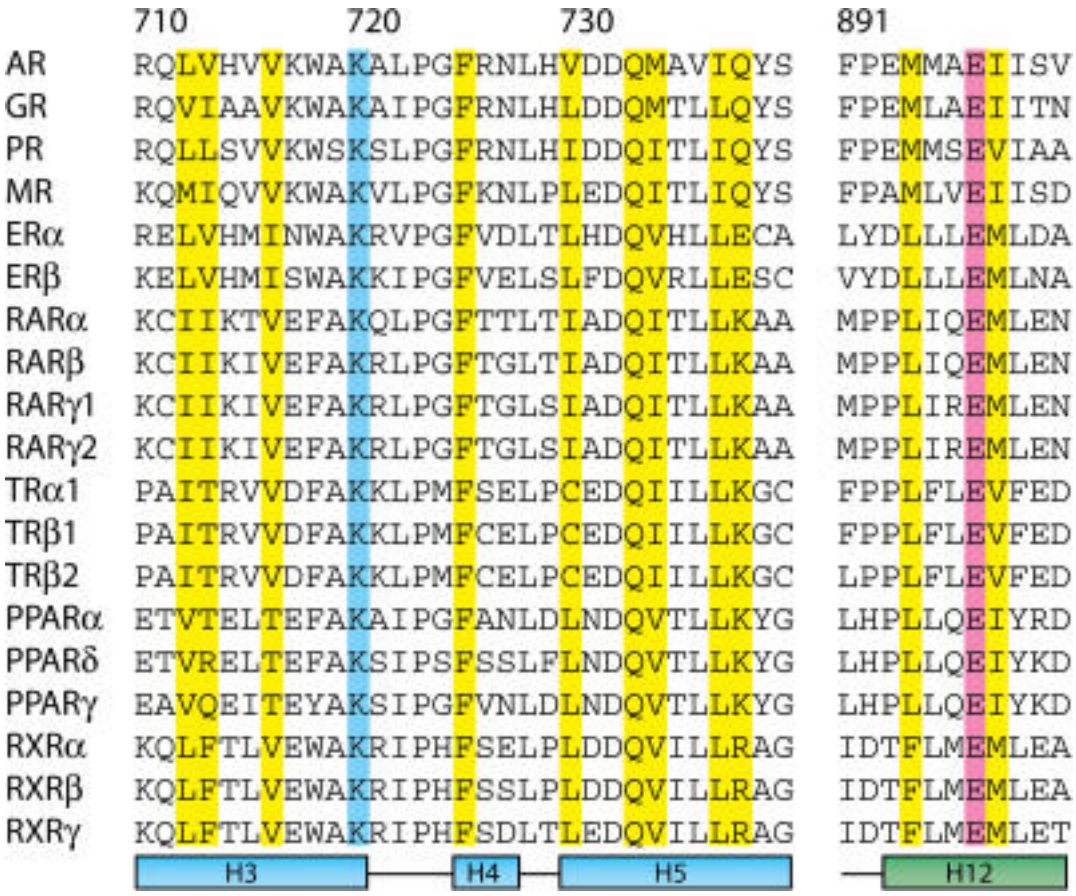

Figure 2-8. Sequence Alignment of the AF-2 Region of NRs

Restrictions of the Three Subsites. Together, the structures described above permit an assessment of the way that individual subsites of the AR AF-2 cleft accommodate hydrophobic groups. The indole rings of tryptophan and the phenyl rings of phenylalanine fit into their pockets analogously with the +1 and +5 residues bound facedown and edgewise, respectively, into the AF-2 cleft. On the other hand, the position of the +4 residue is variable, with binding in this shallow pocket largely dictated by the position of the peptide backbone caused by the bound conformations of the +1 and +5 residues (see Figure 2-2C). Small shifts in the position of the N-terminal of helix 12 can be seen, which reposition Met894 for more optimal contacts with +4 residues bound at that subsite (see Figure 2-2B).

The binding mode detected in the +1 pocket is the most conserved of the three hydrophobic subsites (see Figure 2-2C). The benzyl moiety of the indole side chains superimpose with the corresponding benzyl side chains of the phenylalanine-rich motifs, effectively mimicking interactions of a phenylalanine residue. However, the presence of a hydrogen-bonding partner on the indole side chain enables an additional polar interaction not seen in the phenylalanine-rich motifs between the indole nitrogen and Gln738 (see Figure 2-5B). Unexpectedly, this additional interaction in the +1 pocket does not occur with Trp+1 of WxxVW (see Figure 2-5C). While similarly distanced to make the same interaction, the plane of the indole ring is rotated about 20° relative to that of WxxLF, causing it to be at a poor angle for strong hydrogen bonding to Gln738.

Binding of tryptophans in the +5 pocket is slightly more variable (see Figure 2-2C). Trp +5 of WxxVW is bound similarly to phenylalanine residues at the same position. Only the six-membered ring of the indole group is fully buried in the pocket. The five-membered ring of the

indole side chain sticks out, solvent exposed. In contrast, the +5 indole group of FxxLW is rotated almost 90°, resulting in burial of both rings of the indole group, as well as the formation of a strong hydrogen bond between the indole nitrogen and Gln730 (see Figure 2-5A). Binding in this orientation appears to be highly favorable, as the FxxLW peptide deviates from helical geometry at the +5 position to do so.

DISCUSSION

The crystal structures reported here reveal how AR binds coactivator motifs with bulky aromatic hydrophobic groups and permit construction of a profile of the AR coregulator interface (see Figure 2-2). In some ways, this interface resembles those of other nuclear receptors: it is an L-shaped hydrophobic cleft comprised of three distinct subsites that bind hydrophobic groups at the +1, +4, and +5 positions in cognate peptides. Moreover, the so-called charge clamp residues (Lys720 and Glu897) bracket the cleft. Nonetheless, the AR coregulator recognition site is unique in that it rearranges upon motif binding to form a long, deep, and narrow groove that accommodates aromatic residues at the +1 and +5 positions (Figure 2-9). Sequence alignments of AR with other NRs suggest that a unique combination of substitutions at Val730, Met734, and Ile737 combine to permit the formation of a smoother, flatter interaction surface that displays a higher complimentarily to aromatic substituents than to branched aliphatic (see Figure 2-8). Of these, methionine, the only unbranched hydrophobic amino acid and the most accommodating, at a key position between the +1 and +5 sites, allows the AR AF-2 interface to vary the size and shape of its pockets to associate with a more diverse set of coregulators. GR also contains a methionine residue at this position, raising the possibility that it may also employ induced fit to

broaden motif recognition. While naturally occurring mutations in AR have yet to be observed at Met734, it is interesting to note that mutations at Val730 and Ile737 have been reported in patients with prostate cancer and androgen insensitivity, respectively (Newmark et al. 1992; Quigley et al. 1995; Gottlieb et al. 1998).

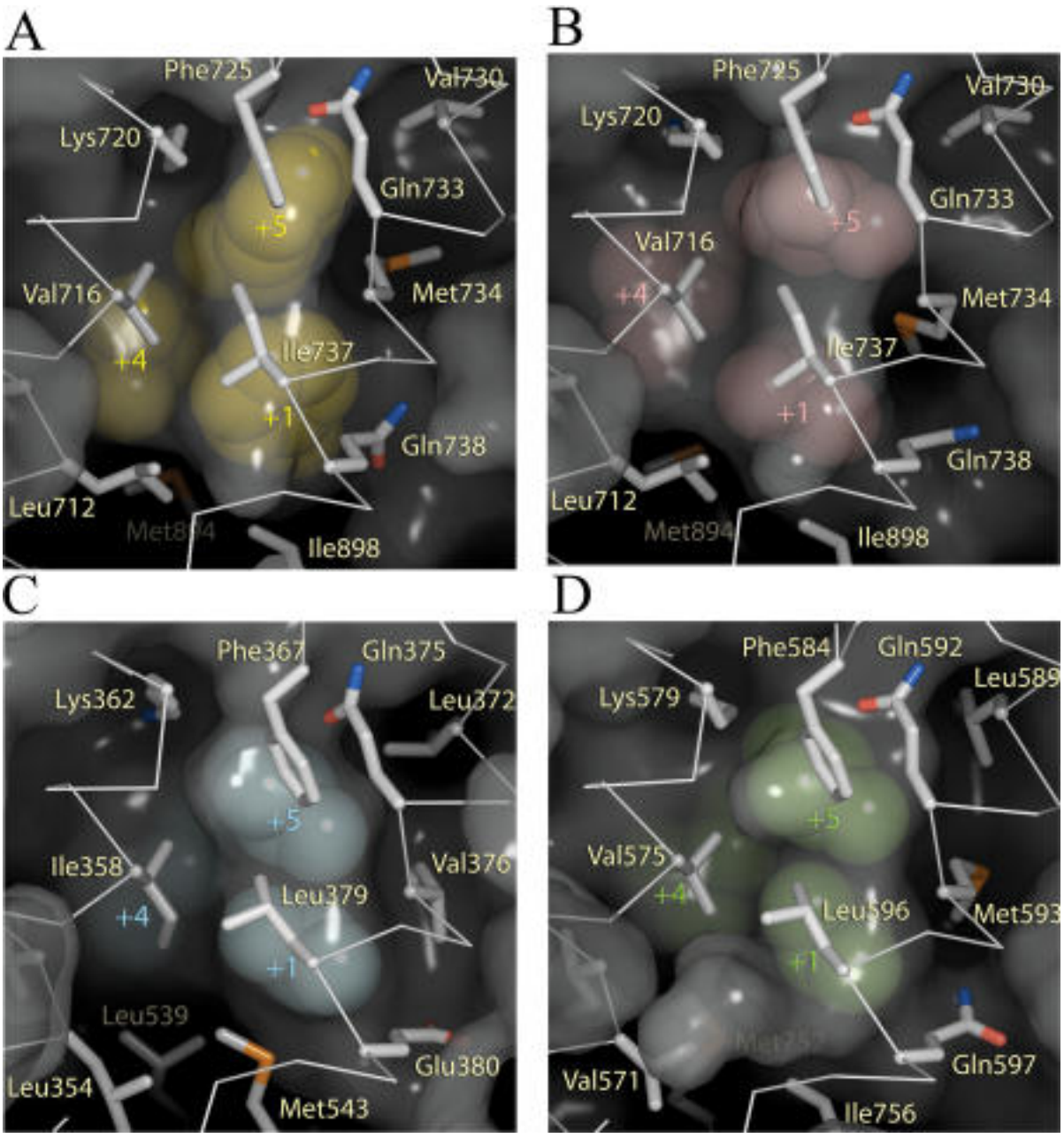

Figure 2-9. Surface Complimentarity of Hydrophobic Motifs in the AR, ERα, and GR AF-2 Clefts

The same characteristics that make the AR AF-2 ideal for binding of longer, aromatic side chains also make it less well suited for binding of shorter, branched side chains. Although changes in the position of Met734 widen the groove towards the +5 subsite to permit binding of leucine residues, the gross features of the groove remain largely the same (see Figure 2-9B). As a result, the +1 and +5 leucines bind in a smooth, elongated groove and interactions between the +1 and +5 residues on the face of the peptide helix, or with a hydrophobic "bump" present in other receptors caused by a isoleucine to leucine substitution between the +1 and +5 subsites, are absent. Thus, a smaller proportion of the available surface area is available for van der Waals interactions.

Unlike the conserved interaction modes of aromatic residues with the +1 and +5 sites, binding interactions at the +4 site are variable and characterized by nonspecific interactions. This finding agrees with the relatively high conservation of residues at the +1 and +5 positions of AR-interacting motifs and suggests that these residues drive peptide interaction with the LBD, whereas the +4 site is less critical. Indeed, the +4 pocket is shallow, surface exposed, and relatively featureless, explaining the assortment of residues selected at the +4 position. It is likely that any hydrophobic residue that does not clash with surrounding residues would be suitable at this subsite.

While peptide motif recognition is governed by hydrophobic interactions, polar interactions from backbone atoms and residues outside the core motif also contribute. With the exception of FxxFF, motifs containing phenylalanines at the +1 and +5 positions present canonical main chain interactions with both charge clamp residues, Lys720 and Glu897. This finding stands in contrast to predictions of previous studies (Alen et al. 1999; He et al. 1999;

Slagsvold et al. 2000; He and Wilson 2003), which concluded that Lys720 was dispensable for FxxLF binding and that Glu897 was required for binding to FxxLF and LxxLL motifs. Lys720 comprises a significant portion of the +5 subsite, making important van der Waals interactions with the Phe+5 benzyl group in addition to hydrogen bonds to the motif backbone. These results suggest that Lys720 is required for binding of FxxLF motifs. However, it may be that enough binding energy is provided by the other residues of the +5 subsite (i.e., Met734), as well as by the other subsites themselves, such that removal of Lys720 would have little effect on binding. Observations that Lys720 plays a greater role in LxxLL motif binding are likely due to the fact that there is less surface area contributing to van der Waals contacts in LxxLL motifs. Disrupting binding contributions from Lys720 would thus have a more detrimental effect on binding.
On the other hand, Glu897 interacts with the FxxLF peptide backbone, but is disengaged from the LxxLL peptide backbone. One possible explanation for the apparent requirement for Glu897 in LxxLL binding is that it might interact with residues outside of the core motif. The corresponding glutamate of GR, Glu 755, forms hydrogen bonds with the −3 asparagine of TIF2 NR box 3 (Bledsoe et al. 2002), and Glu897 of AR participates in noncanonical interactions with the hydroxyl group of a Ser−2 residue that was selected in all of our tryptophan-containing peptides. This is especially intriguing given that the only WxxLF motif known in vivo, located in the AR NTD, also possesses a Ser−2 residue. WxxLF also makes backbone interactions with an alternate charge clamp residue, Glu893, pointing towards adaptability in AR AF-2 charge clamp formation.

Sequence alignment of NR coactivator sequences shows that positively charged residues are favored N-terminal to the core hydrophobic motif while negatively charged residues are

favored C-terminal to the motif (He and Wilson 2003). Our phage-selected peptides are consistent with this trend. Arginines and lysines were observed at the N-terminal −1 position in all peptides, except for LxxLL, in which Arg was present at the −3 position. Moreover, four out of seven peptides contained negatively charged aspartate or glutamate residues C-terminal to the core motif. While previous studies have shown that complementary interactions between charged residues flanking coactivator signature motifs of coactivators and charged residues surrounding the AF-2 cleft modulated binding to the receptor (He and Wilson 2003), we find that the flanking charged residues are typically disordered in the electron density, with only Arg−1 of FxxLF interacting with Glu897, and Lys+2 of FxxYF forming a water-mediated hydrogen bond to Asp731. Thus, if charge–charge interactions between flanking peptide residues and the AR surface occur, they are too weak to be detected crystallographically.

Finally, the AR AF-2 surface is an attractive target for pharmaceutical design. Selective peptide inhibitors that bind the AF-2 surface of liganded ERα, ERβ, and TRβ have been developed (Geistlinger and Guy 2003), and similar α-helix–mediated protein–protein interfaces have successfully been targeted with tight binding small molecule inhibitors (Asada et al. 2003; Vassilev et al. 2004). Drugs that directly interfere with coactivator binding or formation of the AR N/C interaction would likely inhibit AR activity, perhaps even in androgen-resistant prostate cancers in which conventional therapies have failed. Strategies for designing AR coactivator antagonists are revealed in spite of the changes to the structure at the interface. Together the +1, +4, and +5 subsites contribute the majority of buried surface area of the peptide–LBD interaction (Table 2-2). Inhibitors may be designed by varying hydrophobic constituents at these hotspots. The +1 and +5 subsites of AR have a unique preference for aromatic side chains and provide the

most viable starting points for designing AR-specific inhibitors. Aromatic groups, possibly with polar constituents to exploit hydrogen bonding interactions with Gln733 and Gln738 in the +1 and +5 subsites, respectively, may provide promising leads. Indeed, initial screens have yielded compounds that bind to the +1 subsite in such a manner (E. Estébanez-Perpiñá, personal communication). Poorly conserved binding and a lack of strong structural features at the +4 subsite suggest that this site may be incorporated for achieving other characteristics important for inhibitors besides fit. Synthetic strategies that link together groups that bind with moderate affinity to the +1, +5, and possibly +4 subsites may yield tight binding inhibitors of AR coactivator association.

MATERIALS AND METHODS

Protein purification. Expression and purification of the AR LBD for crystallization were performed essentially as described (Matias et al. 2000). The cDNA encoding the chimp AR LBD (residues 663–919—human numbering), which displays 100% identity to the human form in protein sequence, was cloned into a modified pGEX-2T vector (Amersham Biosciences, Piscataway, New Jersey, United States) and expressed as glutathione S-transferase (GST) fusion protein in the E. coli strain BL21 (DE3) STAR in the presence of 10 μM DHT. Induction was carried out with 30 μM IPTG at 17 °C for 16–18 h. E. coli cells were lysed in buffer (10 mM Tris, [pH 8.0], 150 mM NaCl, 10% glycerol, 1 mM TCEP, 0.2 mM PMSF) supplemented with 0.5 μg/ml lysozyme, 5 U/ml benzonase, 0.5% CHAPS, and 10 μM DHT. All buffers for further purification steps contained 1 μM DHT. Soluble cell lysate was adsorbed to Glutathione Sepharose 4 Fast Flow resin (Amersham Biosciences), washed with buffer containing 0.1% n-

octyl β-glucoside, and eluted with 15 mM glutathione. After cleavage of the GST moiety with thrombin, final purification of the AR LBD was carried out using a HiTrap SP cation exchange column (Amersham Biosciences). Eluted AR LBD was dialyzed overnight at 4 °C against buffer containing 50 mM HEPES (pH 7.2), 10% glycerol, 0.2 mM TCEP, 20 μM DHT, 150 mM Li2SO4, and 0.1% n-octyl β-glucoside, then concentrated to greater than 4 mg/ml for crystallization.

Purification of AR LBD for use in phage affinity selection was carried out as above without the final dialysis and concentration steps. The expression construct contained the AR LBD as an inframe fusion with GST in a modified pGEX-2T vector containing both a flexible region and an AviTag sequence (Avidity, Denver, Colorado, United States) allowing in vivo biotinylation. The GST–AR LBD fusion expression plasmid was cotransformed with a plasmid-encoding E. coli biotin ligase (Avidity) into BL21 (DE3) STAR cells. Protein expression was carried out as above but with induction supplemented with 50 μM biotin to ensure quantitative biotinylation of AR LBD.

Phage affinity selections and peptide identification. Phage affinity selections were performed essentially as described (Paige et al. 1999). Biotinylated AR LBD (10 pmol/well) was incubated in streptavidin-coated Immulon 4 96-well plates (Dynatech International, Edgewood, New Jersey, United States) in TBST (10 mM Tris-HCl [pH 8.0], 150 mM NaCl, 0.05% Tween 20) with 1 μM DHT for 1 h at 4 °C. Affinity selections were performed in TBST containing 1 μM DHT. M13 phage distributed among 24 libraries displaying a total of greater than 2 × 1010 different random or biased amino acid sequences were added to the wells containing

immobilized AR LBD and incubated for 3 h at 4 °C. After washing, bound phage were eluted using pH 2 glycine. Enrichment of phage displaying target-specific peptides was monitored after each round of affinity selection using an anti-M13 antibody conjugated to horseradish peroxidase in an ELISA–type assay.

Synthetic peptides corresponding to the deduced amino acid sequences from receptor-specific phage were tested for their ability to interact with purified AR LBD using a FRET–based assay format. Peptides were synthesized according to the deduced amino acid sequence displayed on phage with an additional C-terminal amino acid sequence consisting of SGSGK to allow the attachment of a biotin tag (Anaspec, San Jose, California, United States). Flourophor conjugates were prepared by incubating either biotinylated peptides with streptavidin-cryptate (Cis Bio International, Bagnols Sur Ceze Cedex, France), or biotinylated AR LBD with streptavidin-XL665 (Cis Bio). Interaction between peptide and AR LBD was monitored by the ratio of energy transfer by excitation at 320 nm and emission at 625 nm and 665 nm.

Surface plasmon resonance. Affinities of peptides to the AR LBD were determined with a Biacore (Piscataway, New Jersey, United States) 2000 instrument. A peptide derived from silencing mediator for RXR and TR 2 (SMRT2) served as a negative control. 1 mM peptide stock solutions in DMSO were diluted into HBS-P buffer (10 mM HEPES [pH 7.4], 150 mM NaCl, 0.005% Surfactant P20) to generate 10 μM working solutions. HBS-P buffer was flowed through the cells to achieve a stable baseline prior to immobilization of the biotinylated peptides. To achieve the binding of approximately 250 RU of peptides to individual cells, working

solutions of peptides were diluted to 100 nM in HBS-P buffer. Unbound streptavidin sites were blocked by injection of a 1 mM biotin solution at a rate of 10 µl/min.

Purified AR LBD was diluted into HBS-P buffer to a concentration of 10 µM and injected into all four Flowcells using the Kinject protocol at a flow rate of 10 µl/min (contact time 360 s, dissociation time 360 s). Following the dissociation phase, the surface of the chip was regenerated to remove residual AR LBD by QuickInject of buffer containing 10 mM HEPES and 50% ethylene glycol (pH 11). Following the establishment of a stable baseline, the same procedure was repeated using a series of AR LBD dilutions (5 µM, 1 µM, and 300 nM) in an iterative manner. Analysis of the data was performed using BIAevaluation 3.0 software (Biacore). The SMRT2 signals were subtracted as background from the three remaining peptide signals. Data were best fit using the two-state conformational change model (Warnmark et al. 2001,2002).

Crystallization, data collection, and refinement. Purified, concentrated AR LBD was combined with 3x to 6x molar excess of peptide and incubated 1 h at room temperature before crystallization trials. Complexes were crystallized using the hanging drop vapor diffusion method. Protein–peptide solution was combined in a 1:1 ratio with a well solution consisting of 0.6–0.8 M sodium citrate and 100 mM Tris or HEPES buffer (pH 7–8). Crystals typically appeared after 1–2 d, with maximal size attained within 2 wk. For data collection, crystals were swiped into a cryo-protectant solution consisting of well solution plus 10% glycerol before flash freezing in liquid nitrogen. The addition of ethylene glycol to a well concentration of 10%–20%

was later found to both improve crystal quality and enable the freezing of crystals directly out of the drop.

Datasets were collected at 100K at the Advanced Light Source (Lawrence Berkeley Laboratory, Berkeley, California, United States), beamline 8.3.1, with either a ADSC Quantum 315 or Quantum 210 CCD detector. Data were processed using Denzo and Scalepack (Otwinowski and Minor 1997). Molecular replacement searches were performed with rotation and translation functions from CNS (Brunger et al. 1998). Initial searches for AR–FxxLF were performed using the structure of AR–R1881 (PDB: 1E3G) with R1881 omitted from the search model. Subsequent searches for all other complexes were performed using the refined LBD structure from the AR–FxxLF complex. To minimize the possibility of model bias, FxxLF peptide and DHT were omitted from all molecular replacement searches. Protein models were built by iterative rounds of simulated annealing, conjugate gradient minimization, and individual B-factor refinement in CNS followed by manual rebuilding in Quanta 2000 (Accelrys, San Diego, California, United States) using σA-weighted 2Fo − Fc, Fo −Fc, and simulated annealing composite omit maps. Superposition of structures was performed with LSQMAN (Kleywegt 1996). Buried surface area calculations were performed with CNS. All figures were generated with PyMOL (DeLano 2002). Coordinates and structure factors for all complexes have been deposited in the Protein Data Bank. Accession numbers are listed in Table 2-2.

SUPPORTING INFORMATION

Accession Numbers. The Swiss-Prot (http://www.ebi.ac.uk/swissprot) accession numbers for the gene products discussed in this paper are AR (P10275), ARA54 (Q9UBS8), ARA55 (Q9Y2V5), ARA70 (Q13772), ER (P03372, Q92731), glucocorticoid receptor-interacting protein 1 NR box 3 (Q61026), GR (P04150), NR box 3 of TIF2 (Q15596), and TR β (P10828).
The Protein Data Bank (http://www.rcsb.org/pdb) accession numbers for the structures used in this paper are FxxFF (1T73), FxxLF (1T7R), FxxLW (1T79), FxxYF (1T7M), LxxLL (1T7F), unbound (1T7T), WxxLF (1T74), and WxxVW (1T76).

ACKNOWLEDGEMENTS

We would like to thank Erin Anderson-Chisenhall for assistance in protein purification, James Holton and the staff at ALS beamline 8.3.1 for assistance in data collection, and Paul Webb for critical review of the manuscript. This work was supported by funds from the Prostate Cancer Foundation and National Institutes of Health grant R21 CA95324 to RJF.

Author contributions.

EH, BB, and RF conceived and designed the experiments. EH, SP, ESP, HG, and BB performed the experiments. EH, SP, ESP, HG, BB, and RF analyzed the data. BB and RF contributed reagents/materials/analysis tools. EH, BB, and RF wrote the paper.
Academic Editor: Ueli Schibler, University of Geneva

REFERENCES

1. Alen P, Claessens F, Verhoeven G, Rombauts W, Peeters B. The androgen receptor amino-terminal domain plays a key role in p160 coactivator-stimulated gene transcription. Mol Cell Biol. 1999;19:6085–6097.

2. Asada S, Choi Y, Uesugi M. A gene-expression inhibitor that targets an alpha-helix-mediated protein interaction. J Am Chem Soc. 2003;125:4992–4993.

3. Bledsoe RK, Montana VG, Stanley TB, Delves CJ, Apolito CJ, et al. Crystal structure of the glucocorticoid receptor ligand binding domain reveals a novel mode of receptor dimerization and coactivator recognition. Cell. 2002;110:93–105.

4. Brunger AT, Adams PD, Clore GM, DeLano WL, Gros P, et al. Crystallography & NMR system: A new software suite for macromolecular structure determination. Acta Crystallogr D Biol Crystallogr. 1998;54:905–921.

5. Chang C, Norris JD, Gron H, Paige LA, Hamilton PT, et al. Dissection of the LXXLL nuclear receptor-coactivator interaction motif using combinatorial peptide libraries: Discovery of peptide antagonists of estrogen receptors alpha and beta. Mol Cell Biol. 1999;19:8226–8239.

6. Culig Z, Klocker H, Bartsch G, Hobisch A. Androgen receptors in prostate cancer. Endocr Relat Cancer. 2002;9:155–170.

7. Darimont BD, Wagner RL, Apriletti JW, Stallcup MR, Kushner PJ, et al. Structure and specificity of nuclear receptor-coactivator interactions. Genes Dev. 1998;12:3343–3356.

8. DeLano WL. The PyMOL molecular graphics system. Available: http://www.pymol.org via the Internet. 2002 Accessed 2 July 2004.

9. Ding XF, Anderson CM, Ma H, Hong H, Uht RM, et al. Nuclear receptor-binding sites of coactivators glucocorticoid receptor interacting protein 1 (GRIP1) and steroid receptor coactivator 1 (SRC-1): Multiple motifs with different binding specificities. Mol Endocrinol. 1998;12:302–313.

10. Geistlinger TR, Guy RK. Novel selective inhibitors of the interaction of individual nuclear hormone receptors with a mutually shared steroid receptor coactivator 2. J Am Chem Soc. 2003;125:6852–6853.

11. Glass CK, Rosenfeld MG. The coregulator exchange in transcriptional functions of nuclear receptors. Genes Dev. 2000;14:121–141.

12. Gottlieb B, Lehvaslaiho H, Beitel LK, Lumbroso R, Pinsky L, et al. The Androgen Receptor Gene Mutations Database. Nucleic Acids Res. 1998;26:234–238.

13. Gregory CW, He B, Johnson RT, Ford OH, Mohler JL, et al. A mechanism for androgen receptor-mediated prostate cancer recurrence after androgen deprivation therapy. Cancer Res. 2001;61:4315–4319.

14. He B, Wilson EM. Electrostatic modulation in steroid receptor recruitment of LXXLL and FXXLF motifs. Mol Cell Biol. 2003;23:2135–2150.

15. He B, Kemppainen JA, Voegel JJ, Gronemeyer H, Wilson EM. Activation function 2 in the human androgen receptor ligand binding domain mediates interdomain communication with the NH(2)-terminal domain. J Biol Chem. 1999;274:37219–37225.

16. He B, Kemppainen JA, Wilson EM. FXXLF and WXXLF sequences mediate the NH2-terminal interaction with the ligand binding domain of the androgen receptor. J Biol Chem. 2000;275:22986–22994.

17. He B, Lee LW, Minges JT, Wilson EM. Dependence of selective gene activation on the androgen receptor NH2- and COOH-terminal interaction. J Biol Chem. 2002a;277:25631–25639.

18. He B, Minges JT, Lee LW, Wilson EM. The FXXLF motif mediates androgen receptor-specific interactions with coregulators. J Biol Chem. 2002b;277:10226–10235. 37219–37225.

19. Hsu CL, Chen YL, Yeh S, Ting HJ, Hu YC, et al. The use of phage display technique for the isolation of androgen receptor interacting peptides with (F/W)XXL(F/W) and FXXLY new signature motifs. J Biol Chem. 2003;278:23691–23698.

20. Kleywegt GJ. Use of noncrystallographic symmetry in protein structure refinement. Acta Crystallogr D Biol Crystallogr. 1996;52:842–857.

21. Langley E, Kemppainen JA, Wilson EM. Intermolecular NH2-/carboxyl-terminal interactions in androgen receptor dimerization revealed by mutations that cause androgen insensitivity. J Biol Chem. 1998;273:92–101.

22. Lee HJ, Chang C. Recent advances in androgen receptor action. Cell Mol Life Sci. 2003;60:1613–1622.

23. Matias PM, Donner P, Coelho R, Thomaz M, Peixoto C, et al. Structural evidence for ligand specificity in the binding domain of the human androgen receptor. Implications for pathogenic gene mutations. J Biol Chem. 2000;275:26164–26171.

24. Needham M, Raines S, McPheat J, Stacey C, Ellston J, et al. Differential interaction of steroid hormone receptors with LXXLL motifs in SRC-1a depends on residues flanking the motif. J Steroid Biochem Mol Biol. 2000;72:35–46.

25. Newmark JR, Hardy DO, Tonb DC, Carter BS, Epstein JI, et al. Androgen receptor gene mutations in human prostate cancer. Proc Natl Acad Sci U S A. 1992;89:6319–6323.

26. Nolte RT, Wisely GB, Westin S, Cobb JE, Lambert MH, et al. Ligand binding and co-activator assembly of the peroxisome proliferator-activated receptor-gamma. Nature. 1998;395:137–143.

27. Norris JD, Paige LA, Christensen DJ, Chang CY, Huacani MR, et al. Peptide antagonists of the human estrogen receptor. Science. 1999;285:744–746.

28. Northrop JP, Nguyen D, Piplani S, Olivan SE, Kwan ST, et al. Selection of estrogen receptor beta- and thyroid hormone receptor beta-specific coactivator-mimetic peptides using recombinant peptide libraries. Mol Endocrinol. 2000;14:605–622.

29. Otwinowski Z, Minor W. New York: Academic Press; 1997. Processing of X-ray diffraction data collected in oscillation mode. In: Carter CW, Sweet RM, editors. Methods in enzymology: Macromolecular crystallography, Part A; pp. 307–326.

30. Paige LA, Christensen DJ, Gron H, Norris JD, Gottlin EB, et al. Estrogen receptor (ER) modulators each induce distinct conformational changes in ER alpha and ER beta. Proc Natl Acad Sci U S A. 1999;96:3999–4004.

31. Quigley CA, De Bellis A, Marschke KB, el-Awady MK, Wilson EM, et al. Androgen receptor defects: Historical, clinical, and molecular perspectives. Endocr Rev. 1995;16:271–321.

32. Sack JS, Kish KF, Wang C, Attar RM, Kiefer SE, et al. Crystallographic structures of the ligand-binding domains of the androgen receptor and its T877A mutant complexed with the natural agonist dihydrotestosterone. Proc Natl Acad Sci U S A. 2001;98:4904–4909.

33. Shiau AK, Barstad D, Loria PM, Cheng L, Kushner PJ, et al. The structural basis of estrogen receptor/coactivator recognition and the antagonism of this interaction by tamoxifen. Cell.1998;95:927–937.

34. Slagsvold T, Kraus I, Bentzen T, Palvimo J, Saatcioglu F. Mutational analysis of the androgen receptor AF-2 (activation function 2) core domain reveals functional and mechanistic differences of conserved residues compared with other nuclear receptors. Mol Endocrinol. 2000;14:1603–1617.

35. Vassilev LT, Vu BT, Graves B, Carvajal D, Podlaski F, et al. In vivo activation of the p53 pathway by small-molecule antagonists of MDM2. Science. 2004;303:844–848.

36. Wang Q, Lu J, Yong EL. Ligand- and coactivator-mediated transactivation function (AF2) of the androgen receptor ligand-binding domain is inhibited by the cognate hinge region. J Biol Chem. 2001;276:7493–7499.

37. Warnmark A, Almlof T, Leers J, Gustafsson JA, Treuter E. Differential recruitment of the mammalian mediator subunit TRAP220 by estrogen receptors ERalpha and ERbeta. J Biol Chem. 2001;276:23397–23404.

38. Warnmark A, Treuter E, Gustafsson JA, Hubbard RE, Brzozowski AM, et al. Interaction of transcriptional intermediary factor 2 nuclear receptor box peptides with the coactivator binding site of estrogen receptor alpha. J Biol Chem. 2002;277:21862–21868.

Chapter 3

Purification and characterization of apo glucocorticoid receptor ligand binding domain

INTRODUCTION

The glucocorticoid receptor mediates transcription of target genes in response to steroid binding to its C-terminal ligand binding domain. Prior to ligand binding, GR is maintained in the cytoplasm by a complex of chaperone proteins including Hsp90, Hsp70, Hsp40, HOP, p23, and FKBP-51. Interaction with the chaperone complex is also mediated by the ligand binding domain, and is required for high-affinity ligand binding to the receptor. As the binding of steroid completes formation of the LBD's hydrophobic core, unliganded nuclear receptors are notoriously unstable and have rarely been accessible in the test tube.

Initial Purification of apo GR LBD

After initial attempts to purify functional, recombinant GR LBD in the presence of agonists were unsuccessful, we aimed to purify apo GR. Our strategy was to express a double-mutant form of the human GR LBD (residues 521-777, F602S, C638D) shown to enhance protein solubility. An additional step taken to enhance receptor solubility was to express the LBD as a glutathione-s-transferase (GST) fusion protein. GST is a 26 kDa protein that is commonly used as a fusion partner for recombinant expression due to its high solubility and its ability to be used as an affinity purification tag.

Initial success in GST-GR LBD expression was achieved with a protocol similar to that used in the purification of PR LBD.(Williams & Sigler, 1998) Protein expression in BL21(DE3) *E. Coli* was carried out at 15^{o} C for 16-24 hours in standard LB media with no added ligand. Cells were lysed by sonication in a buffer containing 50 mM Tris pH 8.0, 150 mM NaCl, 10 mM DTT, 2 M Urea. The addition of urea at moderate concentration as a light denaturant had been

previously shown to enhance recovery of NR LBDs from bacterial pellets. The clarified lysate was incubated with glutathione-sepharose resin and subsequently eluted with glutathione while the lysate pellets were resuspended in the above buffer with urea concentration increased to 3 M. The resuspended pellets were incubated on ice overnight before additional sonification, clarification, and affinity purification. Protein yield was typically better from the 3 M urea resuspended pellets, with very little GST-GR remaining soluble after the initial lysis.

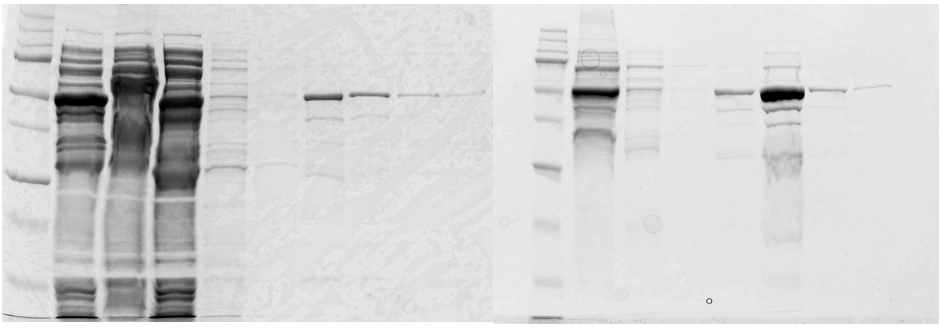

Figure 3-1. *Initial purification of GR LBD (F602S, C638D)*. Left gel lanes from left to right (non-urea lysis): MW ladder, crude lysate, insoluble portion, soluble portion, glutathione column wash, glutathione column elutions. Right gel lanes from left to right (2M urea lysis, 3M urea recovery): 1. MW ladder, 2-4 initial glutathione column elutions, 5-8 3M urea-recovered glutathione column elutions.

In order to assess the functionality of the purified GST-GR LBD, we performed fluorescence polarization (FP) steroid binding assays, using fluorescein-labeled dexamethasone (dex-fl) as the binding probe. Prior to the experiment, GR was dialyzed into a buffer containing 50 mM Tris-HCl pH 8.0, 100 mM NaCl, 10% Glycerol, 10 mM DTT. In order to perform this experiment with GR expressed in the presence of dex, this dialysis step was used to remove bound ligand from the receptor. After dialysis, serial dilutions of GR were mixed with 10 nM dex-fl and allowed to equilibrate for 30-60 minutes. Fluorescence polarization was measured in

opaque, 384-well plates on an Analyst AD plate reader. Two representative experiments (GR expressed ± dex) are shown in figure 3-2.

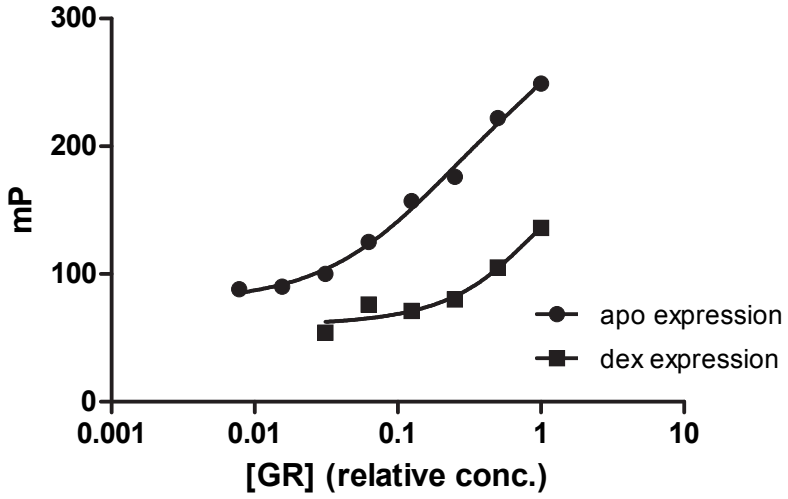

Figure 3-2. *Fluorescence polarization GR ligand binding assay*. GST-GR LBD prepared in the presence of followed by dialysis to remove dex (squares) and GST-GR LBD prepared without dex (circles) binding to 10 nM dexamethasone-fluorescein

As indicated by the increased dynamic range and dose-response of dex-fl polarization, GST-GR expressed without ligand appeared to have greater steroid binding capability in our preliminary experiments. This coupled with the enhanced protein yield, led us to pursue this strategy for protein production.

As our interest was in producing GR for structural and biochemical study, we wanted to simplify the system by completely isolating the LBD. To that end, cleavage of the GST-fusion tag was a necessary step. In addition to introducing a heterologous sequence at the N-terminus of the LBD, GST forms dimers, which may have had unintended consequences on the LBD to which it was fused. Cleavage of GST from GR was performed with thrombin at 4^{o} C for 12-20 hours. Typical cleavage results are shown in figure 3-3.

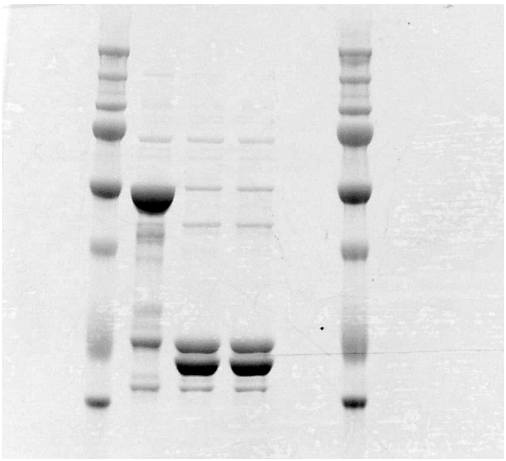

Figure 3-3. *Thrombin cleavage of GST-GR LBD*. Lanes from left to right: 1. MW ladder, 2. uncleaved GST-GR, 3-4 cleaved GST-GR. GST is the lower band and appears more prevalent due to precipitation of GR from solution.

Upon cleavage from GST, much of the GR LBD precipitated out of solution, while GST remained predominantly soluble. Recombinant GR's reputation as an unstable protein made this result predictable, yet disappointing, as our already low protein yield became even lower. Further attempts to purify the remaining soluble GR by FPLC were mostly unsuccessful due to the small quantities of protein available. A partial solution was elucidated based on personal communications with Andy Shiau. His suggestion for prevention of LBD precipitation was to include NR box peptide to the cleavage mixture at high concentration. 2x molar excess GRIP1 box 3 was added to the cleavage mixture henceforth, as indeed its presence reduced the amount of observed precipitant upon thrombin cleavage.

Further purification was again complicated by protein stability issues. Thrombin cleavage products were run on a Superdex-200 (23 mL bed volume) gel filtration column to separate GR LBD from GST and other impurities. Figure 3-4 shows a typical UV absorbance curve resulting from a Superdex-200 run.

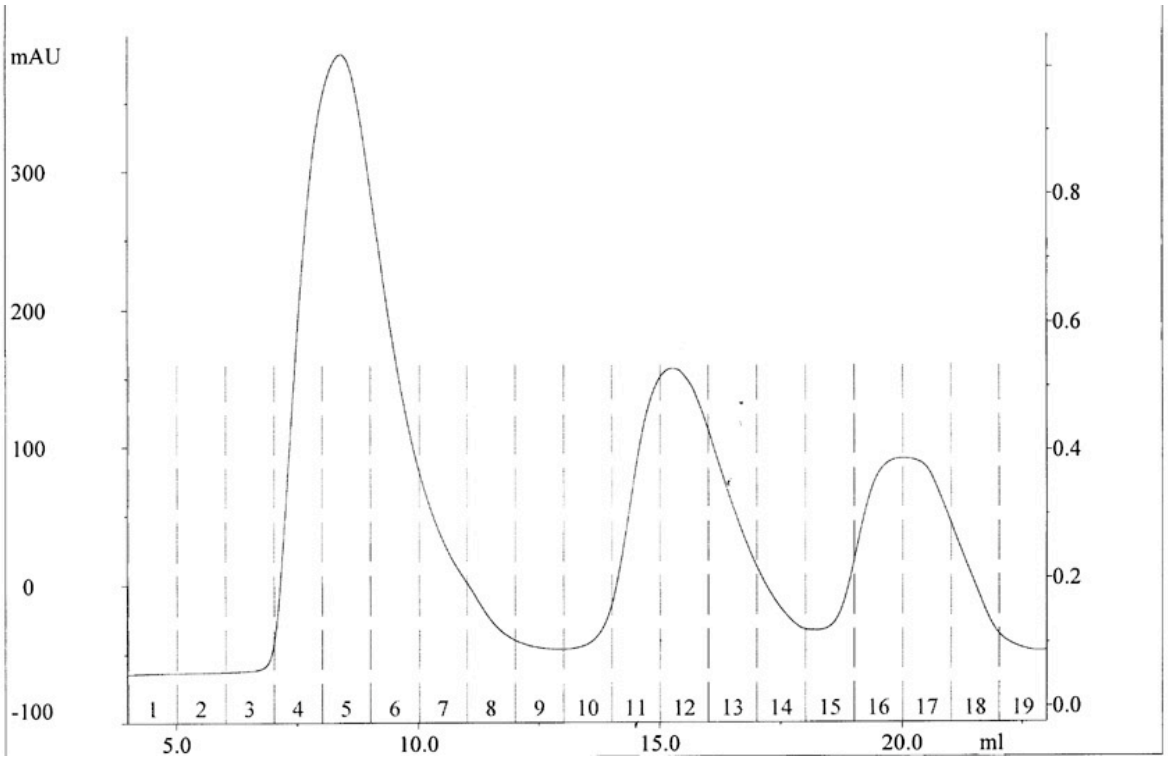

Figure 3-4. *Gel filtration of GST-GR thrombin cleavage products.* First peak is soluble aggregate GR (gel lanes 2-5), second peak is GST (gel lanes 7-9), third peak is co-activator peptide.

The first peak, ~8 mL elution volume, contains GR LBD in addition to several high molecular weight impurities. The GST dimer elutes in a separate peak around 13 mL. Although the prime objective of separating GR from GST had been accomplished, the elution volume of GR was disconcerting. On a gel filtration column, higher molecular weight particles elute faster than LMW particles, due to their inability to fully enter the gel matrix. We expected a GR LBD monomer to elute later than the GST dimer based on weight alone (30 kDa vs. 52 kDa). An early elution profile is indicative of high-order aggregated species. Even with NR box peptide present to prevent precipitation of GR from solution, it appeared as though GR LBD took a soluble aggregate form. Further evidence of protein instability was our inability to concentrate the GR containing fractions. All attempts to concentrate led to a complete loss of protein.

Zwittergent 3-12-aided GR purification

As our previous protocols had failed to yield GR suitable for biochemical study, we began to incorporate various detergents at low to medium concentration in our preparations. A recent study by McLaughlin and Jackson had shown uccess in purifying recombinant apo GR LBD using the zwitterionic detergent Zwittergent 3-12.**(McLaughlin & Jackson, 2002)** Their work had shown biophysical characterizations of WT GR LBD prepared in the presence and absence of zwittergent 3-12. Due to the authors' use of the WT GR sequence, which is highly unstable, they were forced to purify refolded GR from inclusion bodies, as recombinant expression yielded primarily aggregated protein. Notably, they saw differences in GR's elution profile from a Superdex-200 column depending on inclusion of zwittergent 3-12 in the refolding buffer. GR prepared without zwittergent 3-12 eluted ~8 mL, as it had in our hands, while detergent-prepared protein eluted ~14 mL. This elution profile matched standard curves well for a protein with MW = 30 kDa.

We employed a modified version of the McLaughlin protocol for purification of apo GR LBD (F602S, C638D). Cultures were grown and induced similarly as with our previous protocol, with the key difference in prep being the lysis / purification buffer ingredients. GST-GR-containing cells were harvested and lysed in a buffer containing 50 mM Tris-HCl pH 8.0, 150 mM NaCl, 0.1 % Zwittergent, 2 mM mono-thio-glycerol. Passage over glutathione resin was again the first purification step, followed by thrombin cleavage. Our previous protocol had yielded unstable GR LBD that aggregated upon cleavage from GST. GR prepared in zwittergent

3-12 remained completely soluble upon cleavage, with or without the inclusion of NR box peptide.

Several strategies were employed to fully purify zwittergent 3-12-stabilized GR LBD. Separation of GR from GST was accomplished through either a second passage over glutathione resin or passage over a 5 mL HiTrap Q anion exchange column. Both techniques yielded slightly heterogenous GR samples in contrast to our previous samples, we were able to concentrate readily. Final purification was accomplished with a Superdex-200 column. As in McLaughlin and Jackson's paper, GR prepared with zwittergent 3-12 eluted later off of the gel filtration column, indicating a particle of more appropriate size (figure 3-5).

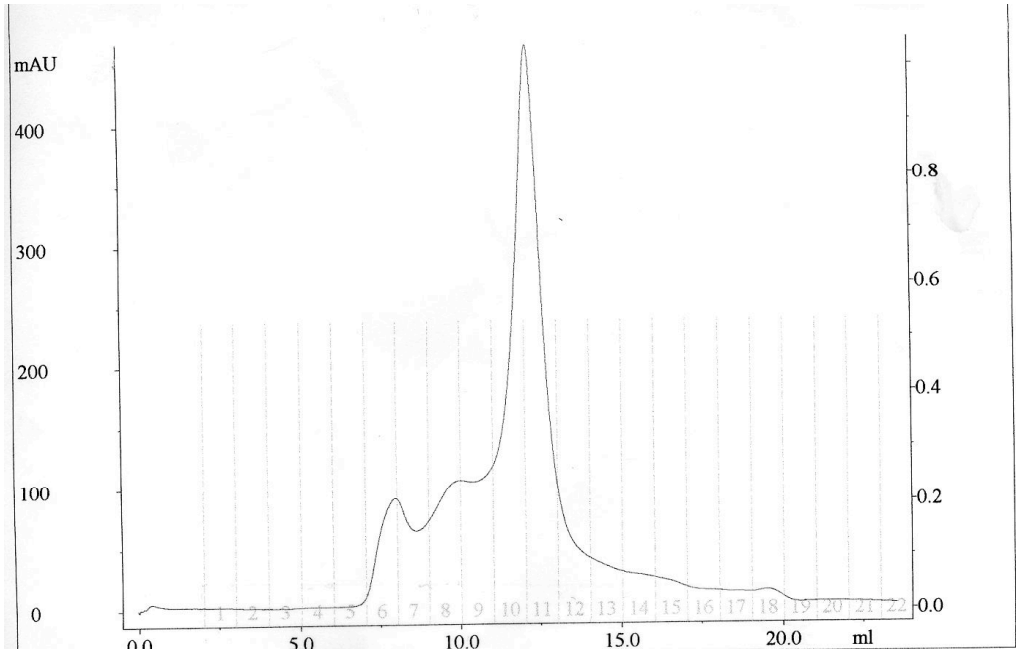

Figure 3-5. *Gel filtration of GR LBD in zwittergent 3-12.* Dominant peak is GR LBD. Gel lanes from left to right: MW ladder, fractions 10-12 concentrated, fractions 9-13.

Biophysical characterization of zwittergent 3-12 purified GR LBD

Various biophysical techniques were employed to characterize GR LBD purified with zwittergent 3-12. Circular dichroism showed GR to be helical in the presence or absence of 10 μM dexamethasone (figure 3-6).

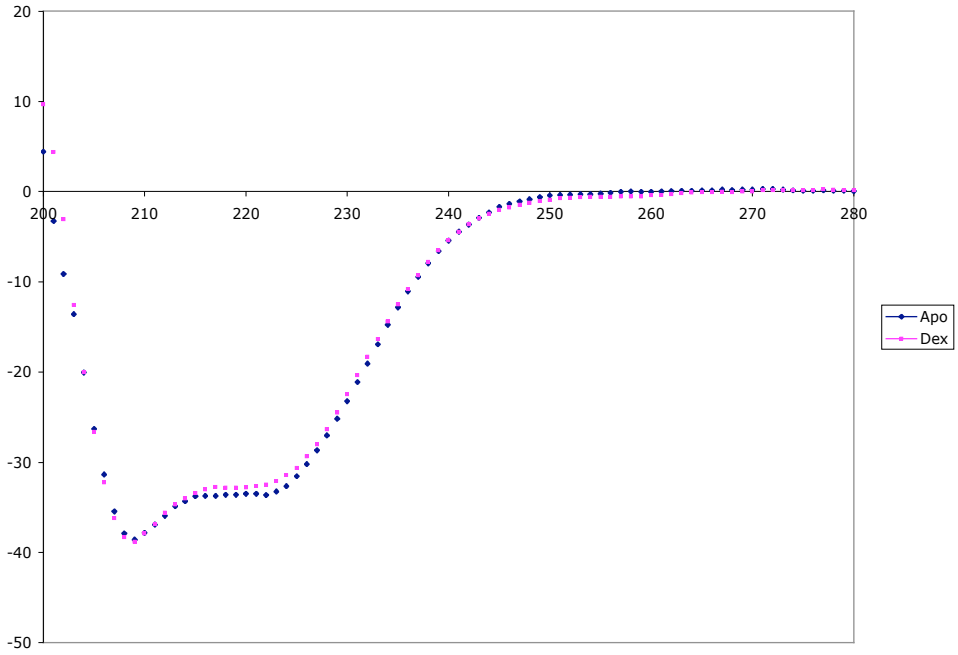

Figure 3-6. *Circular dichroism spectrum of GR LBD in zwittergent 3-12.* CD spectra taken at room temperature in 50 mM Tris-HCl pH 8.0, 150 mM NaCl, 0.1% zwittergent 3-12, 2 mM MTG, ± 10 μM dex shows GR to be helical.

The CD data was reminiscent of results by McLauglin and Jackson. The similarity between + dex and - dex conditions was expected as the LBD is not expected to undergo large scale conformational rearrangement upon ligand binding.

To gauge the particle size of GR in our hands, we used equilibrium analytical ultracentrifugation (AUC). Results and fitting of an AUC run are shown in figure 3-7. AUC was conducted in the zwittergent 3-12-containing lysis buffer listed above, with or without added dex. The best fit to the AUC data was achieved using a two-particle model with particle sizes of

45 kDa and 60 kDa. The lack of a dominant species ~30 kDa, the predicted MW of a GR LBD monomer, was again disconcerting.

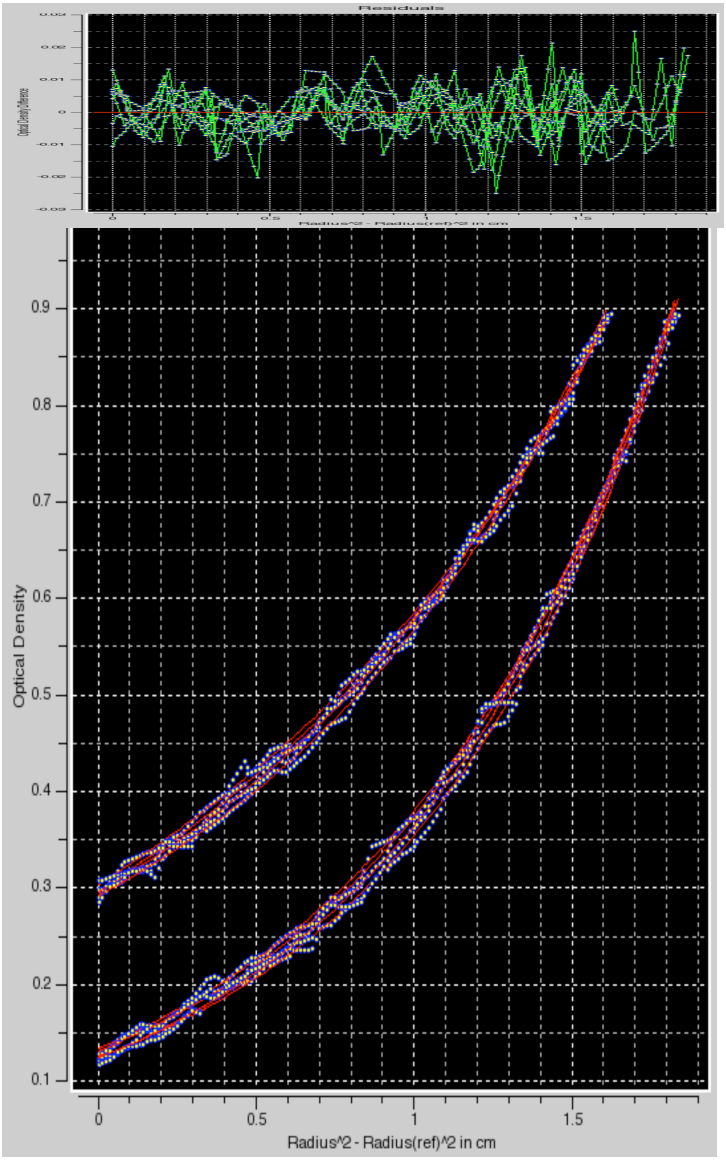

Figure 3-7. *Analytical ultra-centrifugation of GR LBD in zwittergent 3-12.* Equilibrium AUC at 4^0 C in the presence of 0.1% zwittergent 3-12 and 10 μM dex. Top panel, residuals.

As zwittergent 3-12 containing buffers proved unsuitable for fluorescence polarization ligand binding studies (figure 3-8), ligand binding to purified GR LBD was assayed indirectly.

We chose to monitor protein susceptibility to subtillisin cleavage in the presence and absence of dex, as a measure of overall protein stability (figure 3-9). A stable protein samples a small portion of conformational space, providing limited access to segments of the protein that can be cleaved by a protease such as subtillisin. GR was completely cleaved by subtillisin within 30 min at 4^0 C. GR that had been incubated with dex before and during cleavage showed a slightly-enhanced resistance to cleavage, indicating a ligand-induced conformational tightening.

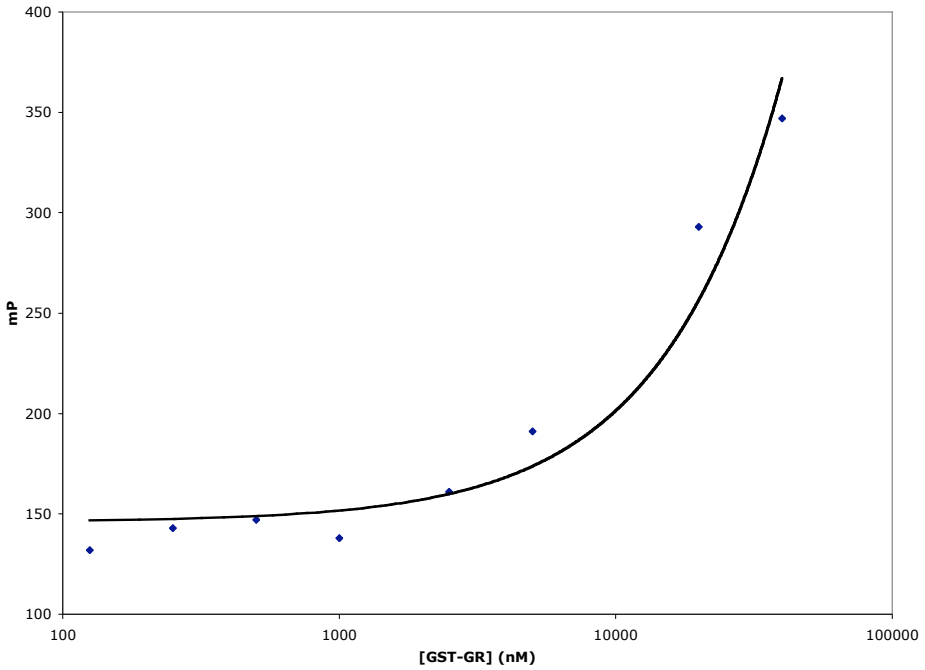

Figure 3-8. *FP ligand binding in the presence of zwittergent 3-12.* GST-GR in 0.1% zwittergent 3-12 titrated against 10 nM dex-fl.

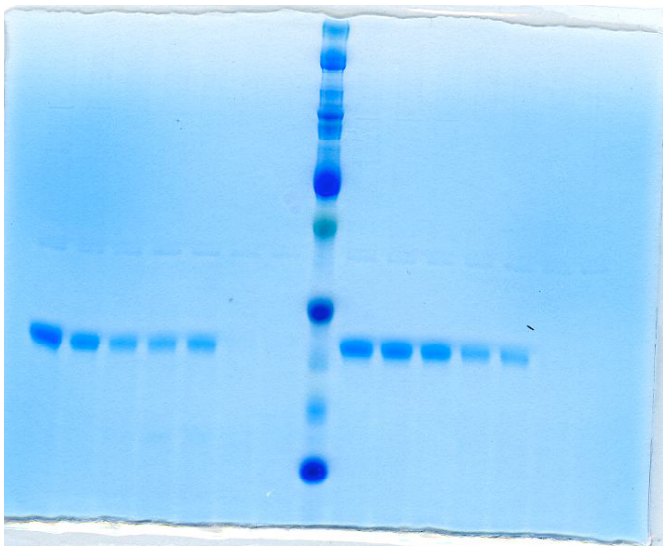

Figure 3-9. *Partial proteolysis of GR LBD.* GR LBD in zwittergent 3-12 was subjected to proteolysis by subtillisin in the absence (left lanes) or presence (right lanes) of dex. Lanes represent time-points 0, 2 min, 5 min, 10 min, 15 min, 20 min, 30 min.

GR in zwittergent 3-12 crystallization trials

Efforts to crystallize apo GR LBD and GR LBD in complex with dex and various coactivator peptides yielded little success. Apo GR LBD in zwittergent 3-12 containing buffer was concentrated to > 3 mg/mL and screened against the following conditions: Nextal Classics, Classics Lite, JCSG+, Cations, Anions, PEGS, pHClear, Pro Complex, and Molecular Dimensions NR LBD 1 and 2. No crystals were obtained, but interesting patterns of phase separation and ordered precipitation were seen (figure 3-10). GR / dex / coactivator peptide complexes were screened against Nextal Classics, Anions, and Molecular Dimensions NR LBD 1 and 2 with similar results.

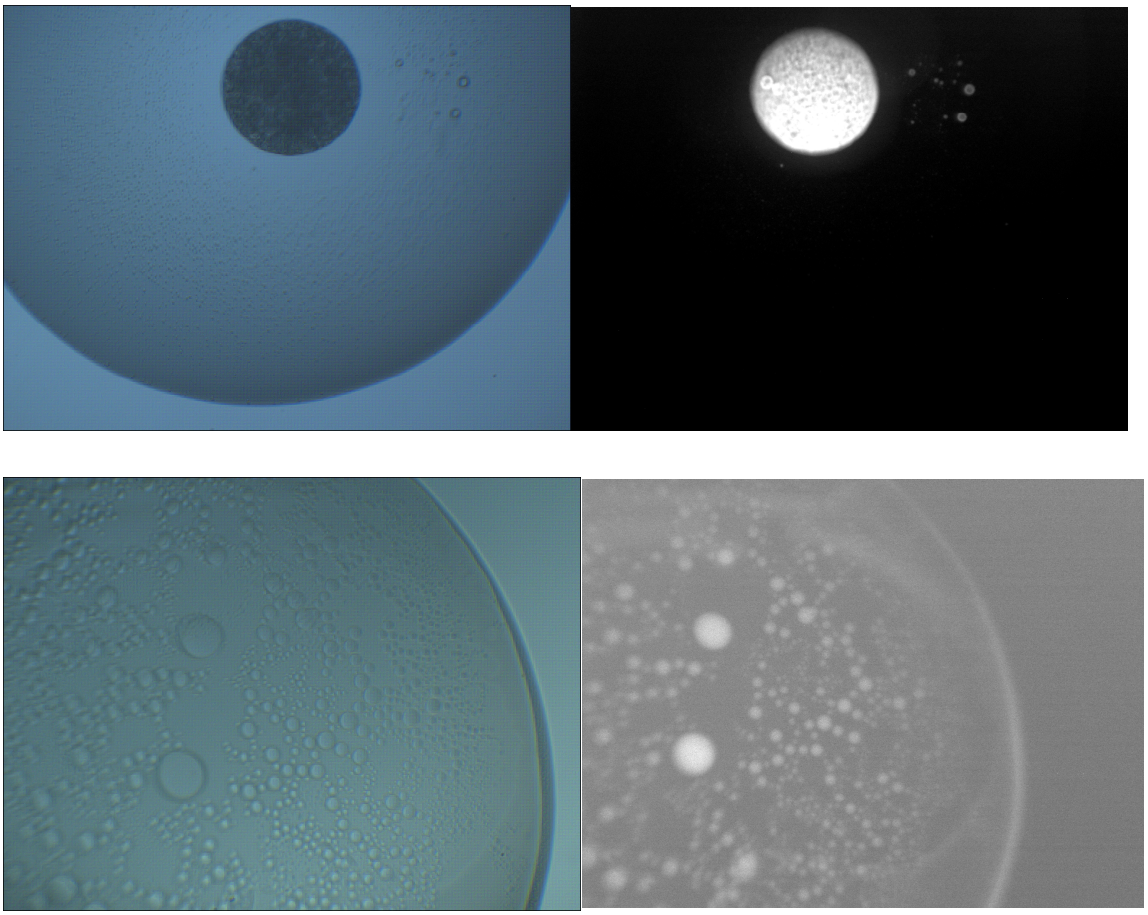

Figure 3-10. *GR LBD crystallization trials.* Left panels, visible light microscope images of ordered precipitates. Right panels, UV microscope images of same drops showing that precipitates are protein.

REFERENCES

McLaughlin SH, Jackson SE (2002) Folding and stability of the ligand-binding domain of the glucocorticoid receptor. *Protein Sci* **11**(8)**:** 1926-1936

Williams SP, Sigler PB (1998) Atomic structure of progesterone complexed with its receptor. *Nature* **393**(6683)**:** 392-396

Chapter 4

Purification and functional characterization of hormone-bound glucocorticoid receptor

INTRODUCTION

Steroid receptors are activated by binding to specific steroid hormones in the cell cytoplasm. Many receptors, including GR and AR, can be activated by diverse sets of ligands, both natural and synthetic, possessing a steroid backbone or not. Genomic output from receptors typically varies based on ligand identity, with many receptors being able to bind agonist, antagonist, partial agonist, and selective modulator compounds. The mechanisms by which different ligands produce different transcriptional outcomes depends on cellular context, notably on the quantities and identities of co-regulators available. In order to explore the mechanisms by which different GR ligands lead to specific patterns of transcription, we aimed to produce GR LBD in several ligand contexts, and determine the ligand-dependent pattern of co-regulator recruitment to the LBD's AF-2 surface.

Purification of hormone-bound GR LBD

Steroid receptors are most commonly expressed recombinantly with the ligand of interest, followed by exchange into a buffer with a different ligand if so desired. Difficulties in expressing AR with ligands other than DHT and the inability to readily exchange out DHT post-purification made us hesitant to pursue the same strategy with GR. Attempting to overcome this, our initial GR strategy, detailed in chapter 3, was to express the receptor in the absence of ligand, allowing easy addition of ligand after purification was complete. This technique, however, failed to produce appropriate quantities of functional receptor for biochemical and structural study.

Although several crystal structures of GR had been solved, the purification protocols detailed in these studies were never able to yield functional receptors in our hands.**(Biggadike et**

al, 2008; Bledsoe et al, 2002; Kauppi et al, 2003; Suino-Powell et al, 2008) A study by Kroe et al., however, provided us a with a protocol that was robust and produced soluble, functional GR LBD.**(Kroe et al, 2007)** The protocol is very similar to our initial purification procedure from chapter 3, with the key differences being the amount of ligand added during expression and addition of the detergent CHAPS at various concentrations throughout preparation. Our modified version of the Kroe protocol follows.

Initially, we used the standard human GR DNA sequence, but later switched with great success to a construct that had been codon-optimized for *E. Coli* expression by GeneArt. Codon optimization improved protein yield from < 0.5 mg/L of culture to > 3 mg/L on average. 6His-tagged GR LBD (F602S, C638D, 521-777) was transformed into BL21(DE3) *E. Coli* and grown in 2x LB media at 30^0 C until OD_{600} ~ 0.8. The temperature was then dropped to 15^0 C and expression was induced with 200 μM IPTG and 200 μM ligand. Cells were grown for 16-20 hours and harvested by centrifugation. Lysis by sonication was carried out on ice in a buffer containing 50 mM Tris-HCl pH 8.0, 150 mM NaCl, 10% glycerol, 2 M urea, 0.2 mM TCEP, 10 mM imidazole, 0.04% CHAPS, 10 μM dexamethasone. Lysates were clarified by centrifugation at 30,000x*g* for 30 min. Clarified lysate was bound in batch to Ni-NTA resin at 4^0 C for ~ 1 hour followed by extensive washing in lysis buffer without urea, and elution in the following buffer: 20 mM Tris-HCl pH 8.0, 150mM Nacl, 10% glycerol, 0.2 mM TCEP, 0.04% CHAPS, 10 μM dexamethasone, 150 mM imidazole. GR containing fractions were pooled and diluted into a buffer containing 20 mM Tris-HCl pH 8.0, 10% glycerol, 0.2mM TCEP, 0.4% CHAPS, 10 μM dexamethasone (AX Buffer A), and then applied to a HiTrap Q HP (GE Healthcare) column on an Akta explorer FPLC (GE Healthcare). Protein was eluted using a 0-30% gradient of AX

Buffer B (Buffer A + 1 M NaCl). Protein yield at this stage was roughly proportional to CHAPS concentration. 0.4% CHAPS was empirically found to be the most suitable concentration. Thrombin cleavage of the 6xHIS tag was carried out during dialysis into storage buffer containing 20 mM HEPES pH 7.4, 150 mM NaCl, 10% glycerol, 0.2 mM TCEP, 0.04% CHAPS, 10 μM dexamethasone. The resultant GR LBD was purified to 100% homogeneity using a Superdex 200 column. GR LBD was expressed in the presence of 4 ligands, dexamethasone, prednisolone, cortisol, and mifepristone. Yield was best when expressed with dex.

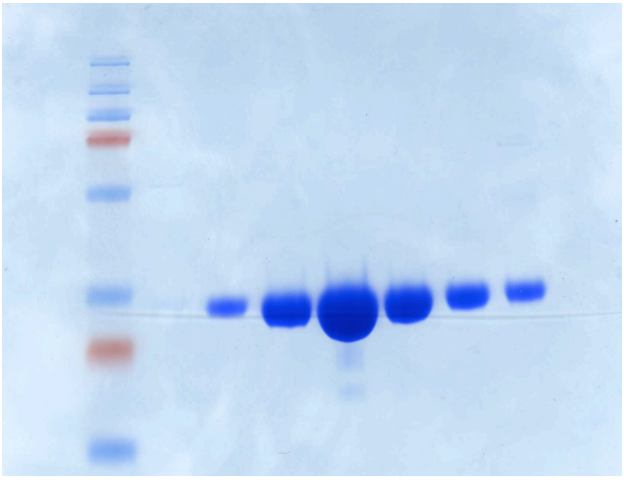

Figure 4-1. *Purified GR LBD : dexamethasone.* Elution fractions from HiTrapQ anion exchange column.

Partial proteolysis by subtillisin was employed to observe the relatively stability of agonist bound GR LBD (figure 4-2). GR expressed and purified in the presence of dex was resistant to proteolysis at 4^0 C for the duration of the experiment, indicating greatly enhanced structural stability compared to zwittergent 3-12 purified GR detailed in chapter 3.

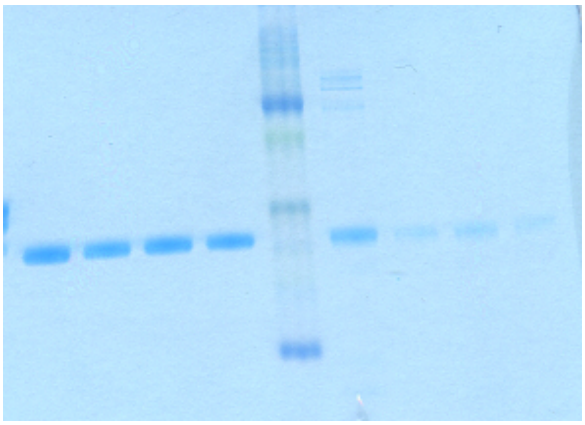

Figure 4-2. *Partial proteolysis of GR LBD expressed in presence of absence of dex.* Left lanes: GR:dex incubated with subtillisin for 0, 10, 20, 30 min. Right lanes: apo-expressed GR incubated with subtillisin for 0, 10, 20, 30 min.

Equilibrium ligand binding studies

Ligand binding to purified GR was assessed with dexamethasone-fluorescein by fluorescence polarization. Prior to the assay, ligand remaining from protein preparation was removed by dialysis or a pass over a NAP-25 desalting column. GR that had been prepared with agonist (dex, prednisolone, cortisol) bound dex-fl in a saturable manner, with slight differences in affinity seen for the differently prepared GRs (figure 4-3).

Competitive ligand binding studies were also carried out using dex-fl (figure 4-4). Agonist dex and antagonist mifepristone were titrated against dex-fl bound GR LBD and the resulting isotherms were fit to yield IC_{50} values of 90 nM for dex and 12 nM for mifepristone. Both ligands have been shown to bind GR with higher affinity in cells.

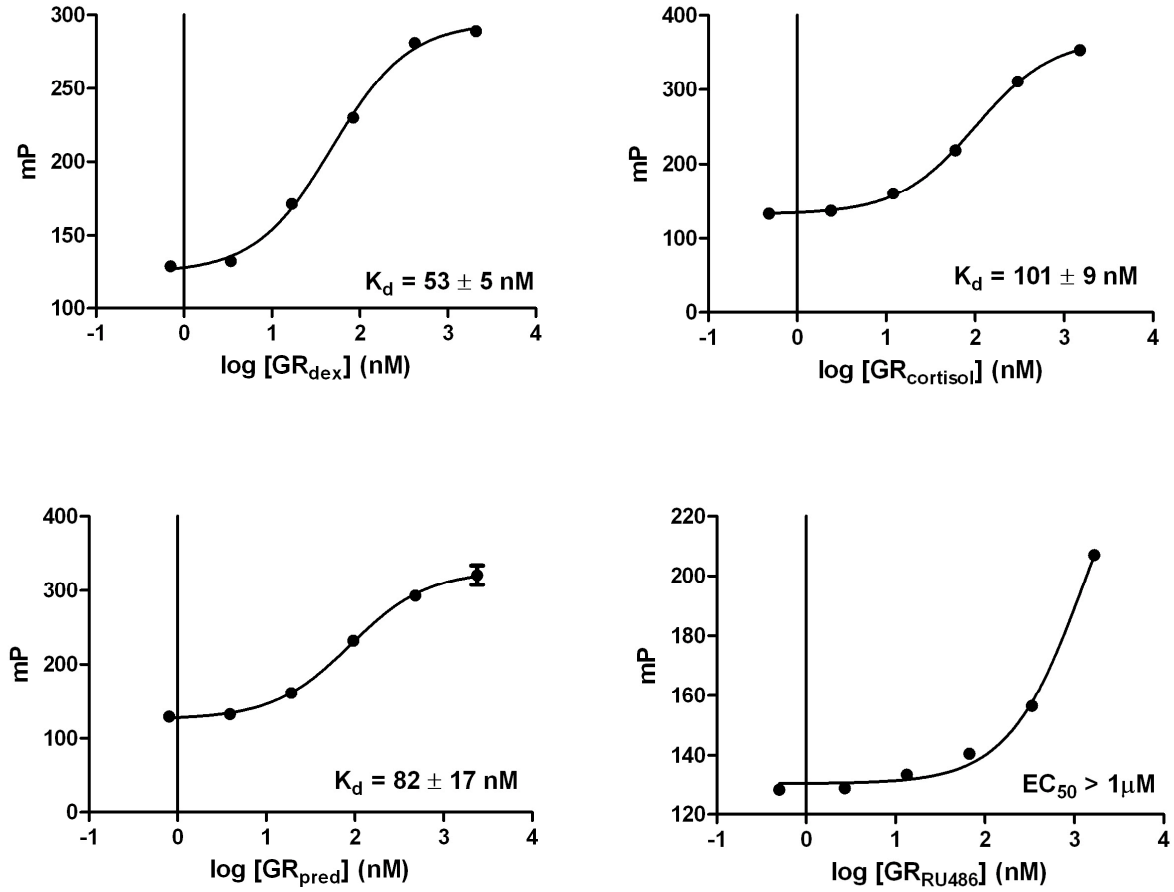

Figure 4-3. *Equilibrium GR binding to dex-fl.* GR was prepared in the presence of 4 ligands, stripped of ligand by dialysis, then assayed for binding to 10 nM dex-fl. K_ds determined by fitting to one-site saturation binding model in Prism 5.

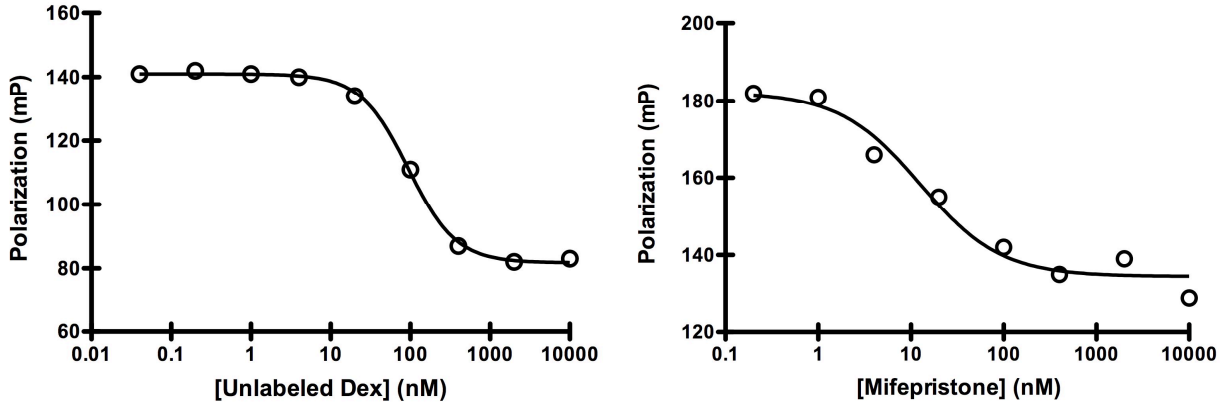

Figure 4-4. *Competitive GR ligand binding assays.* Dex and mifepristone titrated against GR : dex-fl.

Co-regulator peptide binding studies

Significant effort was placed into examining GR's interaction with co-regulator NR box peptides by surface plasmon resonance (SPR). Mirroring Kris Kuchenbecker's AR studies, we attempted to invert the typical SPR experiment by creating GR surfaces that could then be assayed for binding to several NR box peptides in one experiment. Previously published SPR studies of GR LBD had been facilitated by the creation of NR box peptide surfaces, over which GR at varying concentration could be flowed.**(Bledsoe et al, 2002; Kroe et al, 2007)** This technique requires the use of at least two flow cells per peptide, while in theory a single LBD surface on one flow cell can be interrogated with several peptides *ad infinitum*.

Creating GR surfaces that showed full activity proved immensely difficult. Two problems were routinely encountered during the course of these studies: (1) coupling of GR LBD to the SPR chip surface was very inefficient in buffers that are suitable for maintaining active GR, and (2) once coupled to the chip, GR surfaces produced low responses to peptide binding, with typical experiments indicating less than 20% surface activity. In comparison, similarly treated AR surfaces maintain 100% peptide binding activity on the order of days to weeks. Two partial solutions to problem (1) were identified. Coupling to the SPR surface was typically attempted by covalent amide linkage to a CM-5 chip. Commonly, proteins show pH dependent shifts in coupling capacity over a wide pH range. Several pH conditions were scouted for GR, with the the highest efficiency seen at pH 4.0. Although low pH enhanced coupling, it did not improve the activity of the surfaces.

Another strategy employed to increase coupling capacity was biotinylation of GR followed by non-covalent coupling to a streptavidin chip. This was attempted in two contexts: a

non-specific biotin reagent that labeled protein N-termini and lysine residues, and the engineered enzyme subtilligase that specifically labels N-termini.**(Mahrus et al, 2008)** Both techniques enhanced coupling efficiency greatly, but again failed to yield active surfaces.

The second problem above was never fully rectified. Conditions that yield fully active GR surfaces have yet to be identified. Still, the SPR experiments produced some data that is in line with our later findings detailed in chapter 1. The sensorgrams and resulting fits from our most successful experiments are shown in figure 4-5. The conditions for this set of experiments was as follows. 0.3 mg/mL GST-GR LBD : dex was covalently coupled to a CM-5 chip in a buffer containing 20 mM HEPES pH 7.5, 150 mM NaCl, 0.04% CHAPS, 0.2 mM TCEP, and 1 μM dex. All peptides were serially diluted in triplicate from 80 or 60 μM to 1.25 or 0.94 μM in 2-fold steps in the same buffer. Each peptide condition was injected over the GR surface for 60s, followed by a 60s dissociation phase.

The resulting K_D values were somewhat in agreement with our findings in chapter 1. SRC2-3 (GRIP1-3) bound 3-fold weaker than in our FP assay, while SRC1-2 (improperly labeled SRC1-1 in the figure) and SHP-1 showed weak to moderate affinity as they had by FP. An engineered fragment of the co-repressor NCoR containing two of its NR interacting domains unexpectedly showed weak, but saturable binding to the GR surface. As the NCoR peptides are highly insoluble and prone to aggregation, this result may is likely artifactual.

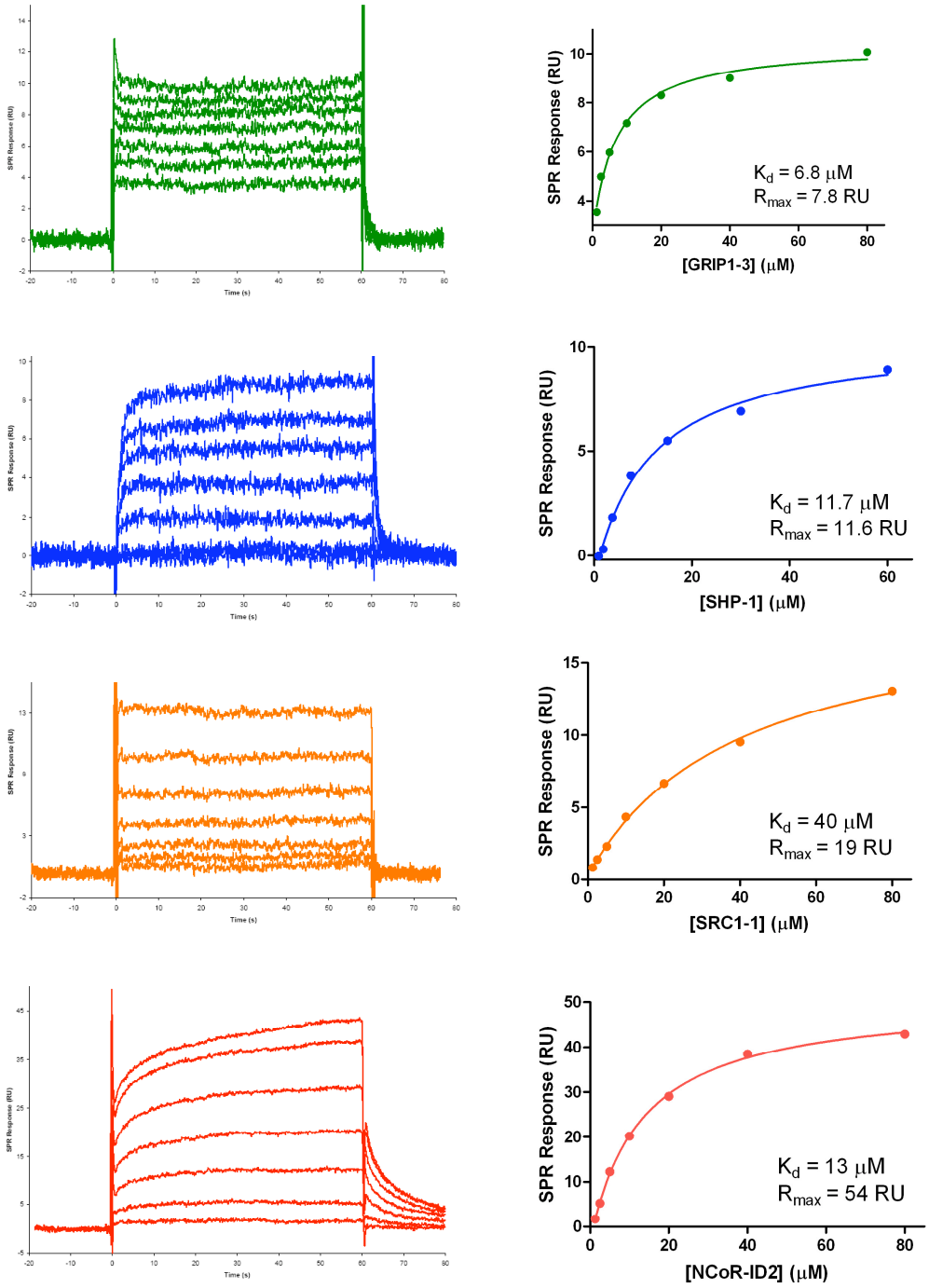

Figure 4-5. *GR binding to co-regulator peptides by SPR.* Left panels are baseline-subtracted sensorgrams of NR box peptides interacting with a GR surface. Right panels are fits to the sensorgram data that yielded K_{DS} and R_{max} values listed. SRC1-2 is mislabeled at SRC1-1 in this figure.

Isothermal titration calorimetry

Another technique employed to assay GR's interactions with co-regulator peptides was isothermal titration calorimetry (ITC). These experiments were limited, as the amount of protein required for each condition is extremely high. The results of one ITC experiment with GR_{M752I} (see chapter 1) and NR box SRC1-4 is shown in figure 4-6.

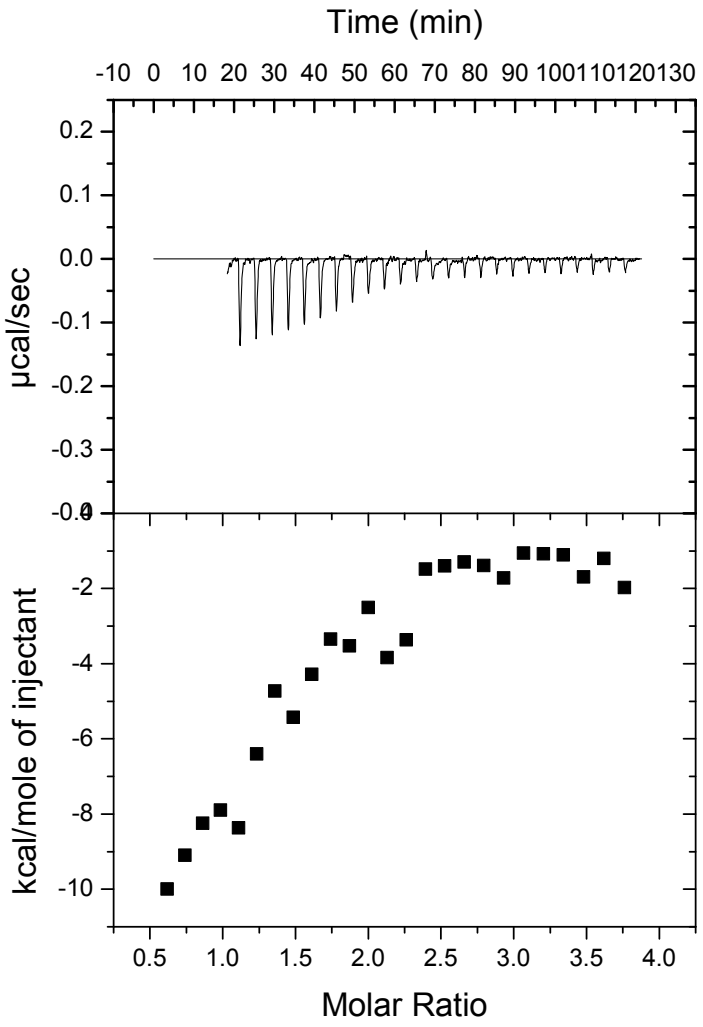

Figure 4-6. *GR_{M752I} binding SRC1-4 by ITC*. Top panel, baseline-subtracted ITC injection data. Bottom panel, heat exchange calculated by Origin software. K_D = 1.2 µM for the interaction.

Experiments were carried out at 25^0 C in a buffer containing 20 mM HEPES pH 7.4, 150 mM NaCl, 10 μM dex, and 0.2 mM TCEP. GR was at 3 μM while SRC1-4 peptide was at 50 μM. The fit K_D value for the above interaction was 1.2 μM, 4-fold weaker than observed by FP. Further experiments were not conducted due to limitations in protein availability, however, ITC appears to be a method well suited to studying GR's interactions with co-regulators and potentially small molecule ligands.

REFERENCES

Biggadike K, Bledsoe RK, Hassell AM, Kirk BE, McLay IM, Shewchuk LM, Stewart EL (2008) X-ray crystal structure of the novel enhanced-affinity glucocorticoid agonist fluticasone furoate in the glucocorticoid receptor-ligand binding domain. *J Med Chem* **51**(12)**:** 3349-3352

Bledsoe RK, Montana VG, Stanley TB, Delves CJ, Apolito CJ, McKee DD, Consler TG, Parks DJ, Stewart EL, Willson TM, Lambert MH, Moore JT, Pearce KH, Xu HE (2002) Crystal structure of the glucocorticoid receptor ligand binding domain reveals a novel mode of receptor dimerization and coactivator recognition. *Cell* **110**(1)**:** 93-105

Kauppi B, Jakob C, Farnegardh M, Yang J, Ahola H, Alarcon M, Calles K, Engstrom O, Harlan J, Muchmore S, Ramqvist AK, Thorell S, Ohman L, Greer J, Gustafsson JA, Carlstedt-Duke J, Carlquist M (2003) The three-dimensional structures of antagonistic and agonistic forms of the glucocorticoid receptor ligand-binding domain: RU-486 induces a transconformation that leads to active antagonism. *J Biol Chem* **278**(25)**:** 22748-22754

Kroe RR, Baker MA, Brown MP, Farrow NA, Gautschi E, Hopkins JL, LaFrance RR, Kronkaitis A, Freeman D, Thomson D, Nabozny G, Grygon CA, Labadia ME (2007) Agonist versus antagonist induce distinct thermodynamic modes of co-factor binding to the glucocorticoid receptor. *Biophys Chem* **128**(2-3)**:** 156-164

Mahrus S, Trinidad JC, Barkan DT, Sali A, Burlingame AL, Wells JA (2008) Global sequencing of proteolytic cleavage sites in apoptosis by specific labeling of protein N termini. *Cell* **134**(5)**:** 866-876

Suino-Powell K, Xu Y, Zhang C, Tao YG, Tolbert WD, Simons SS, Jr., Xu HE (2008) Doubling the size of the glucocorticoid receptor ligand binding pocket by deacylcortivazol. *Mol Cell Biol* **28**(6)**:** 1915-1923

Appendix 1

6-azido-7-nitro-1,4-dihydroquinoxaline-2,3-dione (ANQX) forms an irreversible bond to the active site of the GluR2 AMPA receptor

In collaboration with:

Leslie A. Cruz, Eva Estébanez-Perpiñá, Sabine Borngraeber, Ning Bao, Justin Blethrow, Robert J. Fletterick and Pamela M. England

Reprinted with permission from:

Cruz LA, Estébanez-Perpiñá E, Pfaff S, Borngraeber S, Bao N, Blethrow J, Fletterick RJ, England PM. (2008) *6-azido-7-nitro-1,4-dihydroquinoxaline-2,3-dione (ANQX) forms an irreversible bond to the active site of the GluR2 AMPA receptor.* J Med Chem. 51(18): 5856–5860

ABSTRACT

AMPA receptors mediate fast excitatory synaptic transmission and are essential for synaptic plasticity. ANQX, a photoreactive AMPA receptor antagonist, is an important biological probe used to irreversibly inactivate AMPA receptors. Here, using X-ray crystallography and mass spectroscopy, we report that ANQX forms two major products in the presence of the GluR2 AMPAR ligand-binding core (S1S2J). Upon photostimulation, ANQX reacts intramolecularly to form FQX or intermolecularly to form a covalent adduct with Glu705.

INTRODUCTION

α-amino-3-hydroxy-5-methyl-4-isoxazolepropionic acid (AMPA) receptors (AMPARs) are a subtype of glutamate-gated ion channels that mediate most fast excitatory synaptic transmission by ensuring rapid responses to synaptically released glutamate. (1-3) In addition, activity-dependent changes in the number of AMPARs at synapses modulates the strength of synaptic transmission, an essential component of the mechanism underlying various forms of synaptic plasticity including learning and memory. (4-8)

AMPARs are composed of four modular subunits (GluR1−4 or GluRA−D), each consisting of an amino-terminal domain (NTD) that modulates receptor assembly, a ligand-binding domain (LBD) that gates the pore of the receptor, three transmembrane segments (M1, M3, M4), a reentrant loop (M2) that lines the pore of the channel, and a cytoplasmic C-terminal domain that influences receptor trafficking (Figure A1-S1, Supporting Information). (1-3)

High-resolution crystal structures of an engineered ligand-binding core (S1S2J) with several bound ligands have provided insight into the structure and function of full-length receptors. (9, 10) Gouaux and co-workers provided the first high-resolution structures of the GluR2 AMPAR ligand-binding core (Figure A1-S1, Supporting Information). (11-13) These structures revealed that the ligand-binding core, formed from two discontinuous polypeptide segments (Figures A1-S1 and A1-S2, Supporting Information), adopts a clamshell-like shape that is open in two states, unliganded (apo) and with a competitive antagonist bound. The clamshell is closed with agonist bound. Notably, structurally related ligands within a given class produce distinct degrees of clamshell closure. (14-17) Coupled with electrophysiological experiments carried out on full-length receptors, these studies suggested that the degree of closure affects the

conductance (ion permeation) of the channel, providing a model for channel gating. In addition to modulating channel biophysics, ligand binding also appears to influence the trafficking of AMPARs. For example, both agonists and antagonists have been shown to induce the internalization of AMPARs from neuronal plasma membranes. (18) Although the mechanistic basis for this effect is not understood, it is likely that conformational changes within the ligand-binding domain are translated to the intracellular C-terminal domains, which play a critical role in receptor trafficking.

Quinoxaline-2,3-diones are a major class of competitive AMPAR antagonists, frequently used in studies focused on characterizing the activity of AMPARs. (19) Key members of this family of antagonists are 6,7-dinitroquinoxaline-2,3-dione (DNQX) and 6-cyano-7-nitroquinoxaline-2,3-dione (CNQX). Recently we reported the development of ANQX, a new member of the family of quinoxaline-2,3-diones containing an ortho-nitrophenylazide, which irreversibly inhibits AMPARs in the presence of ultraviolet light and provides a means of rapidly inactivating receptors expressed on the surfaces of neurons. (20-22) In the absence of ultraviolet light, ANQX reversibly inhibits AMPARs. The mechanism by which ANQX irreversibly antagonizes AMPARs has not been previously described. Here we report that ANQX forms two products upon photolysis in the presence of the GluR2 ligand-binding core (S1S2J). Following irradiation with ultraviolet light, ANQX loses dinitrogen to form a highly reactive nitrene that either reacts intramolecularly to form [1,2,5]oxadiazolo[3,4-G]quinoxaline-6,7(5H,8H)-dione 1-oxide (FQX) or intermolecularly to form a covalent adduct with Glu705 located in the binding pocket. The high-resolution crystal structure of FQX bound to the S1S2J revealed that FQX binds in the same orientation and promotes the same degree of closure of the S1S2J around the

ligand as the previously reported structures complexed with DNQX and CNQX. (12, 23) Together, these data indicate a common orientation of quinoxaline-2,3-diones within the AMPAR LBD and reveal the mechanism of receptor photoinactivation with ANQX.

RESULTS

ANQX is a photoreactive quinoxaline-2,3-dione that, upon irradiation with ultraviolet light, loses dinitrogen to form a highly reactive nitrene that undergoes either intra- or intermolecular reactions. We identified the products of both reactions using X-ray crystallography and mass spectrometry. Irradiation of S1S2J-ANQX cocrystals provided a high-resolution structure of the intramolecular reaction product, FQX, reversibly bound to S1S2J. Irradiation of S1S2J in solution in the presence of ANQX yielded sufficient quantities of the intermolecular reaction product to identify GluR705 as the site of cross-linking.

Crystal Structure of the S1S2J−FQX Complex. The high-resolution X-ray structure of the GluR2 ligand-binding core (S1S2J) in complex with FQX was solved at 1.87 Å resolution (Figure A1-1, Table A1-1 of Supporting Information). The complex crystallized in the orthorhombic P212121 space group with four protein monomers in the asymmetric unit (Table A1-1 of Supporting Information). Only two of the monomers are related by noncrystallographic 2-fold symmetry axis. A monomer of the S1S2J dimer complexed with DNQX was used as the search model for molecular replacement. Pairwise superposition of the Cα-atoms of the four molecules yielded pairwise rmsd values ranging between 0.21−0.41 Å.

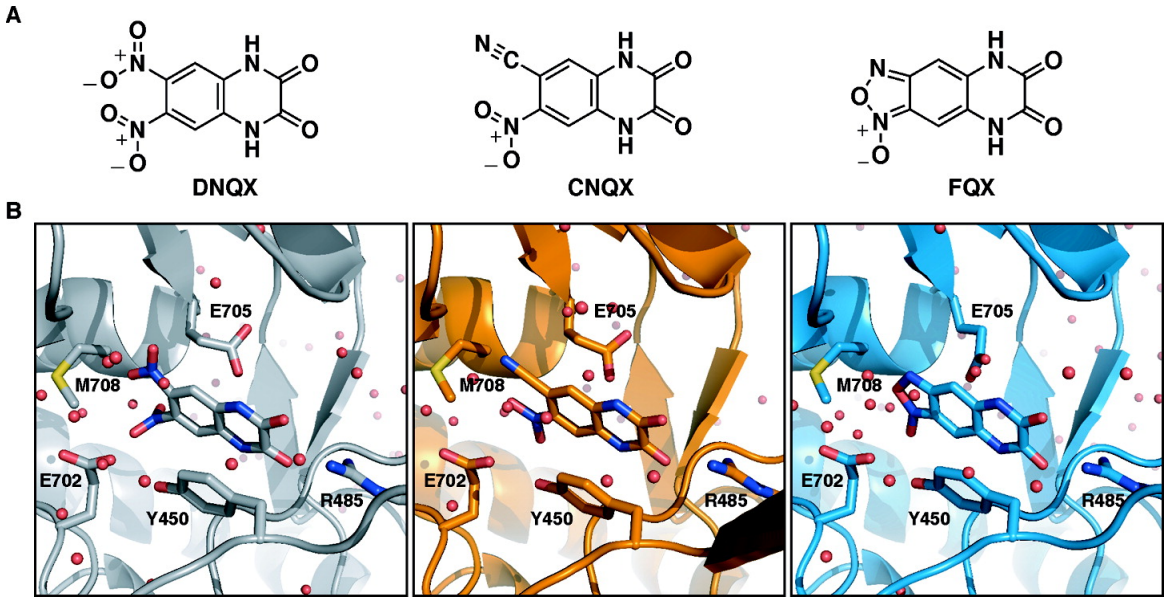

Figure A1-1. Structural formulas and orientation of the quinoxaline-2,3-diones discussed in the present study within the GluR2 ligand-binding core (S1S2J). (A) The competitive antagonists 6,7-dinitroquinoxaline-2,3-dione (DNQX), 6-cyano-7-nitroquinoxaline-2,3-dione (CNQX), and [1,2,5]oxadiazolo[3,4-G]quinoxaline-6,7(5H,8H)-dione 1-oxide (FQX). (B) Close-up views of DNQX, CNQX and FQX bound to the S1S2J.

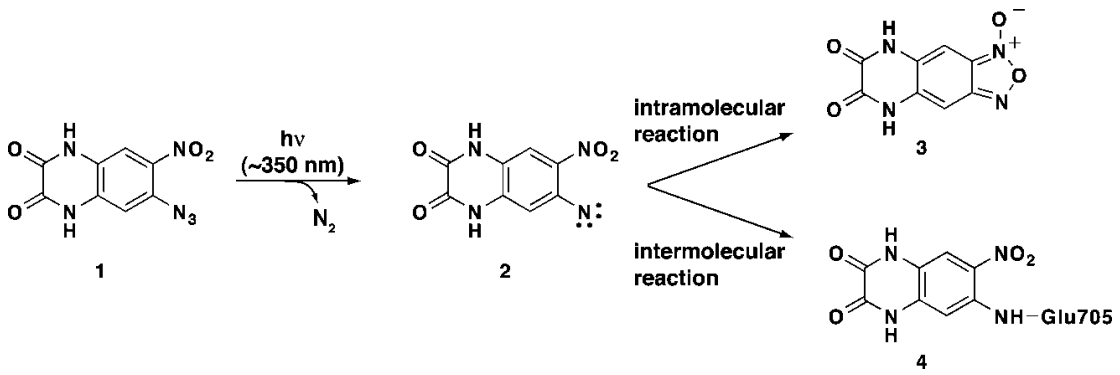

Scheme A1-1. Photochemistry of ANQX. Upon irradiation with UV light, ANQX (1) forms a highly reactive nitrene (2), which forms two products within the S1S2J binding pocket. The intramolecular reaction results in the formation of FQX (3). The intermolecular reaction results in the formation of a covalent bond with Glu705 in the ligand-binding core (4).

Superposition of the S1S2J−FQX monomers with the previously reported S1S2J−DNQX monomer revealed that FQX binds analogously to DNQX within the S1S2J, with an average rmsd of 0.40 Å (Figure A1-2). The degree of clamshell closure in the S1S2J−FQX structure is identical to that observed in the previously reported S1S2J−DNQX and S1S2J−CNQX structures. (12, 23) In all three structures, the clamshell is opened by 15° compared to the glutamate-bound structure. In addition, key residues positioning FQX in the binding site are identical to those orienting DNQX (Figure A1-2) and CNQX in the ligand-binding core. The quinoxaline ring of FQX is positioned directly below Tyr450, forming a favorable π-stacking interaction. The FQX carbonyl oxygens form hydrogen bonds with Arg485, and the amide nitrogens form hydrogen bonds with the backbone carbonyl of Pro478 and a well-defined water molecule, respectively. The two oyxgens of the FQX furoxan ring form a hydrogen bond with a water molecule that is held in position through hydrogen bonds with Tyr405 and Met708. The only binding site residue that differs between the S1S2J−FQX structure and the DNQX and CNQX structures is Glu705, which adopts different conformations in each of the S1S2J−FQX monomer structures due to rotation about the Cβ-Cγ bond.

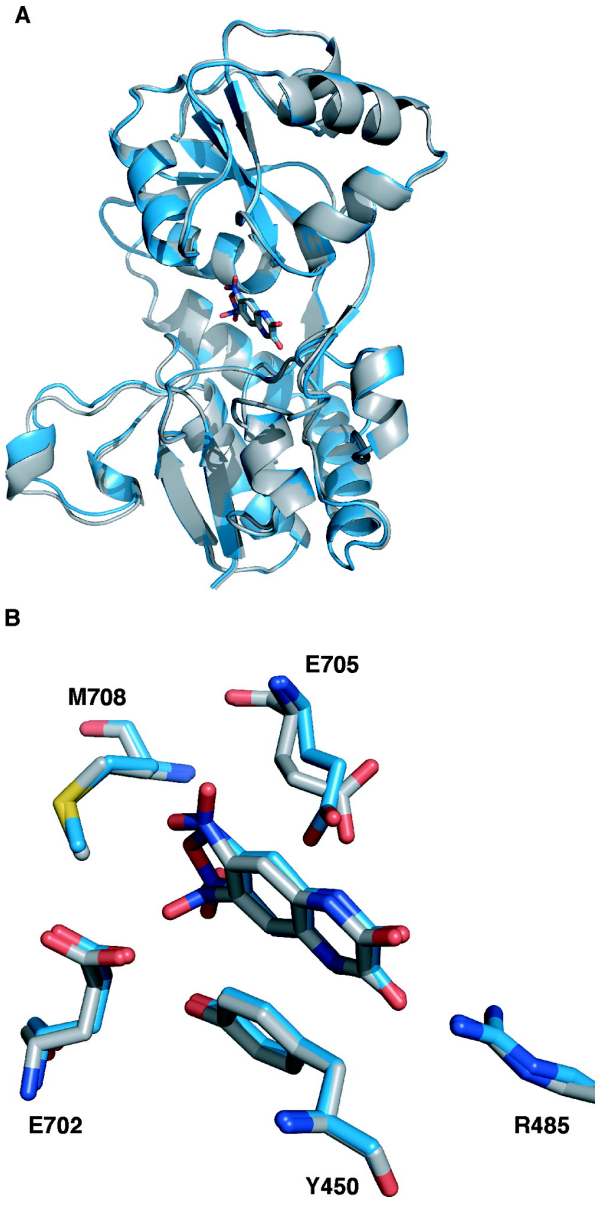

Figure A1-2. Aligned structures of FQX and DNQX bound to the GluR2 ligand-binding core (S1S2J). (A) FQX (blue ribbon), DNQX (gray ribbon), and CNQX (not shown) produce the same degree of closure of the ligand-binding core. (B) Close-up view of the ligand-binding core showing the residues in close proximity to the ligands FQX and DNQX. Glutamate (E) 705 adopts a different conformation in the FQX structure (blue sticks) than the DNQX structure (gray sticks) and CNQX structure (not shown).

Mass Spectral Analysis of the S1S2J -ANQX Solution Complex. The photocross-linked S1S2J−ANQX adduct was obtained through continuous irradiation and perfusion with "fresh" (unphotolyzed) ANQX over the histidine (6X) tagged S1S2J protein immobilized on Ni-NTA beads. Treatment of S1S2J with ANQX and ultraviolet light, but not ultraviolet light alone, resulted in the formation of covalently modified S1S2J bearing a 220 Da mass increase as determined by electrospray ionization orthogonal-time-of-flight (ESI-o-TOF) (Figure A1-3A). This is the expected mass increase for the formation of a covalent adduct between photolyzed ANQX (−N2, MW 220) and S1S2J (MW 32218). To determine the location of this adduct, the covalently modified S1S2J was digested with trypsin and the resulting peptides were analyzed by nanoscale liquid chromatography and tandem mass spectrometry (MS/MS). A peptide fragment containing the active site residues Glu705 and Met708 was found bearing a 220 Da adduct in the ANQX-treated sample, which corresponds to the expected mass increase for the formation of a peptide-ANQX fragment (Figure A1-3B, top panel). In control samples treated with UV light in the absence of ANQX, the 220 Da adduct was not observed (Figure A1-3B, bottom panel). Comparison of the fragment analysis for the ANQX treated versus untreated samples showed that an adduct formed with Glu705 (y11, E*, top panel, Figure A1-3B, top panel) and not Met708 (y8, M, Figure A1-3B, top panel). That is, there is a 220 Da mass difference between the Glu705 fragment in the ANQX treated sample (y11, E*, m/z 1602.72 + NH4, Figure3B, top panel) compared to that of the Glu705 fragment in the untreated sample (y11, E, m/z1399.38, Figure A1-3B, bottom panel). There is no mass difference for the Met708 fragment between the ANQX treated and untreated samples (y8, M, Figure A1-3B). This peptide fragmentation data provides sufficient coverage to assign the site of covalent modification to Glu705 (E*) and not

Met708 (M). We conclude that Glu705 is the preferred site of reaction with photoactivated ANQX.

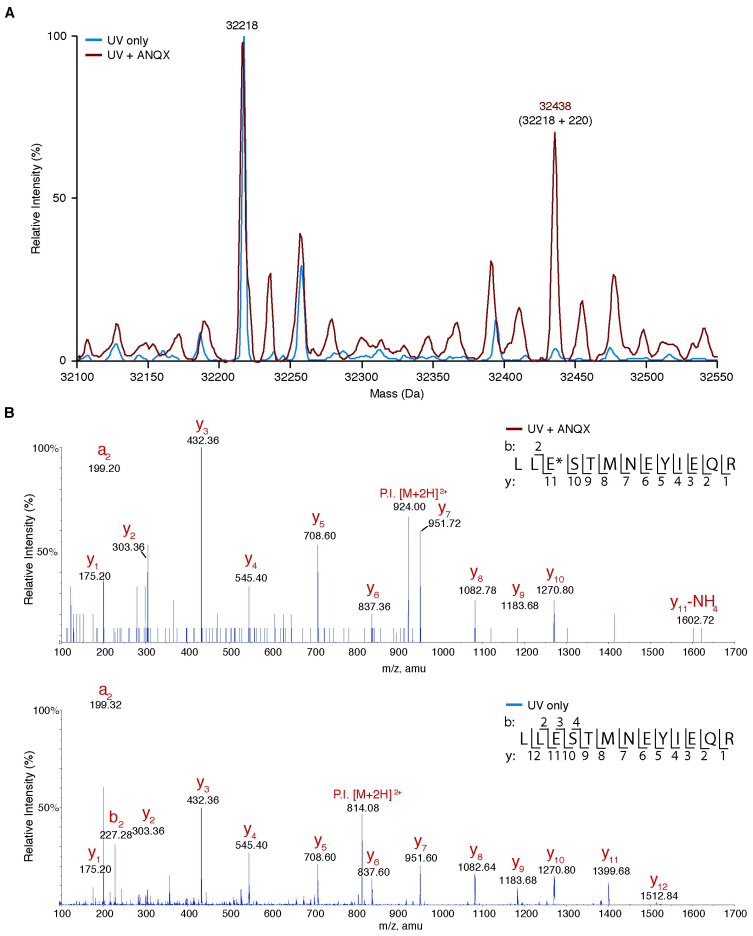

Figure A1-3. Photocross-linking of ANQX to the GluR2 ligand-binding core (S1S2J) analyzed using mass spectrometry. (A) ESI-o-TOF mass spectrum of the S1S2J (32218 Da) following irradiation (90 s) in the absence (blue trace) and presence (red trace) of ANQX (100 μM). Irradiation in the presence of ANQX produces a new major peak (32438 Da) that corresponds to the expected increase in mass (+220 Da) for the ANQX−protein adduct. (B) Mass spectra (MS/MS) of the peptide fragment spanning Glu705 following irradiation (90s) in presence (top panel) and absence (bottom panel) of ANQX. Irradiation in presence of ANQX produced a new peak (m/z 1602.72, E*, top panel), corresponding to the expected mass increase for the formation of an ANQX adduct, and the loss of unlabeled Glu705 (m/z 1399.68, E, bottom panel) peak.

DISCUSSION

In the present study, we used X-ray crystallography and mass spectroscopy to identify the products of photolyzing ANQX in the presence of the GluR2 ligand-binding core (S1S2J). Photolysis of ANQX−S1S2J cocrystals yielded a 1.87 Å crystal structure of the intermolecular reaction product, FQX reversibly bound to the GluR2 ligand-binding core (S1S2J). FQX is formed via intramolecular reaction of the nitrene formed following the loss of dinitrogen from ANQX (Scheme A1-1).

Upon irradiation with UV light, ANQX (1) forms a highly reactive nitrene (2), which forms two products within the S1S2J binding pocket. The intramolecular reaction results in the formation of FQX (3). The intermolecular reaction results in the formation of a covalent bond with Glu705 in the ligand-binding core (4).

In a previous electrophysiological study, ANQX was used to irreversibly photoinactivate AMPARs on neurons. (21) In these experiments, we noted an initial increase in the AMPAR current following the first pulse of ultraviolet light, which suggested that a major product of photolyzed ANQX is the formation of a lower affinity antagonist. Consistent with this observation, the IC50 of FQX (7.6 μM25) is nearly 8-fold higher than the IC50 for ANQX (1.0 μM(20)). The cross-linking efficiency of nitrenes is notoriously poor, with ortho-nitrophenylazides tending to react intramolecularly upon photolysis.24 Therefore, it is not surprising that we only observed the major reaction product (FQX) reversibly bound to the S1S2J, following irradiation of ANQX−S1S2J cocrystals. An intense effort was made to obtain

crystals of the intermolecular reaction product, covalently modified S1S2J−ANQX. However, irradiation of S1S2J−ANQX cocrystallization drops resulted in protein that did not form crystals even after several months and irradiation of the S1S2J immobilized on Ni-NTA beads in the presence of ANQX resulted in protein that was too impure for protein crystallography even after FPLC purification.

Comparison of the FQX structure with the previously reported DNQX and CNQX structures revealed that all three antagonists bind in the same orientation and produce the same degree of clamshell closure within the ligand-binding core. Mass spectral analysis revealed that Glu705 is the site covalently modified by ANQX. On the basis of the position of FQX in the binding pocket in one of the monomers, the nitrene nitrogen on ANQX is positioned 2.5 Å from Glu705. This residue can adopt a range of conformations with distances of 1.7−6.2 Å from the nitrene nitrogen on ANQX. Thus, the cross-link can occur within the range of a single bond without distortion. Together, these data suggest that the formation of the covalent adduct with photolyzed ANQX does not produce a change in the degree of clamshell closure around the ligand. Because Glu705 is a flexible residue in the S1S2J−FQX crystal structure, it may be the case that only certain rotamers of Glu705 react with the activated ANQX nitrene.

Taken together, these data demonstrate that ANQX is a useful biological probe for inactivating AMPARs because it is not a promiscuous cross-linker. We have shown that ANQX forms a covalent adduct with Glu705 and not Met 708. If this reaction does not occur, ANQX reacts intramolecularly to form FQX, which is a low-affinity antagonist of AMPARs.

EXPERIMENTAL SECTION

ANQX was synthesized as previously reported. (20) The GluR2 ligand-binding core was expressed in Escherichia coli and purified to homogeneity as previously reported by Gouaux and co-workers. The purified S1S2J protein was cocrystallized with ANQX at 4 °C using vapor-diffusion (hanging-drop) with a 1:1 ratio of protein to well solution. While submerged in liquid nitrogen, S1S2J−ANQX cocrystals were exposed to ultraviolet light. Synchrotron data for the resulting S1S2J−FQX complex were collected at 100 K on the Advanced Light Source beamline 8.3.1 at Lawrence Berkeley National Laboratory. Data processing was performed using Elves and HKL2000. A complete data set from an S1S2J−FQX crystal diffracted to 1.87 Å, exhibited the space group P212121 and contained four molecules per asymmetric unit (Table A1-1 of Supporting Information). Molecular replacement solutions for S1S2J−ANQX crystal structure were obtained using as a search model one of the monomers of S1S2J−DNQX dimer structure. Photocross-linking of ANQX to the S1S2J was accomplished by irradiating a solution of the 6-HIS tagged S1S2J immobilized on Ni-NTA beads in the presence of ANQX. The resulting sample was denatured and digested with trypsin/chymotrypsin and then analyzed by nanoscale LC/MS2using a Q TRAP mass spectrometer coupled to a liquid chromatography system. Tandem mass spectra were acquired automatically in IDA mode, and the resulting data were analyzed with MASCOT.

ACKNOWLEDGEMENTS

We thank James Holton at the Advance Light Source (ALS) 8.3.1 beamline, Pascal Egea (UCSF) for assistance collecting and processing data, and Eric Gouaux for the S1S2J construct. This work was supported by grants from the Sandler Foundation and the Herbert Boyer Foundation.

REFERENCES

1. Hollmann, M.; Heinemann, S. Cloned glutamate receptors Annu. Rev. Neurosci. 1994 17 31 108

2. Dingledine, R.; Borges, K.; Bowie, D.; Traynelis, S. F. The glutamate receptor ion channels. Pharmacol. Rev. 1999 51 7-61

3. Palmer, C. L.; Cotton, L.; Henley, J. M. The molecular pharmacology and cell biology of alpha-amino-3-hydroxy-5-methyl-4-isoxazolepropionic acid receptors. Pharmacol. Rev.2005 57 253-277

4. Bliss, T. V. P.; Collingridge, G. L. A Synaptic Model of Memory: Long-Term Potentiation in the Hippocampus. Nature 1993 361 31-39

5. Bredt, D. S.; Nicoll, R. A. AMPA receptor trafficking at excitatory synapses. Neuron 2003 40 361-379

6. Song, I.; Huganir, R. L. Regulation of AMPA receptors during synaptic plasticity. Trends Neurosci. 2002 25 578-588

7. Malinow, R.; Malenka, R. C. AMPA receptor trafficking and synaptic plasticity. Annu. Rev. Neurosci. 2002 25 103-126

8. Collingridge, G. L.; Isaac, J. R.; Wang, Y. T. Receptor trafficking and synaptic plasticity. Nat. Rev. Neurosci. 2004 5 952-961

9. Gouaux, E. Structure and function of AMPA receptors. J. Physiol. 2004 554 249-253

10. Mayer, M. L. Glutamate receptor ion channels. Curr. Opin. Neurobiol. 2005 15 282-288

11. Armstrong, N.; Sun, Y.; Chen, G. Q.; Gouaux, E. Structure of a glutamate-receptor ligand-binding core in complex with kainate. Nature 1998 395 913-917

12. Armstrong, N.; Gouaux, E. Mechanisms for activation and antagonism of an AMPA-sensitive glutamate receptor: crystal structures of the GluR2 ligand binding core. Neuron 2000 28 165-181

13. Sun, Y.; Olson, L.; Horning, M.; Armstrong, N.; Mayer, M. Mechanism of glutamate receptor desensitization. Nature 2002 417 245-253

14. Jin, R.; Banke, T. G.; Mayer, M. L.; Traynelis, S. F.; Gouaux, E. Structural basis for partial agonist action at ionotropic glutamate receptors. Nat. Neurosci. 2003 6 803-810

15. Hogner, A.; Kastrup, J. S.; Jin, R.; Liljefors, T.; Mayer, M. L. Structural basis for AMPA receptor activation and ligand selectivity: crystal structures of five agonist complexes with the GluR2 ligand-binding core. J. Mol. Biol. 2002 322 93-109

16. Jin, R.; Gouaux, E. Probing the function, conformational plasticity, and dimer−dimer contacts of the GluR2 ligand-binding core: studies of 5-substituted willardiines and GluR2 S1S2 in the crystal. Biochemistry 2003 42 5201-5213,

17. Jin, R.; Clark, S.; Weeks, A. M.; Dudman, J. T.; Gouaux, E. Mechanism of positive allosteric modulators acting on AMPA receptors. J. Neurosci. 2005 25 9027-9036

18. Lin, J. W.; Ju, W.; Foster, K.; Lee, S. H.; Ahmadian, G. Distinct molecular mechanisms and divergent endocytotic pathways of AMPA receptors internalization. Nat. Neurosci. 2000 3 1282-1290

19. Nikam, S. S.; Kornberg, B. E. AMPA receptor antagonists. Curr. Med. Chem. 2001 8 155-170

20. Chambers, J. J.; Gouda, H.; Young, D. M.; Kuntz, I. D.; England, P. M. Photochemically knocking out glutamate receptors in vivo. J. Am. Chem. Soc. 2004 126 13886-13887,

21. Adesnik, H.; Nicoll, R. A.; England, P. M. Photoinactivation of native AMPA receptors reveals their real-time trafficking. Neuron 2005 48 977-985

22. England, P. M. Rapid photoinactivation of native AMPA receptors using ANQX. Sci. STKE2006 331 11

23. Menuz, K.; Stroud, R. M.; Nicoll, R. A.; Hays, F. A. Subunits switch AMPA receptor antagonists to partial agonists. Science 2007 318 815-817

24. Murata, S.; Tomioka, H. Photochemistry of o-Nitrophenylazide in Matrices. The First Direct Spectroscopic Observation of o-Dinitrosobenzene. Chem. Lett. 1992 57-60

25. Baudy, R. B.; Sulkowski, T. S. 5h,8h-2-oxa-1,3,5,8-tetraaza-cyclopenta[b]-naphthalene-6,7-diones neuroprotective agents. U.S. (1998), USXXAM US 5719153 A 19980217 CAN 128:176169 AN 1998:146566.

SUPPLEMENTAL INFORMATION

Expression and Purification of the GluR2 S1S2J Domain. The GluR2 ligand-binding core (S1S2J) construct, consisting of the GluR2 S1 segment linked to the GluR2 S2 segment via two amino acids (GT), was kindly provided by Dr. Eric Gouaux (HHMI Investigator, Oregon Health & Science University). The S1 and S2 domains correspond to amino acids 390–506 and 632–763, respectively, in the full-length GluR2 subunit. The S1S2J core was expressed in E. coli and purified to homogeneity as previously reported Gouaux and co-workers (1).

Crystallization, Structure Determination and Refinement. The purified S1S2J protein was co-crystallized with the competitive antagonist ANQX. Apo-S1S2J was concentrated to 10 mg/ mL in 10 mM HEPES buffer (10 mM HEPES, 20 mM NaCl, 1 mM EDTA, pH 7.0) and incubated with ANQX (6 mM final concentration). Crystals were grown at 4 °C using vapor-diffusion (hanging-drop) with a 1:1 ratio of protein to well solution. Crystals grew to full dimensions after one month in 12.5%-25% PEG 4000, 0.25-0.4 M ammonium sulfate, and 0.1 M NaOAc pH 5.0. Just prior to data collection, the crystals were soaked in 25% ethylene glycol as cryoprotectant and then flash-cooled in liquid nitrogen. While submerged in liquid nitrogen, S1S2J-ANQX co- crystals were exposed to ultraviolet light for 10 s using a Hg/Xe arc lamp (1000 Watt) outfitted with a UV bandpass filter (#51660, Oriel Instruments: transmitting 300–400 nm, peak 360 nm) and a heat absorbing filter (#51944, Oriel Instruments: transmitting 300-1000nm). Synchrotron data for S1S2J-FQX was collected at 100K on S2 the Advanced Light Source beamline 8.3.1 at Lawrence Berkeley National Laboratory. Data processing was performed using Elves2 and HKL2000. For additional details see Table A1-1 (supplementary material).

A complete dataset from an S1S2J-FQX crystal diffracted to 1.87 Å and exhibits the space group P212121 and contains four molecules per asymmetric unit (Table A1-1). Molecular replacement solutions for S1S2J-ANQX crystal structure was obtained using as a search model one of the monomers of S1S2J-DNQX dimer structure.3 The molecular replacement solutions were obtained using rotation and translation functions from Crystallography & NMR Systems (CNS, http://cns.csb.yale.edu/v1.1/). Protein model

refinement consisted of simulated annealing, group and individual B-factor refinement, and conjugate gradient minimization in CNS followed by model building (monitored by free-R factor) using COOT.4,5 Visual inspection of electron density using COOT allowed identification of the ligand FQX bound to the S1S2J domain. Using CNS, a composite omit map was also calculated in which a different 5% of the model was omittedin an attempt to minimize model bias. Calculation of the electron density maps and crystallographic refinement was performed with CNS using the target parameters of Engh and Huber.6 Several cycles of model building, conjugate gradient minimization and simulated annealing using CNS resulted in models with good stereochemistry. A Ramachandran plot shows that all but three of the residues fall into the favored regions. The statistics for data collection and refinement of each one of the data sets are in Table A1-1.

Photocrosslinking ANQX to S1S2J. A solution of Ni-NTA beads bound to the 6-HIS tagged S1S2J in 10 mM HEPES buffer was placed on a piece of filter paper (Whatmann) in a Petri dish outfitted with a perfusion inlet, supplying unphotolyzed ANQX (100 μM), and an outlet attached to an in house vacuum, removing photolyzed ANQX from the beads. Unphotolyzed ANQX in 10 mM HEPES buffer was continuously perfused (20 mL/min) over the S1S2J Ni-NTA beads while exposing the beads to ultraviolet light for 90 s (1000 Watt Hg/Xe arc lamp outfitted with a UV bandpass filter (#51660,Oriel Instruments: transmitting 300–400 nm, peak 360 nm) and a heat absorbing filter (#51944, Oriel Instruments: transmitting 300-1000nm). In control experiments S1S2J Ni-NTA beads were similarly irradiated in the absence of ANQX. The S1S2J Ni-NTA beads were washed with 10 mM HEPES buffer to remove any remaining photolyzed ANQX. The

S1S2J domain was eluted with elution buffer (50 mM NaH2PO4, 300 mM NaCl, 250 mM imidazole, pH 8.0), dialyzed against 10 mM HEPES, pH 7.0, 20 mM NaCl, 1 mM EDTA, and concentrated (4 mL 10,000 MWCO Amicon centrifuge tubes, Millipore). The samples were analyzed by high-throughput mass spectrometry using a CIT Analytics Autosampler and a LTC premier mass spectrometer (Waters Micromass).

Trpysin-digestion and Tandem Mass Spectrometric Analysis. The experimental (UV light, ANQX) and control (UV light only) S1S2J cores (2.5 μg) were treated with 8 M urea and sonicated for 10 min in a 37 °C water. The resulting denatured proteins were digested overnight at 37 °C with a mixture of trypsin/chymotrypsin. Approximately five picomoles of each sample were then analyzed by nanoscale LC/MS2 using a Q TRAP mass spectrometer (Applied Biosystems, Foster City, USA) coupled to an LC Packings Ultimate/Famos/Switchos liquid chromatography system (Dionex). Peptides were resolved over a 75 micron x 150 mm C18 column using a two hour gradient at a flow rate of 150 nL/min. Tandem mass spectra were acquired automatically in IDA mode, and the resulting data were analysed with MASCOT (Matrix Science).

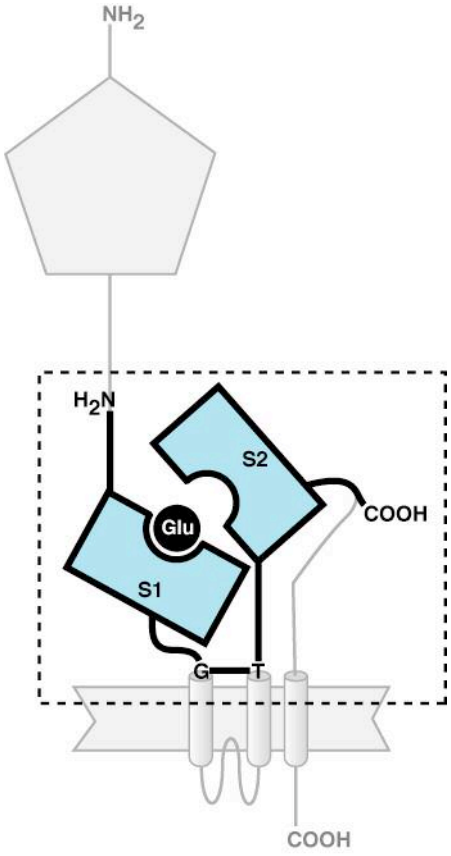

Figure A1-S1. Cartoon depicting the AMPAR ligand-binding core (S1S2J) with respect to the subunit topology. The portion of the subunit corresponding to the S1S2J (dashed box) is comprised of the S1 segment linked to the S2 segment via two amino acids (GT). The S1 and S2 segments correspond to amino acids 390–506 and 632–763, respectively, in the full-length GluR2 subunit.

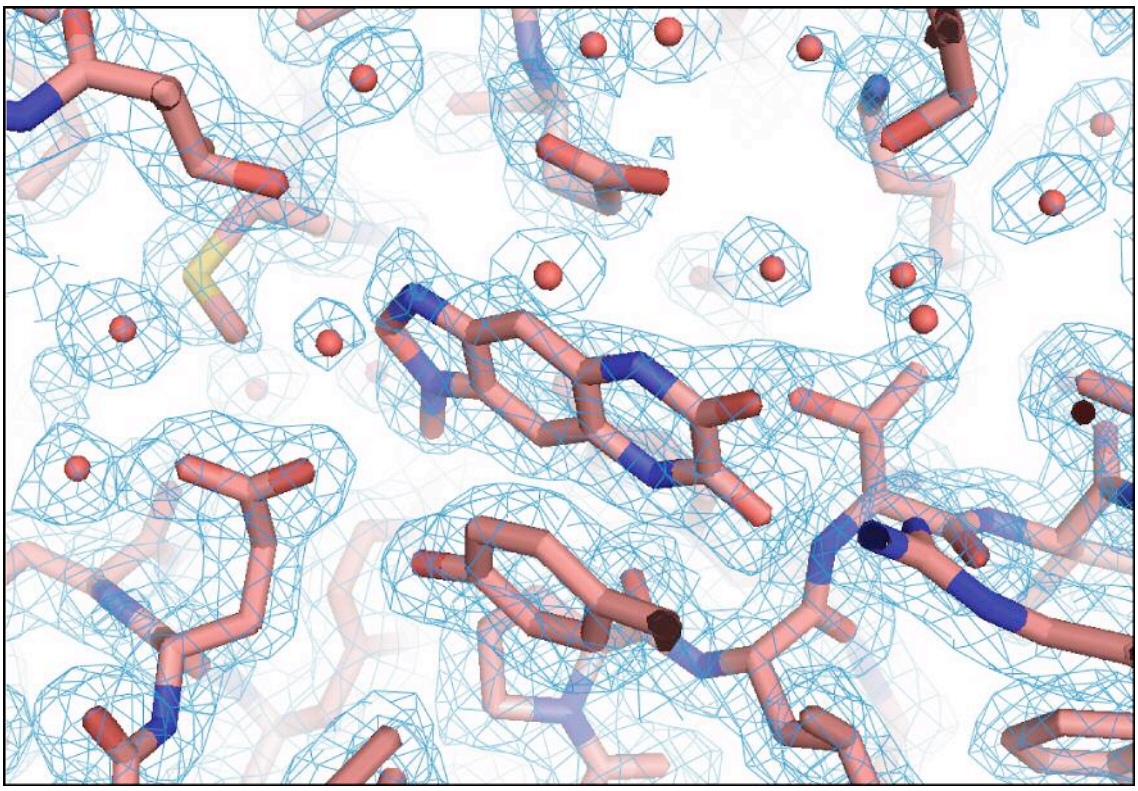

Figure A1-S2. Fo-Fc omit electron density for FQX and surrounding ligands contoured at 1.0 sigma. At 1.5 sigma, the electron density shows the good shapes for the side chains and aromatic rings and has reliable solvent peaks. At 3.0 sigma contouring, there is significant loss of information.

	S1S2J-FQX
Data Collection Statistics	
Space group	$P2_12_12_1$
Cell constants a/b/c (Å)	62.34
	92.26
	195.24
# Molecules/ASU	4
Total Reflections	191553
Unique Reflections	90300
Reflections used refinement	90300
R-merge(%)[a,b]	5.6 (51.2)
Redundancy	2.1
I/ σ (I)[b]	8.0 (2.0)
Completeness (%)[b]	97.0 (92.8)
Refinement Statistics	
Resolution (Å)	1.87
R-factor (%)[c]	21.2
R-free (%)[d]	22.0
B-factors	
Protein	17.677
Ligand	23.172
Solvent	24.521
R.M.S.D bonds	0.017
R.M.S.D angles	1.7
Waters	875
Matthews Coefficient (Da-1)	2.34
Solvent content (%)	47.4
Ramachandran plot (%)	
Most Favored	94%
Allowed	6%
PDB code	3BKI

Table A1-1. Statistics for X-ray Data Collection and Refinement.

ASU=asymmetric unit

[a]R merge (%)= $\sum_{hkl} |\langle I \rangle - I| / \sum_{hkl} |I|$

[b]Values in parentheses refer to the highest resolution shell (1.87-1.97 Å).

[c]R factor (%)= $\sum_{hkl} ||Fo| - |Fc| / \sum_{hkl} |Fo|$

[d]5% of the reflections were set aside for the calculation of the R free value.

SUPPLEMENTAL REFERENCES

1. Chen, G. Q.; Sun, Y.; Jin, R.; Gouaux, E. Probing the ligand binding domain of the GluR2 receptor by proteolysis and deletion mutagenesis defines domain boundaries and yields a crystallizable construct. Protein Sci 1998, 7, 2623-2630.

2. Holton, J., Alber, T. Automated protein crystal structure determination using ELVES. Proc Natl Acad Sci U S A. 2004, 101, 1537-1542.

3. Armstrong, N.; Gouaux, E. Mechanisms for activation and antagonism of an AMPA-sensitive glutamate receptor: crystal structures of the GluR2 ligand binding core. Neuron 2000, 28, 165-181.

4. Brunger, A. T.; Adams, P. D.; Clore, G. M.; DeLano, W. L.; Gros, P. et al. Crystallography & NMR system: A new software suite for macromolecular structure determination. Acta. Crystallogr. D. Biol. Crystallogr. 1998, 54, 905-921.

5. Emsley P.; Cowtan K.; Coot: model-building tools for molecular graphics Acta Crystallographica Section D-Biological Crystallography2004, 60, 2126-2132

6. Engh, R. A.; Huber, R. Accurate bond and angle parameters for X-ray protein structure refinement. Acta Cyrstallographica 1991, A47, 392-400.

Publishing Agreement

It is the policy of the University to encourage the distribution of all theses, dissertations, and manuscripts. Copies of all UCSF theses, dissertations, and manuscripts will be routed to the library via the Graduate Division. The library will make all theses, dissertations, and manuscripts accessible to the public and will preserve these to the best of their abilities, in perpetuity.

Please sign the following statement:

I hereby grant permission to the Graduate Division of the University of California, San Francisco to release copies of my thesis, dissertation,or manuscript to the Campus Library to provide access and preservation, in whole or in part, in perpetuity.

12/1/2009

Author Signature Date